

NONLINEAR PARTICLE DYNAMICS OF PLASMA DIODES IN PRESENCE OF EXTERNAL MAGNETIC FIELD

by

Sourav Pramanik

(Enrolment No.-PHYS05201104004)

Plasma Physics Division, Saha Institute of Nuclear Physics, 1/AF-Bidhannagar,
Kolkata-700064, India

*A thesis submitted to the
Board of Studies in Physical Sciences
In partial fulfillment of requirements
for the degree of
DOCTOR OF PHILOSOPHY*



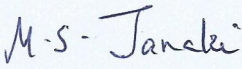
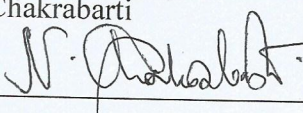
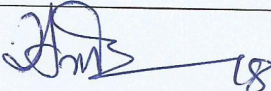
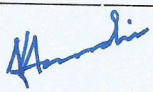
HOMI BHABHA NATIONAL INSTITUTE

July, 2016

Homi Bhabha National Institute

Recommendations of the Viva Voce Committee

As members of the Viva Voce Committee, we certify that we have read the dissertation prepared by Sourav Pramanik entitled "Nonlinear particle dynamics of Plasma Diodes in presence of external magnetic field" and recommend that it may be accepted as fulfilling the thesis requirement for the award of Degree of Doctor of Philosophy.

Chairman - Prof. M. S. Janaki		Date: 20/10/2016.
Guide / Convener - Prof. Nikhil Chakrabarti		Date: 20.10.2016
Co-guide - (if any)		Date:
Examiner - Prof. H. Bailung		Date: 20.10.2016
Member 1- Prof. Munshi Golam Mustafa		Date: 20/10/2016
Member 2- Prof. Samita Basu		Date: 20/10/2016

Final approval and acceptance of this thesis is contingent upon the candidate's submission of the final copies of the thesis to HBNI.

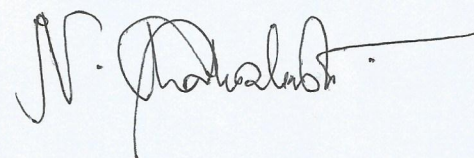
I/We hereby certify that I/we have read this thesis prepared under my/our direction and recommend that it may be accepted as fulfilling the thesis requirement.

Date: 20.10.2016

Place: SINP, KOLKATA

Co-guide (if applicable)

Guide



STATEMENT BY AUTHOR

This dissertation has been submitted in partial fulfillment of requirements for the doctoral degree at Homi Bhabha National Institute (HBNI) and is deposited in the Library to be made available to borrowers under rules of the HBNI.

Brief quotations from this dissertation are allowable without special permission, provided that accurate acknowledgement of source is made. Requests for permission for extended quotation from or reproduction of this manuscript in whole or in part may be granted by the Competent Authority of HBNI when in his or her judgment the proposed use of the material is in the interests of scholarship. In all other instances, however, permission must be obtained from the author.

Sourav Pramanik

DECLARATION

I, hereby declare that the investigation presented in the thesis has been carried out by me. The work is original and has not been submitted earlier as a whole or in part for a degree / diploma at this or any other Institution / University.

Sourav Pramanik

List of Publications

(Publications in peer reviewed Journals)

1. *The transverse magnetic field effect on steady-state solutions of the Bursian diode.*
S. Pramanik, A. Ya. Ender, V. I. Kuznetsov and N. Chakrabarti, *Physics of Plasmas* **22**, 042110 (2015).
2. *Stability analysis of steady state solutions of Bursian diode in presence of transverse magnetic field.*
S. Pramanik, V. I. Kuznetsov and N. Chakrabarti, *Physics of Plasmas* **22**, 082103 (2015).
3. *A study on the steady-state solutions of a Bursian diode in the presence of transverse magnetic field, when the electrons of the injected beam are turned back partially or totally*
S. Pramanik, V. I. Kuznetsov and N. Chakrabarti, *Physics of Plasmas* **22**, 112108 (2015).
4. *Non-neutral plasma diode in the presence of a transverse magnetic field.*
S. Pramanik, V. I. Kuznetsov, A. B. Gerasimenko and N. Chakrabarti, *Physics of Plasmas*, **23**, 062118 (2016).
5. *A study on the steady-state solutions of a relativistic Bursian diode in the presence of a transverse magnetic field.*
S. Pramanik, V. I. Kuznetsov, L. A. Bakaleinikov and N. Chakrabarti, *Physics of Plasmas*, **23**, 082110 (2016).
6. *Time-independent states of a non-neutral plasma diode when emitted electrons are partially turned around by a transverse magnetic field.*

- S. Pramanik**, V. I. Kuznetsov, A. B. Gerasimenko and N. Chakrabarti, *Physics of Plasmas*, **23**, 103105 (2016).
7. *Wave breaking of nonlinear electron oscillations in a warm magnetized plasma.*
S. Pramanik, C. Maity and N. Chakrabarti, *Physics of Plasmas* **21**, 022308 (2014).
8. *Phase-mixing of ion plasma modes in pair-ion plasmas.*
S. Pramanik, C. Maity and N. Chakrabarti, *Physics of Plasmas* **22**, 052303 (2015).
9. *The phase mixing of an upper hybrid wave in a magnetized pair-ion plasma.*
S. Pramanik, C. Maity and N. Chakrabarti *Physica Scripta* **91**, 065602 (2016).

Sourav Pramanik

Dedicated to my “Baba”, “Maa” and “Bon”

Acknowledgements

The research included in this dissertation could not have been performed without the assistance, patience, and support of many individuals. I would like to express my sincere gratitude first to my supervisor Prof. Nikhil Chakrabarti for his careful guidance, encouragement and moral support throughout my tenure. Under his guidance, I successfully overcame many difficulties and learned a lot. It has been a great pleasure and honour to work with him at Saha Institute of Nuclear Physics.

I express my heartiest thanks to my collaborator Prof. Victor Kuznetsov of Ioffe Institute, Russia for his invaluable helps and suggestions as well as for guiding me to solve different problems regarding my Ph.D works. I have learned so many things from him in the field of my research. This thesis would not have been possible without his constant support. I would also like to acknowledge A. B. Gerasimenko and L. A. Bakaleinikov for their cooperations.

My special words of thankfulness should also acknowledge Prof. R. Pal, Prof. A. N. S. Iyenger and Prof M. S. Janaki for their fruitful comments and discussions.

This research would not have been possible without the assistance and cooperation of my seniors Subir Da, Chandan Da, Sudip da, Debu Da, Avik da and Anwesha di. I must thank Chandan da individually who loved me like his brother and motivated me greatly by sharing his knowledge and insights. I also feel very lucky to spend innumerable joyful moments with Abhijit, Satyajit, Pankaj, Debajyoti, Sabuj, Sayanee, Mithun and Subha. I should extend my words of appreciation to Subhasish Da, Monobir Da, Santanu Da, Partha Da, Dipankar Da and many other colleagues in SINP. I would also like to acknowledge Pallabi Das (Tata Institute of Fundamental Research, Mumbai) who contributed to our investigations of the vacuum diodes during her visit at Saha Institute of Nuclear Physics as a project-trainee.

I thank my doctoral committee members in making yearly evaluation of my progress report and giving valuable suggestions.

The five years journey of my doctoral work would not have been easy without my friends. Whenever I needed them, they have always been there, in front of my

eyes for last five years, motivating and inspiring every bit of me. Prasanta, Faruque, Gouranga, Kuntal, Achyut, Abhijit, Goutam, Ashish, Santanu, Rajendra, Arka, Sabyasachi, Mithun, Minakshi, Sucheta... thanks to one and all for making my journey memorable.

I should convey my deepest gratitude to my beloved parents and sibling. Without their love, support and understanding I could never have completed this doctoral degree.

Lastly, I want to express my sincere apologies for my inability to individually acknowledge many others, who might have helped me in the completion of this Ph.D. work one way or another.

SINP, Kolkata

July, 2016

Sourav Pramanik

Contents

Synopsis	xii
List of figures	xix
1 Introduction	1
1.1 Brief Historical Overview	2
1.1.1 Basic structures of the Plasma Diodes	2
1.1.2 Bursian diode (pure electron diode)	6
1.1.3 Pierce diode	10
1.1.4 Further progress in this field	13
1.2 Applications of the “Bursian-Pierce” Instabilities	14
1.3 Motivation to study the effect of the transverse magnetic field	16
1.4 Outline of the thesis	18
2 Effect of transverse magnetic field on the steady-state solutions of a Bursian diode	21
2.1 Introduction	22
2.2 The electron dynamics	23
2.3 Steady-state solutions. The Euler method	26
2.4 Features of steady-states. The Lagrange method	34
2.5 Summary	42
3 Stability analysis of the steady state solutions of Bursian Diode in presence of transverse magnetic field	43
3.1 Introduction	44
3.2 Steady State Solutions	45
3.3 Stability of the steady states with respect to Aperiodic Perturbation	49
3.4 The Dispersion equation	51
3.5 Stability Analysis	53
3.6 Summary	59

4	Stationary states of a Bursian diode in presence of transverse magnetic field representing partial or total electron reflection	61
4.1	Introduction	62
4.2	Complete electron-reflection: The Euler method	63
4.3	Partial electron-reflection: The Euler method	67
4.4	Partial electron-reflection: The Lagrange method	73
4.5	Total electron-reflection: The Lagrange method	80
4.6	Summary	84
5	Stationary states of a relativistic Bursian diode in the presence of a transverse magnetic field	87
5.1	Introduction	88
5.2	The electron dynamics	89
5.3	Steady-state solutions. The Euler method	93
5.3.1	Regime of no electron-reflection	100
5.3.2	Regime of electron reflection	102
5.4	Features of the steady-states. The Lagrange method	106
5.5	Summary	112
6	Effect of transverse magnetic field on non-neutral plasma diodes	115
6.1	Introduction	116
6.2	Basic equations	117
6.3	The steady state solutions	119
6.4	Summary	132
7	The regime of electron-reflection of a non-neutral plasma diode in the presence of a transverse magnetic field	133
7.1	Introduction	134
7.2	Model and the dimensionless variables	135
7.3	Steady state solutions	137
7.4	Summary	147
8	Conclusion	149
8.1	A quick recapitulation	150
8.2	Future prospects and conclusive remarks	154
	Bibliography	159

Synopsis

The contents of this thesis are mainly centered around the effects of externally applied transverse magnetic field on the steady state characteristics of plasma diodes. A detailed analytical and numerical study on plasma diodes in presence of uniform transverse magnetic field is carried out in this doctoral research. A plasma diode, in its simplest form, consists of two electrodes and a certain potential (V) is applied across them. Charge carriers which are injected by the emitter and collected by the collector, contribute a net current across the circuit. The problems in deep space research as well as in near-earth space study, have actualized the need of electrical energy sources of hundreds KW to tens MW power. To obtain such values, a source with high efficiency up to more than 30 percent is needed. This criteria is well satisfied with the Thermionic Energy Converter (TIC) of new generation [1]. It is a diodic system which operates in a collisionless (Knudsen) regime with surface ionization. The high-temperature TIC yields a very high current density. As a result, there is a strong inherent magnetic field within the interelectrode gap and it is transversal to the electron motion. This field reorients the flow of the emitted electrons partially, resulting in lowering the output current. The simplest example of the Knudsen diode is the Bursian diode [2], where a monoenergetic beam of electrons is injected from the emitter. Not only in thermionic energy converters [3], diode like phenomena are also exhibited by many physical systems which are used for scientific and technological purposes, such as, microwave generators [4], electronic switches [5], low pressure discharges and processing [6], xerographic technologies [7], Q machines [8] etc. One of the most interesting diodic features is “space-charge-limited flow” and it severely controls the operating conditions of such systems.

In the first quarter of 20-th century, collective nature of bounded charge particles was firstly analyzed by Child and Langmuir [9, 10]. They studied a vacuum diode with a certain potential bias V , and showed that the current transported between two electrodes is proportional to $V^{3/2}/L^2$ by assuming the velocity of the charge particles to be zero at the emitter. It is known as the famous “Child-Langmuir” law. Almost in the same time, the Russian scientists Bursian and Pavlov studied a short circuited vacuum diode for monoenergetic electron beam [2] and depending upon the values of external parameters, they found three distinct types of solutions in steady state. The solutions are as follows: stable solution without electron reflection, unstable solution without electron reflection and stable

solution with partial electron reflection for which potential distribution corresponds to virtual cathode (VC). It has been shown that, if the diode gap value exceeds a certain critical value, an aperiodic instability appears in the system. As a result of it, the regime without electron reflection disappears and the system ends up with a state of partial electron reflection. So, there is a threshold value of the current that can pass through the vacuum diode in steady state. It is known as “Bursian threshold” and the phenomena involved behind it, is called as “Bursian instability”. This threshold situation, where the diode current reaches to its maximum value, is called “space-charge-limit”. Later, Gill studied a vacuum diode experimentally with a small velocity spread in the injected electron beam and confirmed the existence of the threshold value of the diode current [11].

Kuznetsov *et al.* studied the Bursian diode, both analytically and numerically, with arbitrary external voltage and discussed the solutions with and without electron reflections in detail [12, 13, 14, 15, 16]. In their works, all the steady state solutions have been visualized through $\varepsilon_0 - \delta$ parametric plot for a certain value of applied voltage; where ε_0 and δ are the electric field strength at emitter and the diode gap respectively. For a particular value of external voltage, each point on the “ $\varepsilon_0 - \delta$ ”-curve denotes a steady state. From this diagram, they pointed out two special situations which were mentioned as “*SCL*” point and “zero-point” (or, “0”-point) in this diagram. The “*SCL*” point corresponds to the state with maximum diode current and the “zero-point” appears for the situation when longitudinal velocity of an electron of the injected beam becomes zero within the inter-electrode region for the first time. They showed that the ‘S’-shaped curves in $\varepsilon_0 - \delta$ parametric space consist of three distinct regions where each region represents a solution of particular type in steady state, and the “*SCL*” point and “zero-point” differentiate these regions. Following the convention, introduced by Fay *et al.* [17], these regions were termed as : “C normal branch” ($\varepsilon_0 \leq \varepsilon_{0,SCL}$), “C overlap branch” ($\varepsilon_{0,SCL} < \varepsilon_0 \leq \varepsilon_{0,0}$) and “virtual cathode branch”, the branch corresponding to partial electron reflection ($\varepsilon_0 > \varepsilon_{0,0}$). Here the notations $\varepsilon_{0,SCL}$ and $\varepsilon_{0,0}$ represent the value of electric field strength at emitter (ε_0) for *SCL* and “zero-point” conditions respectively. Potential distributions corresponding to the states for no electron reflection, maximum diode current and electron reflection were also developed. To explain the stability properties of the steady state solutions, “collector potential (η_c) vs emitter field strength (ε_0)” diagram was utilized

as well as, a relevant dispersion relation was derived by employing first order perturbation theory. It was shown that for every “ $\varepsilon_0 - \delta$ ”-curve, C overlap branch is unstable and the other two branches are stable under small aperiodic perturbation [18].

To utilize the interesting properties of space charge limited flow for different applications, the plasma diodes have been diagnosed extensively in recent years [19, 20, 21, 22, 23]. In these works, a number of parameters (e.g., applied voltage, temperature etc.) are identified to control the space charge current in diodic systems. In this thesis, efforts are focussed to study how the presence of external magnetic field modifies the space charge limit of the plasma diodes. For this purpose, we have employed a simplified planar model with uniform magnetic field which is perpendicular to the plane of electron motion. With the aid of basic fluid equations, the relevant problems have been approached with two techniques: the Euler and the Lagrange formalism.

In our first study, assuming the emitted electrons to be purely monoenergetic, we have explored the steady states up to the situation where the longitudinal velocity of an electron vanishes for the first time within the interelectrode region. Using emitter electric field as a characteristic function, the steady state solutions have been evaluated in accordance with the diode length, applied voltage and magnetic field strength. This investigation shows that in a Bursian diode with a transverse magnetic field, potential distributions remain single minimum functions, but the height of minimum turns out to be below the initial kinetic energy of electrons. It happens because of the fact that a part of the longitudinal kinetic energy of the electrons is converted into transversal kinetic energy due to the presence of magnetic field. Like the case of vacuum diode without magnetic field, the steady-state solutions are demonstrated through the “emitter field strength vs diode gap” diagram and the “*SCL*” and “zero-point” situations are investigated in detail. It has also been explained from the energy conservation principle that, for the case of “zero-point” solution, at the position of zero electron-velocity, potential profile approaches to a threshold value. In presence of strong magnetic field, the trajectories of the emitted electrons are bent and they start to lose their beam characteristics. The value of the maximum diode current at space charge limit also decreases with increasing strength of applied magnetic field. As a consequence, (ε_0, δ) -curves are displaced as magnetic field strength is enhanced. The *SCL* points are displaced to the left, and at its right, solutions with no electron reflection are

absent.

Next, we have investigated the stability properties of the steady state solutions of a Bursian diode in presence of uniform transverse magnetic field. The dispersion relation is obtained from the time dependent basic equations by using first order perturbation theory. It is shown that the solutions corresponding to C normal branch are always stable, and those of C overlap branch are unstable with respect to the small aperiodic perturbation. When the strength of the magnetic field is increased, the width of the unstable region (branch II) gradually decreases and vanishes at a particular strength of the magnetic field. The method of “ $\eta_c - \varepsilon_0$ ” diagram leads us to same results, where η_c is the collector potential.

In these works, emitted electrons have been assumed to be purely monoenergetic. As soon as the potential distribution within interelectrode region reaches a threshold value, emitted electrons are completely turned about by the magnetic field. But, if there is a small velocity spread in the emitted electron beam, they can be reflected back partially or completely depending on the strength of the applied magnetic field, and as a result of it, the diode current decreases. To study this behaviour, a reflection coefficient r is introduced, which is the ratio of reflected to injected electron fluxes. This coefficient takes the value zero for the solution without electron turning and one for complete electron turning. The situation of partial electron turning appears in the limit $0 < r < 1$. The branch (virtual cathode branch or B branch) for partial electron reflection for which potential distribution corresponds to the virtual cathode formation, has been also plotted in (ε_0, δ) -diagram.

However, unlike the classical Bursian diode, a new region with non-unique solutions has been explored. This region contains the solutions for which the longitudinal velocity of the injected electrons vanishes for several times within the inter-electrode space. The coefficient r , which controls the amount of the electrons to be turned back by the magnetic field, is more than about 0.9 in this region.

Motivated by the fact that sometimes, electrons of the injected beam may possess relativistic velocity, we next scrutinized the steady-states of a relativistic planar vacuum diode driven by a cold relativistic electron beam in presence of external transverse magnetic field. The situations where no electrons are turned around by the magnetic field and they are turned around partially or totally, are treated in a generalized way. The solutions are compared with similar ones obtained for the Bursian diode with a non-relativistic electron beam. It was explained

that the region of non unique solutions is enlarged as relativistic factor γ_0 of the emitted beam increases. It will be communicated soon.

Bursian diode is a purely non-neutral diode with only single kind of charge carriers (electrons). We have also attempted an analytical study of the steady states of the plasma diodes, where the injected electron beam propagates through the background of stationary and positively charged ions and in presence of external transverse magnetic field. We have introduced an arbitrary neutralization parameter γ , which is the ratio of background ion density to injected electron density. Note that, γ takes the value zero for the Bursian diodes and it is one for Pierce diodes [24]. Along with the transverse magnetic field, the parameter γ is found to play an important role to control the steady state properties as well as the stability criteria. It will also be communicated soon.

As an application of our works, we can suggest to design the fast electronic switches based on Bursian diode. The working mechanism of this electronic switch involves a transition between the states of the normal C branch and the B branch. Let us imagine a diode operating without magnetic field and the initial state lies just to left of the *SCL* point. Here, the relevant current through the diode is nearly equal to the maximum one ($J_{max} \sim \delta_{SCL}^2$). When magnetic field is turned on, the *SCL* points are displaced to the left, and to its right, the solutions without electron reflection are absent. As a result, a transition process occurs in the diode resulting to the final state corresponding to the branch with limited current. It is shown that if the strength of the applied magnetic field exceeds a certain critical value, the current turns out to be zero after switching, i. e., current cut-off is complete. Otherwise the state corresponds to the regime with an incomplete current cut-off.

In summary, the results and conclusion presented in this thesis, would enrich the understanding of different nonlinear aspects of plasma diodes.

The submission of this synopsis is recommended and approved by the Doctoral committee.

Bibliography

- [1] V. I. Babanin, I. N. Kolyshkin, V. I. Kuznetsov, V. I. Sitnov, and A. Ya. Ender, *2nd Intersoc. Conf. on Nuclear Power Eng. in Space. Physics of Thermionic Energy Converters, Sukhumi, Georgia: 9* (1991).
- [2] V. R. Bursian and V. I. Pavlov, *Zh. Rus. Fiz.-Khim. Obshch* **55**, 71 (1923) (in Russian).
- [3] F. G. Baksht *et al.*, in: Moizhes, Pikus (Eds.), *Thermionic Converters and Low-Temperature Plasma, Washington, DC*, (1976).
- [4] V. L. Granatstein and I. Alexe (Eds.), *High-Power Microwave Sources*, (Artech House, Norwood 1987).
- [5] W. Hertz, *Phys. Technol.* **10**, 195 (1979).
- [6] R. T. Farouki, M. Dalvie and L. F. Pavarino, *J. Appl. Phys.* **68**, 6106 (1990).
- [7] Yu. N. Gartstein and P. S. Ramesch, *J. Appl. Phys.* **83**, 2037 (1998).
- [8] R. W. Motley, *Q-Machines*, (Academic Press, New York, 1975).
- [9] C. D. Child, *Phys. Rev., Ser. 1*, **32** 492 (1911).
- [10] I. Langmuir, *Phys. Rev.* **2**, 450 (1913).
- [11] E. W. B. Gill, *Philos. Mag.* **49**, 993 (1925).
- [12] V. I. Kuznetsov and A. Ya. Ender, *Sov. Phys. Tech. Phys.* **22**, 1295 (1977).
- [13] V. I. Kuznetsov, A. V. Solov'yev and A. Ya. Ender, *Sov. Phys. Tech. Phys.* **39**, 1207 (1994).
- [14] V. I. Kuznetsov, A. Ya. Ender, H. Schamel and P. V. Akimov, *Phys. Plasmas* **11**, 3224 (2004).

- [15] V. I. Kuznetsov and A. Ya. Ender, Plasma Phys. Rep. **36**, 226 (2010).
- [16] V. I. Kuznetsov and A. Ya. Ender, Tech. Phys. **58**, 1705 (2013).
- [17] C. E. Fay, A. L. Samuel and W. Shockly, Bell Syst. Tech. J. **17**, 49 (1938).
- [18] P. V. Akimov, H. Schamel, A. Ya. Ender, and V. I. Kuznetsov, J. Appl. Phys. **93**, 1246 (2003).
- [19] V. F. Tarasenko, Plasma Phys. Rep. **37**, 409 (2011).
- [20] A. Roy, A. Patel, R. Menon, A. Sharma, D. P. Chakravarthy, and D. S. Patil, Phys. Plasmas **18**, 103108 (2011).
- [21] A. Pedersen, A. Manolescu, and A. Valfells, Phys. Rev. Lett. **104**, 175002 (2010).
- [22] M. S. Rosin and H. Sun, Phys. Rev. E **87**, 043114 (2013).
- [23] V. I. Kuznetsov and A. Ya. Ender, Plasma Phys. Rep. **41**, 905 (2015).
- [24] A. Ya. Ender, H. Kolinsky, V. I. Kuznetsov and H. Schamel. Phys. Rep. **328**, 1 (2000).

List of Figures

1.1	Schematic representation of a planar plasma diode. In case, there is any transverse magnetic field, the direction of it is shown by the cross mark.	3
2.1	Normalized potential $e\varphi/(mv_0^2)$ as a function of normalized space z/λ_D for two $\varepsilon_0 = eE_0\lambda_D/(mv_0^2)$ values: (1) $\varepsilon_0 = 0.6$ and (2) 1.0. Dashed curve corresponds to $\varphi = p(z, \omega) = (e/2m)(\omega^2 z^2 - v_0^2)$; $\omega/\omega_0 = 1.0$; $U = 0$	26
2.2	Velocity distribution in the interelectrode gap drawn for different ε_0 values: (1) $\varepsilon_0 = 0.6$, (2) 0.7, (3) 0.8, and (4) 1.0; $\Omega = 1.0$; $V = 0$. Closed circles mark position of the potential minimum.	32
2.3	Plots of positions of (1) the collector, (2) the potential minimum, as well as (3) the velocity minimum vs ε_0 for $\Omega = 1.0$; $V = 0$	33
2.4	Curves $\varepsilon_0(\delta)$ drawn for various values of Ω : (1) $\Omega = 0$, (2) 0.3, (3) 0.6, (4) 1.0, (5) 1.2, and (6) 1.321; $V = 0$. In the curves $u_\zeta(\zeta) > 0$ everywhere.	33
2.5	Dependences (1) δ_{SCL} , (2) δ_0 , and (3) ζ_0 (a) and (1) $\varepsilon_{0,SCL}$ and (2) ε_0^0 (b) as functions of Ω . The lines denote the calculation involving the Lagrange method, and circles – the Euler one. $V = 0$	36
2.6	Plots of the minimum potential η_m (a) and its position ζ_m (b) for the PDs, relating to (1) <i>SCL</i> and (2) 0 points, vs Ω ; $V = 0$	39
2.7	The PDs, relating to (1) <i>SCL</i> ($\varepsilon_0 \approx 0.7185$) and (2) 0 ($\varepsilon_0 \approx 1.0$) points, for $\Omega = 1$; $V = 0$. The open circles mark positions of the potential minimum, closed circle shows the place where a velocity vanishes.	40
2.8	Plots of positions of the point where a velocity vanishes (curve 1) as well as the collector (2) and the potential minimum (3) positions vs Ω . $V = 0$	41
3.1	Curves $\varepsilon_0(\delta)$ drawn for various values of Ω : (1) $\Omega = 0$, (2) 0.3, (3) 0.6, (4) 1.0, (5) 1.2, and (6) 1.321; $V = 0$. In the curves $u_\zeta(\zeta) > 0$ everywhere.	48

3.2	The η, ε -diagram for $\Omega = 1.0$ and various values of δ : (1) $\delta = 0.85$, (2) 0.90, (3) $\delta_{SCL} = 0.947747$, (4) 1.00; $V = 0$. Open circle corresponds to an unstable steady state, closed circle – to an aperiodic stable one.	50
3.3	Growth rate γ vs gap δ for various values of Ω : (1) $\Omega = 0$, (2) 0.3, (3) 1.0, (4) 1.32; $V = 0$	54
3.4	(a) Imaginary part of the dispersion equation (3.22) vs ε_0 for the branch II of the steady state solutions at $\gamma = 0$; (b) the radicand of Eq. (3.29) vs ε_0 for the branch I of the steady state solutions. Positions of SCL and 0 point are marked. $\Omega = 1.0$. $V = 0$	55
3.5	Dispersion curves for branches I and II of steady state solutions: the solid curves correspond to branch I, and the dashed curves, to branch II. Curves A are aperiodic branches, and curves O are oscillatory branches. (a) Growth rate γ and (b) frequency ω . Positions of SCL and 0 point are marked. $\Omega = 0.3$. $V = 0$	56
3.6	Dispersion curves for branches I and II of steady state solutions: the solid curves correspond to branch I, and the dashed curves, to branch II. Curves A are aperiodic branches, and curves O are oscillatory branches. (a) Growth rate γ and (b) frequency ω . Positions of SCL and 0 point are marked. $\Omega = 1$. $V = 0$	58
4.1	Normalized potential $e\varphi/(mv_0^2)$ as a function of normalized space $\zeta = z/\lambda_D$ for various values of $\varepsilon_0 = eE_0\lambda_D/(mv_0^2)$: (1) $\varepsilon_0 = 0.6$ (no electrons are turned due to a magnetic field), (2) 1.0 and (3) 1.61 (a portion of the injected electrons is turned due to a magnetic field), and (4) 1.7321 (all electrons are turned due to a magnetic field). Dashed curve corresponds to $\varphi = p(z, \omega) = (e/2m)(\omega^2 z^2 - v_0^2)$; $\omega/\omega_0 = 1.0$; $U = 0$	63
4.2	The “ $\varepsilon_0 - \delta$ ” curves are drawn for various values of Ω : (1) $\Omega = 0$, (2) 1.0, (3) 1.35, (4) 1.5 and (5) 1.7; $V = 0$. Two regimes are only included: no electrons are turned by magnetic field, and all electrons are turned (marked by open circles).	66
4.3	Coefficient r vs ε_0 for $\Omega = 1.0$; $V = 0$	69
4.4	Velocity profile within the interelectrode gap drawn for different ε_0 values: Fig. (a): $\Omega = 1$; (1) $\varepsilon_0 = 1.20$, (2) 1.55, (3) 1.60, (4) 1.65, and (5) 1.664; Fig. (b): $\Omega = 1.35$; (1) $\varepsilon_0 = 1.10$, (2) 1.20, (3) 1.30, (4) 1.35, and (5) 1.375. $V = 0$	70
4.5	The “ $\varepsilon_0 - \delta$ ” curves are drawn for various values of Ω : (1) $\Omega = 0$, (2) 1.0, (3) 1.35, (4) 1.5, and (5) 1.7; $V = 0$. The regions with partial electron turning are included here. Dashed vertical lines corresponds to a dependence $\delta = 1/\Omega$	71

- 4.6 The dependence of the position of velocity minimum (curve 1), collector position (curve 2) and the position of potential minimum (curve 3) on ε_0 , for $\Omega = 1$ and $V = 0$. Closed circles refer to the bifurcation points. 72
- 4.7 Velocity profile within the interelectrode gap drawn for case of several turning-about points: (1) $\varepsilon_0 = 1.673499(r = 0.9003)$, (2) $\varepsilon_0 = 1.675$ – second turning-about point lies within the gap, (3) $\varepsilon_0 = 1.7027(r = 0.949697)$ – third turning-about point lies on the collector. $\Omega = 1, V = 0$ 73
- 4.8 The position of the *SCL* and *BF* points vs Ω : (1) δ_{SCL} , (2) δ_{BF} ; $V = 0$ 78
- 4.9 Fig. (a): Variation of δ_{max} (curve 1), δ_{min} (curve 2), and δ_{SCL} (curve 3) with Ω ; Fig. (b) coefficient r_1 vs Ω ; $V = 0$ 81
- 4.10 Fig. (a) r and (b) ε_0 vs δ . Vertical dashed line corresponds to position of the *SCL* point, dashed-dotted line is for δ_{max} , and horizontal solid line is for $r = 1.0$. $\Omega = 1.0, V = 0$ 83
- 5.1 Normalized potential $e\varphi/(2W_b)$ is plotted as a function of normalized space $\zeta = z/\lambda_D$ for various values of $\varepsilon_0 = eE_0\lambda_D/(2W_b)$: (1) $\varepsilon_0 = 0.72$ (no electrons are turned due to the magnetic field), (2) 0.9029 and (3) 1.0793 [for (2) and (3), there is a point within the diode gap in which the longitudinal velocity vanishes for the first time]. Dashed curve corresponds to $\varphi = p(z, \omega) = (mc^2/e) \left(\sqrt{1 + (\omega^2/c^2)z^2} - \gamma_0 \right)$; $\gamma_0 = 2$; $\omega/\omega_0 = 1.0$; $U = 0$ 92
- 5.2 Debye length λ_D vs V_b for $j_b = 1\text{kA/cm}^2$. The relativistic and non-relativistic Debye lengths are represented by the solid and dashed lines respectively [69]. 95
- 5.3 The $\varepsilon_0(\delta)$ curves are drawn for various values of γ_0 : (1) $\gamma_0 = 1$, (2) 2, (3) 10; $\Omega = 1, V = 0$. The regime where no electrons are turned by the magnetic field. 99
- 5.4 The dependencies (a) $\delta_{SCL}(\gamma_0)$ and (b) $\varepsilon_{0,SCL}(\gamma_0)$ are drawn for various values of Ω : (1) $\Omega = 0$, (2) 0.3 and (3) 1.0; $V = 0$ 101
- 5.5 The dependencies (a) $\delta(\gamma_0)$ and (b) $\varepsilon_0(\gamma_0)$ are shown for (1) “*SCL*”, (2) “0” and (3) “*BF*” points; $\Omega = 1, V = 0$ 102
- 5.6 The ε_0 vs r curves are drawn for various values of γ_0 : (1) $\gamma_0 = 1$, (2) 1.5, (3) 10; $\Omega = 1, V = 0$ 104
- 5.7 The $\varepsilon_0(\delta)$ curves are drawn for various values of γ_0 : (1) $\gamma_0 = 1$, (2) 1.5, (3) 10. $\Omega = 1, V = 0$. Solid circles correspond to the *SCL* points, hollow circles refer to the *BF* points and zero-points are marked by “0”. 105
- 5.8 The dependencies (a) $\varepsilon_0(\delta)$ and (b) $r(\delta)$ are plotted for $\gamma_0 = 1.5, \Omega = 1$ and $V = 0$ in the vicinity of $r \rightarrow 1$ 108

- 5.9 The dependencies (a) $\varepsilon_0(\delta)$ and (b) $r(\delta)$ are plotted in the vicinity of $r \rightarrow 1$, for a number of γ_0 values: (1) $\gamma_0 = 1$ (blue), (2) $\gamma_0 = 1.5$ (red), (3) $\gamma_0 = 2$ (green) and (4) $\gamma_0 = 3$ (magenta); $\Omega = 1$ and $V = 0$ 109
- 5.10 The profile of (a) velocity [$u_\zeta(\zeta)$] and (b) potential [$\eta(\zeta)$] for a number of γ_0 values: (1) $\gamma_0 = 1$ (blue), (2) $\gamma_0 = 2$ (red), (3) $\gamma_0 = 3$ (green) and (4) $\gamma_0 = 5$ (magenta); $r = 0.99$, $\Omega = 1$ and $V = 0$. The dashed curves in Fig. 10(b) refer to the corresponding η_c for each case. 110
- 6.1 (a), (b) Potential distribution and (c), (d) electron longitudinal velocity one within the inter-electrode space drawn for various values of Ω : (1) $\Omega = 0$, (2) 0.1, (3) 0.2, (4) 0.3, (5) 0.4 and (6) 0.806225; (a), (c) $\varepsilon_0 = 0.5$; (b), (d) $\varepsilon_0 = -0.5$; $\gamma = 1.1$ 122
- 6.2 Curves $\varepsilon_0(\delta)$ drawn for three values of γ and various values of Ω : (a) $\gamma = 0.9$; $\Omega = 0$ (curve 1), 0.1 (2), 0.12 (3), 0.15 (4), 0.3 (5), 0.5 (6), 0.8 (7) and 1.04 (8); (b) $\gamma = 1.0$; $\Omega = 0$ (curve 1), 0.1 (2), 0.14 (3), 0.18 (4), 0.3 (5), 0.5 (6), 0.75 (7) and 0.99 (8); (c) $\gamma = 1.1$; $\Omega = 0$ (curve 1), 0.05 (2), 0.09 (3), 0.1 (4), 0.15 (5), 0.2 (6), 0.3 (7), 0.4 (8), 0.5 (9) and 0.806225 (10). $V = 0$. In the curves, $u_\zeta(\zeta) > 0$ everywhere. 124
- 6.3 Dependencies of (a) $\delta_{SCL}(\Omega)$, (b) $\varepsilon_{0,SCL}(\Omega)$ and (c) $u_{\zeta,SCL}$ for various values of γ : (1) $\gamma = 0$, (2) 0.5, (3) 0.8, (4) 0.9, (5) 1.0, (6) 1.05, (7) 1.1, (8) 1.2 and (9) 1.25. $V = 0$ 126
- 6.4 Dependence $\Omega(\gamma)$ corresponding to $\varepsilon_{0,SCL} = 0$; $V = 0$ 128
- 6.5 Dependencies of (a) ζ_0 , (b) δ_0 , and (c) ε_0^0 for various values of γ : (1) $\gamma = 0$, (2) 0.1, (3) 0.5, (4) 1.0, (5) 1.5, (6) 1.9. The dashed line in Fig. (a) corresponds to $\varepsilon_0^0 = 0$. $V = 0$ 130
- 7.1 (a), (b) Potential distribution and (c), (d) electron longitudinal velocity profile within the inter-electrode space drawn for various values of ε_0 : (1) $\varepsilon_0 = 1.4$, (2) 0.8, (3) -1.1, (4) -1.1. Fig. (a), (c) correspond to $\Omega = 0$ with $r = 0.43$ on curve (1), 0 (2), 0 (3), 0.055 (4); Fig. (b), (d) – $\Omega = 0.1$ with $r = 0.435$ on curve (1), 0 (2), 0 (3), 0.06 (4). $\gamma = 0.9$. The real PDs terminate at points with $V = 0$. The dashed line corresponds to Eq. 10. 140

- 7.2 Curves $\varepsilon_0(\delta)$ drawn for three values of γ and various values of Ω : (a) $\gamma = 0.9$; $\Omega = 0$ (curve 1), 0.1 (2), 0.2 (3), 0.3 (4), 0.5 (5), 0.8 (6) and 1.0 (7); (b) $\gamma = 1.0$; $\Omega = 0$ (curve 1), 0.1 (2), 0.3 (3), 0.5 (4), 0.8 (5) and 0.99 (6); (c) $\gamma = 1.1$; $\Omega = 0$ (curve 1), 0.09 (2) 0.1 (3), 0.2 (4), 0.3 (5), 0.5 (6) and 0.9 (7). Open circles correspond to the *SCL* points, closed circles – to the *BF* points. 143
- 7.3 Dependencies of characteristic points (*SCL*, *BF* and 0-points) on the Bursian family $\varepsilon_0(\delta)$ for $\gamma = 0.9$ and $V = 0$; (a) $\delta(\Omega)$, (b) $\varepsilon_0(\Omega)$. Curve 1 corresponds to *SCL* point, 2 – 0-point, 3 – *BF* point. 146

Chapter 1

Introduction

An objective of this thesis is to contribute to the knowledge of nonlinear phenomena observed in the electron beam driven plasma diodes (like space charge limited flow, phase-transitions, aperiodic instabilities etc.) in the context of the nonlinear diode theory. A systematic theoretical study of the dynamics of the charge particles is presented for the planar plasma diodes. The methods to study the solutions defining the steady states of a plasma diode are solely based on the Eulerian and Lagrangian descriptions. Before going deep into the investigation, we present a brief historical overview on the past works as well as the motivation of studying a plasma diode in presence of a transverse magnetic field.

1.1 Brief Historical Overview

The space charge limited flow in a diodic system has attracted the attention since the beginning of the twentieth century. Many systems in physical science which are used in various technological purposes, such as, Q-machines [1, 2], thermionic converters [3, 4, 5], microwave generators [6, 7], electronic switches[8], low-pressure discharges and processing [9, 10], accelerators [11, 12], inertial confinement devices [13, 14, 15, 16], pinch reflex diodes for intense ion beam generation [17], xerographic technologies [18], semiconductor devices [19, 20, 21], ion diodes with inertial fusion [22, 23, 24], vacuum microelectronics [25], metal-semiconductor layered cathode [26, 27] etc., exhibit diodic behavior. In simplest form, each of the devices mentioned above, can be modeled as a planar diode. The space charge limit, which usually corresponds to the condition of the maximum allowable current in diode like systems, also restricts the optimum operation conditions in these devices. In the Refs. [12, 28, 29, 30, 31], the basic physics and applications of the space charge limit and virtual cathode are reviewed thoroughly. The existence of the limiting value of the current indicates a transition from a state with high current density to a state with negligible charge flow. Hence, it is crucial to study the impact of the space charge limit on the operation condition for such systems systems where diode like phenomena take place.

1.1.1 Basic structures of the Plasma Diodes

Due to its simplicity in basic structure, the particle transport in such a device, can be well approximated as a one-dimensional, ballistic and monoenergetic flow in a planar device. The descriptions of diodic systems by assuming such a planar

model was started from the beginning of the twentieth century [32, 33, 34, 35, 36, 37, 38, 39, 40]. It has attracted many researchers even in modern days, mainly due to its wide range of applicability in contemporary technologies [41, 42, 43].

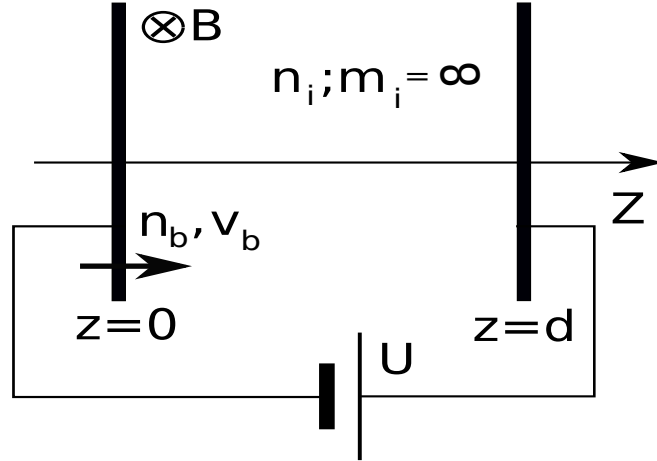


Figure 1.1: Schematic representation of a planar plasma diode. In case, there is any transverse magnetic field, the direction of it is shown by the cross mark.

A diodic system generally consists of two electrodes, where charge carriers are injected by the emitter plate and collected at the collector plate, contributing a net current through the overall circuit. Fig. 1 shows a schematic diagram of a planar diode model. An electron beam of density n_b and velocity v_b is injected into the diode region from the emitter electrode at $z=0$, where it is kept at zero potential. If no reflection occurs, all electrons reach the collector surface, at $z = d$. A bias voltage U is applied across the diode region. Electrons which are reflected by the internal space charge potential return to the emitter electrode and are totally absorbed. The diode region can be assumed to be vacuum or to be occupied uniformly by infinitely massive ions of constant density n_i . The ratio, $\gamma = n_i/n_b$ determines the level of the neutralization. Depending on the operation conditions of the diodes, the neutralization factor γ can take any values. For example, in Bursian diodes, $\gamma = 0$, i.e., background ions are totally absent [35] and it is totally

non-neutral system. On the other hand, the condition of charge neutrality ($\gamma = 1$) appears in classical Pierce diodes [44]. For non-neutral Pierce diodes, γ can take any possible values. As we are focussing mainly on the fast electron dynamics, the ions can be treated as immobile. However, the necessary background of ions with homogeneous distribution can also be provided if ions are injected into the diode region with sufficiently large velocity perpendicular to the direction of the electron motion. In this situation, the ions will leave the diode region without any change in the density distribution in both longitudinal and transverse direction.

The adjective ballistic signifies that the charges flow within the diode gap without collisions, i.e. the mean free path of the charge carriers is larger enough than the diode length. This is a practical situation which occurs very often in diodic devices like Q-machines [1, 2], thermionic energy converters [3, 4], cold electron beam evaporation diode (or triode) systems etc [21]. Such a regime of a plasma diode is referred as the Knudsen regime.

If we consider a planar diode where a monoenergetic beam of electrons is injected by the emitter surface, the potential distribution $[\phi(z)]$ forms a minimum within the inter-electrode region as a result of the space charge effects. This potential minimum (say, ϕ_m) serves as a barrier to the electron flow. As long as the kinetic energy of the injected electrons at the emitter is greater than the potential barrier height ($|e\phi_m|$), the emitted electrons can cross the barrier and reach to the collector surface. However, if for certain values of the relevant parameters, the value of the potential barrier height ($|e\eta_m|$) becomes equal to the kinetic energy of an emitted electron, the longitudinal velocity of the electron vanishes at the position of potential minima. This is the situation when potential distribution

corresponds to the virtual cathode (VC). The steady-state solutions with a virtual cathode arises when the potential minimum reaches a value for which longitudinal velocities of the emitted electrons become zero for the first time. If the emitted electrons are purely monoenergetic, i.e., if the velocity distribution function of the emitted electron beam is a δ -function, all the electrons are reflected back by the potential barrier (virtual cathode). But in reality, the electrons are always injected from the emitter with a small velocity spread. So, in practical situations, there will be always a few number of electrons which can overcome the potential barrier. This is what happens in case of partial electron reflection.

The current-voltage characteristic curves of the diodic systems show a non-Ohmic nature as a result of the space-charge accumulation. A current limitation is also observed in these devices, whenever one of the following quantities exceeds the critical value, the particle density, the current density and the gap distance. This is space-charge-limit [32, 33, 34, 35, 45, 46, 47, 48]. In this situation, an aperiodic instability develops in the system which destabilizes the diode. At this critical point, the diode current reaches its maximum value and once this critical point is crossed the system switches into a state with very negligible charge flow. It happens due to the formation of the virtual cathode which reflects the electrons partially or totally, depending on the parameters involved. The reason behind such complex dynamical pattern in such devices lies in the boundary conditions. For fixed boundary conditions, the flow characteristics at the emitter surface are generally different from the collector end. In contrast to the periodic systems the flow at the injection point has therefore no information about the actual status of the diode. The linear stability analysis shows that, in case of time-dependent

behavior, to meet the fixed boundary conditions, a small perturbation can lead to the aperiodic instability.

The ballistic nature of the flow also provides a window to analyze the diode phenomena in Lagrangian picture, where the dynamics is described in a reference system co-moving with a fluid element. In some situations, the Lagrangian description is found to be more useful than Eulerian description, as it reduces analytical complexity. The Lagrangian description also allows us to investigate the aperiodic and oscillatory instabilities in the case of nonreflective equilibria.

Based on the different working conditions, plasma diodes can be classified into few categories.

1.1.2 Bursian diode (pure electron diode)

A Bursian diode is non-neutral vacuum diode, where only electrons contribute in charge transport between the electrodes. In the first quarter of 20-th century, the study on the collective nature of the charge particles was initiated by Child and Langmuir [32, 33]. Assuming zero electron velocity at the emitter, they studied a vacuum diode and showed that, in steady state, the current transported between two electrodes maintains a specific relation with the applied potential and inter-electrode gap distance. It is known as the famous “Child-Langmuir” law. Almost in the same time, the Russian scientists Bursian and Pavlov studied a short circuited vacuum diode, where a monoenergetic electron beam of electrons is injected by the emitter and transported toward the collector plate [35]. They explained for the first time that, if there is a velocity spread in the emitted electron beam profile, at some certain condition, injected electrons can be reflected back to the emitter partially or totally. Depending upon the values of external parameters, they reported

three distinct types of solutions in steady state. The solutions are as follows: the stable solution without electron reflection, the unstable solution without electron reflection and the stable solution with partial electron reflection for which potential distribution corresponds to virtual cathode (VC). It has been shown that, if the diode gap value exceeds a certain critical value, an aperiodic instability appears in the system. As a result of it, the regime without electron reflection disappears and the system ends up with a state of partial electron reflection. So, there is a threshold value of the current that can pass through the vacuum diode in steady state. It is known as “Bursian threshold” and the phenomena involved behind it, is called as “Bursian instability”. This threshold situation, where the diode current reaches to its maximum value is called “space-charge-limit”. Later on, this kind of devices are named as “Bursian diode”. Gill studied a vacuum diode experimentally with a small velocity spread in the injected electron beam and confirmed the existence of the threshold value of the diode current [49]. He reported that collector current initially grew with the increasing value of the emitter current and after reaching a maximum value the collector current dropped down sharply. The dependence of the collector current on the emitter current was observed to follow a hysteresis pattern. Further experiment was carried out by a number of researchers [50, 51, 52, 53, 54]. Fay *et. al.* [55] studied the stationary states of a vacuum diode by considering cold electron flow and variable collector potential. They obtained the analytical expressions for the potential distributions (PD) and current-voltage relationships for the cases of no electron reflections, partial electron reflections and total electron reflections. They introduced the notations, “normal C-flow” and “C-overlap flow” for the respective steady state solutions when no electrons are

reflected and when a fraction of the emitted electrons is reflected. These different types of solutions were presented through the different regions of current-voltage ($I - V$) characteristic curves. The authors also pointed out that for specific values of the parameters, more than one type of PD may exist. Llewellyn [56] first introduced a Lagrangian-type treatment for the Bursian diodes where solutions were presented in terms of the transit time of the electrons. This idea was later used by Lomax [57] to study the aperiodic instabilities of the steady states. For a fixed value of the dimensionless diode gap, different types of solutions were identified depending on the transit times of the emitted electrons. These were as follows: stable solutions without reflections, unstable solutions without reflection and the solutions with electron reflections. Nezlin [58], in his study on the experimental conditions of the beam propagation in rarefied plasmas, discussed the development of various instabilities including the Bursian instability. Coutsiias [59, 60] used Lagrangian formalism to analyze the formation of the virtual cathode. He also investigated the effect of thermal spread of the electron beam on the space charge limit for a short-circuited vacuum diode and found that the current at space charge limit decreases with increasing beam temperature. Later Alyeshin and Kuz'menkov [61] showed that with the increasing ratio of the thermal velocity and beam velocity at the emitter, the region narrows where two kinds of solutions coexist with each other. When the value exceeds a critical value, only one type of solution remains. Birdsall and Bridges [62] studied the time-dependent states of Bursian diode with the help of particle-in-cell (PIC) code.

Kuznetsov *et. al.* studied the Bursian diode both analytically and numerically

with arbitrary external voltage and discussed the solutions in detail for the situations when electrons do not suffer reflection and when they are partially reflected [63, 64, 65, 66, 67]. In their works, all of the steady state solutions were visualized through the $\varepsilon_0 - \delta$ parametric plot for a certain value of applied voltage where ε_0 and δ are the electric field strength at emitter and diode gap respectively. For a particular value of external voltage, each point on the “ $\varepsilon_0 - \delta$ ”-curve denotes a steady state. They showed that the curve in $\varepsilon_0 - \delta$ parametric space consists of three distinct regions where each region represents the solutions of a particular type in steady state. Each curve also contains a right bifurcation point which corresponds to the state with maximum diode current. This point is named as “SCL”. There is also a “zero-point” (or “0”-point) in this curve, for which an electron of the injected beam loses its velocity within inter-electrode region for the first time. The point “SCL” and “zero-point” define different regions of the “ $\varepsilon_0 - \delta$ ”-curve. Following the convention introduced by Fay *et. al.* [55], these regions are termed as : “C normal branch” ($\varepsilon_0 \leq \varepsilon_{0,SCL}$), “C overlap branch” ($\varepsilon_{0,SCL} < \varepsilon_0 \leq \varepsilon_{0,0}$) and the branch corresponding to partial electron reflection which is also called “virtual cathode branch” ($\varepsilon_0 > \varepsilon_{0,0}$). The symbols $\varepsilon_{0,SCL}$ and $\varepsilon_{0,0}$ refer to the values of ε_0 at SCL and “zero-point”, respectively. In order to explain the stability properties of the steady state solutions, “collector potential vs emitter field strength” diagram was utilized and a relevant dispersion relation was derived employing first order perturbation theory. It is shown that for every “ $\varepsilon_0 - \delta$ ”-curve, C overlap branch is unstable and the other two branches are stable under small aperiodic perturbation [68, 69]. With the help of “collector potential vs emitter field strength” plot, it was also discussed that the solutions which belongs to virtual cathode branch, are

stable with respect to the small perturbation. The stability of the steady states corresponding to virtual cathode branch was also analyzed numerically using PIC codes [70, 71]. Finally, Kolinsky and Schamel [72] studied the different states of a Bursian diode with an arbitrary applied voltage with the help of Lagrangian formalism. They labeled the solutions with no reflection as type-I flow, and the other one with partial reflection as type-II flow. A dispersion relation associated with the type-I flow was obtained which coincides with that of Lomax [57]. They also showed that the solutions corresponding to the branches of type-II flow (the one called C-overlap in the notation of Fay *et. al.* [55]) are unstable with respect to the aperiodic perturbations. They also presented an analytical expressions for various equilibrium quantities, such as the splitting rates in case of reflection, the transmitted current etc.

1.1.3 Pierce diode

1.1.3.1 Neutral Pierce diodes:

Next we discuss another kind of plasma diode where the monoenergetic electron beam leaves the emitter and is transported to the collector through the background of uniformly distributed immobile ions. These types of diodes are called ‘‘Pierce diode’’. The term was first used by Kuhn [73, 74, 75]. In classical Pierce diode, the emitted electrons are also completely neutralized by the uniform immobile ions ($\gamma = 1$). Pierce [44], in his classical paper, studied theoretically a planar short-circuited diode with a cold electron flow moving through the uniform background of infinitely massive ions which neutralized altogether the electronic space charge. He identified that a limiting value of the diode current also exists for this kind of systems in the steady state. He also pointed out that this limiting value of the

current is greater than the Bursian threshold value of current by a factor of 5.6. He explained that the existence of this current limit arises due to the development of the electron aperiodic instability which is also correlated with the feedback mechanism between the electrodes through the external circuit. It is named as “Pierce Instability” [73, 74, 76]. Pierce also derived the dispersion relation and evaluated the maximum growth rate. Nezlin and Solntzev [77] studied a Pierce diode experimentally to determine the threshold point of Pierce instability.

The stability properties of the stationary bounded plasma states were analyzed by Kuznetsov and Ender [78] for an arbitrary spatial distribution of infinitely heavy ions and for a nonzero thermal spread of the electron beam. A differential equation for the perturbed potential was derived and solved analytically for two cases. Firstly, they assumed emitted electrons to be monoenergetic. Secondly, the distribution function of the emitted electrons was considered to be waterbag-like. Boundaries of the aperiodic instability in the η_c, δ -plane were plotted for these two cases, where η_c is the collector potential and δ is the dimensionless gap distance. They found that the perturbed potential profile can be obtained in terms of the Bessel and Neumann functions. Later, the analysis of the stability properties of the Pierce diode was extended by many authors [79, 80, 81, 82]. Godfrey [83] investigated the stability criteria of the short circuited Pierce diode without electron reflection at equilibrium. With the help of an integral formalism, they derived a dispersion relation for linear perturbations, involving aperiodic as well as oscillatory solutions. In this study, the boundary effects to the electron dynamics were also taken into account and the bifurcations were detected for $\delta \approx 2.9\pi$. An analytic treatment of weak nonlinear oscillations in terms of three-harmonic

approximation was presented by Hörhager and Kuhn for Pierce diodes [84]. And finally Ender *et al.* [85] used the Pierce diode as a basic model for a Knudsen diode with surface ionization (abbreviated by KDSI). The effect of the finite thermal spread was incorporated. A linear eigenmode theory of the KDSI was developed and the profiles of the eigenmodes for the Pierce diode and the KDSI were shown to be similar. Furthermore, the nonuniform, time-independent potential distributions were developed corresponding to the situations of no electron reflection, electron reflection and ion distribution corresponding to the ground states.

1.1.3.2 Non-neutral Pierce diode:

In case of non-neutralized Pierce diodes, the neutralization parameter (γ) which is the ratio of background ion density to injected electron density, can take any value other than ‘unity’. The steady states of non-neutralized Pierce diodes ($\gamma_0 \neq 1$) were studied and the stability properties were analyzed by many authors [86, 87]. The case of electron reflection where the potential distributions (PD) corresponds to the virtual cathode (VC), was also explored. Vybornov [88] studied in detail the stationary states of the planar, short-circuited, non-neutralized Pierce diode with infinitely massive ions and for different γ values in the regime where electron reflection does not occur. He demonstrated different kind of solutions through the $\varepsilon_0 - \delta$ -plots, for a number of γ values. He also derived the dispersion relation to evaluate the aperiodic stability properties for various γ values. He concluded that for fixed γ in the range $0 < \gamma < 1$, the steady states are aperiodically stable for any value of diode current. Later, the Lagrangian approach was used by Chen and Lindsay [89] to investigate the short-circuited non-neutral Pierce diode. They reported the existence of oscillatory solutions without reflection and showed the

regions of unstable, stable, oscillatory and chaotic solutions in the (γ, δ) -plane.

Yuan [90] and Kolyshkin [91] considered the effect of the finite ion mass and the electron thermal spread on the aperiodic instability of a neutralized electron beam in a planar diode. They derived a dispersion relation and plotted the branches of the aperiodic Pierce instability. It was concluded that the finite ion mass can increase the threshold value of the current at the transition point. An aperiodic instability can only appear if the electron flow's Mach number "M" exceeds unity. The growth rate and the threshold current are found to be reduced from their values in the cold beam case.

1.1.4 Further progress in this field

The effect of the finite velocity of the background ions on the plasma diodes was investigated using the Lagrangian formulation by several authors [92, 93, 94, 95]. When the stability criteria of such systems were analyzed, few new growing modes and damped oscillatory modes were observed, which in the limit $v_i \rightarrow 0$ become Pierce-Buneman modes and undamped ion plasma oscillations, respectively. Kolin-sky and Schamel [95] also showed that the counter injections of ions can introduce new unstable oscillatory branches which can destabilize the diode for any values of the Pierce parameter (δ) [94]. Kolinsky *et. al.* [96] tried to study theoretically the mechanism of the Pierce-type hydrodynamic instability which is often found experimentally in the thermionic discharges at low pressure. The influence of the ion dynamics, collisions with neutrals and the sheath capacitance were taken into account and the general Lagrangian description [93, 94, 95] was employed. They asserted that few ion-neutral collisions can resist the coupling between the electron and ion dynamics on the electronic time scale. As a result, the growth of

the oscillatory Pierce-Buneman modes is prevented. They also revealed the nature of the “Hopf-bifurcation” at the instability threshold which is responsible for the nonlinear relaxation oscillations. The transient behavior during the rise of the instability is qualitatively described with the help of hydrodynamic model.

The classical works of Child, Langmuir and Schottky were extended further to the quantum regime by Lau et. al. [97, 98]. The limiting value of the diode current was also reinvestigated with an external transverse magnetic field [99] as well as for a diode where electrons are emitted in a self-regulating way [100]. The features of the diodic systems were also explored for the multidimensional geometry [101, 103]. The analysis on the plasma diodes was also executed for the time-dependent states by several authors [104, 105, 106]. Kuznetsov and Ender developed a numerical code (EK code) to study the time-dependent processes in plasma diodes [107, 108].

To utilize the interesting properties of the space charge limited flow for different purposes, the plasma diodes were diagnosed extensively in recent years [109, 110, 111, 112, 113, 114]. In these works, a number of parameters (e.g., applied voltage, temperature, injection velocity of electrons etc.) are identified to control the space charge current in diodic systems.

1.2 Applications of the “Bursian-Pierce” Instabilities

In the new generation of Thermionic Converters (TIC), heat energy is converted into electrical energy when the emitter is heated up to a high temperature ($\gtrsim 2000$ K) to vaporize electrons. The electrons move across a small electrode gap and are collected by the cooler collector surface. This kind of TIC operates in collisionless (Knudsen) regime with surface ionization. At high temperatures, the

efficiency of the Knudsen TIC becomes very close to that of the Carnot cycle. Thus, it is the most promising converter of thermal to electrical energy [115].

In the TIC, a Pierce type instability develops when operation point is switched from the retarding potential region of the I-V-curve to the saturation current region. As a result, a virtual cathode appears within diode gap and current is diminished. This effect was utilized to generate directly an alternating current with the help of a TIC [116, 117]. As a basic model for the thermionic energy converter (TIC), Gverdtziteli *et. al.* [118] studied experimentally the nonlinear current oscillations in a Knudsen diode with surface ionization (KDSI) and measured the time to excite virtual cathode which in turn triggers the course of the nonlinear oscillations at space charge limit. They also asserted that the occurrence of the current limitation is closely related to the Pierce instability. Babanin *et. al.* [119] experimentally determined the threshold condition of the large amplitude oscillations of a KDSI (TIC) for a number of values of the neutralization parameter.

The double-layer dynamics and low-frequency oscillations of diode current were studied by Iizuka *et. al.* [120] in a Q-machine which is effectively a KDSI. They have measured the spatial potential distributions at different times which was useful to distinguish a slow and a fast stage of the process which were developed due to a Pierce-type instability.

As it was discussed previously, as soon as the beam current exceeds the limiting value, the aperiodic instability is developed. As a result, virtual cathode is formed and it begins to oscillate. The electron beam interacts with the time dependent electric field generated between the emitter and the VC. In this process, the beam energy is converted into microwave radiation. Devices operating on the basis of

the VC oscillations are called vircators [121, 122].

A successful application of the SCL current was reported by Modukuru *et. al.* where they showed that the numerically predicted onset of current self-quenching in a metal/CdS/LaS cold cathode in the presence of inelastic scattering in the CdS layer can be explained by the SCL-theory [123].

A model for fast electron switches based on the event of state transition between high and low current branches was also proposed. Here external voltage ensures the rapid transition of states by controlling the space charge limit [107, 124].

1.3 Motivation to study the effect of the transverse magnetic field

The advancement in modern deep space research actualized the need of electrical energy sources of hundreds KW to tens MW power with an efficiency more than 30% . These criteria are well satisfied with the Thermionic Energy Converter (TIC) of new generation. To achieve such high efficiency, the required collector temperature is around 1300-1500 K. The device operates in a collisionless (Knudsen) regime with surface ionization. To decrease the relative amount of power loss (due to the radiation) with respect to the electrical power yield, the temperature of the emitter should be high. As a matter of fact, the efficiency of high-temperature TIC can achieve the maximum limit which is very close to the efficiency of a Carnot cycle. For higher emitter temperature, the optimum temperature of the collector also becomes higher. Theoretical studies suggest that, with an emitter temperature of 2600K and collector temperature of 1500K, the specific power and the efficiency of the TIC can be achieved up to $50\text{W}/\text{cm}^2$ and 30%, respectively [115].

The diodic devices like high-temperature TIC [125, 126, 127], high power microwave sources (viractors) [128, 129, 130], etc. yield a very high current density. High injection velocity also occurs in case of ferroelectric emission and field induced emission from plasma cathodes [131, 132]. As a result of it, a strong inherent magnetic field generates within the inter-electrode gap. It is generally transversal to the electron motion. This field is strong enough to reorient partially the flow of the emitted electrons in reverse direction reducing the net diode current. Development of the virtual cathode and nonlinear oscillation is also common for a TIC which operates in the Knudsen regime [5, 118, 120, 133]. It was reported that the presence of strong magnetic field deviates the electron distribution function from the beam like character and helps in quenching the instabilities and oscillations. In the results [5, 118], it was shown that, with an increase in the external transverse magnetic field, first, oscillation amplitude decreases, then, ultimately these oscillations are suppressed. Thus, the investigation of the effect of the transverse magnetic field on the development of instability and non-linear oscillations in the Knudsen diodes are crucial for diodic systems. In order to check the effect of such a transverse magnetic field on the diode features, throughout this thesis, we shall consider a planar model for the plasma diode where an external magnetic field is applied along the transverse direction. We shall also assume that the electron beam current has little influences on this field, but the external magnetic field can affect the beam profoundly. Such a model will allow us to obtain the analytical results for the diode with an electron beam.

1.4 Outline of the thesis

The outline of this thesis is briefly described below:

In chapter-II, the analysis on the steady-states of a planar vacuum diode driven by a cold electron beam (the Bursian diode) under an external transverse magnetic field is presented. The analysis is performed up to the regime when the longitudinal velocity of an electron becomes zero within the inter-electrode gap for the first time. Solutions are represented through the different branches of “emitter electric field vs diode gap” diagram. It is shown that the transverse magnetic field modifies the “space-charge-limit” significantly.

In chapter-III, we have performed a stability analysis of the steady-state solutions which have been presented in the chapter-II. For this purpose we have used the Lagrangian description. With the help of a perturbative approach, a dispersion relation has been derived to study the effect of the transverse magnetic field on the stable and unstable states.

Chapter-IV covers the analysis on the Bursian diode for the situation when the emitted electrons suffer partial or total reflection in the presence of a transverse magnetic field. It is shown that an extra branch of solutions appears in the “emitter electric field vs diode gap” diagram to represent the time-independent states corresponding to the case of electron reflection. The dependencies of the bifurcation points on the external magnetic field have also been studied.

In chapter-V, we have extended our study on the steady state solutions of Bursian diode into the relativistic regime taking into account a constant magnetic field along transverse direction.

Chapter-VI is devoted to investigate a generalized Pierce diode in the presence of an external magnetic field applied along the perpendicular direction. A new family of steady states have been found along with the Bursian ones. It have been observed that the non-Bursian solutions are very sensitive to the magnetic field and disappear when the strength of the magnetic field crosses a critical value.

Chapter-VII extends the investigation of the steady states of the non-neutral Pierce diode to the regime where a portion of the emitted electrons are reflected back to the emitter due to the presence of the uniform magnetic field in transverse direction.

In chapter-VIII, a summary of the results and discussions made in this doctoral research work is presented. The problems remain unsolved are also discussed point wise which could be interesting to pursue further.

Chapter 2

Effect of transverse magnetic field on the steady-state solutions of a Bursian diode

In chapter one, we have presented our analysis on the steady-states of a planar vacuum diode driven by a cold monoenergetic electron beam (the Bursian diode) under an external transverse magnetic field. The analysis covers the regime of no electron reflection only. For fixed values of the diode length, the applied voltage, and the magnetic field strength, the solutions are evaluated using emitter electric field as a characteristic function.

2.1 Introduction

A TIC in its simplest form can be modeled by a Bursian diode. In the Bursian diode, a mono-energetic (nearly) beam of electrons enters from the emitter and travels within the inter-electrode space under the self-consistent electric field [35, 67, 69]. For a fixed value of the applied potential (U), the steady state solutions can be imaged as a continuous S -curve in the “electric field near emitter vs diode gap”- parametric space. For any U , different regions of these curves represent steady state solutions of different types. One of the regions represents the solutions which correspond to the case where the particle flux at the collector is always lesser than the same at the emitter. This is the solution with a virtual cathode (VC) [134, 135]. The right boundary of each curve refers to the situation when diode current can reach its maximum value (space charge limit). In literature, this maximum value of the current is denoted by the term SCL -current (Space Charge Limited current). The presence of such critical current value in diodic systems is utilized to develop fast electronic switches [136, 137]. On the other side, an inherent non-linear oscillation arises in the Bursian diode once virtual cathode is formed [66, 138]. The transient processes between an open state of diode and a state with virtual cathode are related with the development of the Bursian-Pierce instability [136].

A number of theoretical works [139, 140, 141, 142, 143, 144, 145, 146] dealt with the effect of the magnetic field on the Knudsen TIC parameters. In references [144, 145], the velocity distributions (DF) of the emitted electrons were assumed as the superposition of a large number of separate groups. The particles of each group have the velocity in a narrow region from v_0 to $v_0 + \Delta v_0$. These are named as

the beams. The formulas of particle trajectories were deduced, and contributions from each separate beam to the beam density were determined. An analytical expression was obtained for the beam density at any point of the diode gap.

In this chapter, we investigate how the space charge limit and other characteristic points of a planar vacuum diode get modified due to the presence of the magnetic field. Our analysis is limited up to the regime when longitudinal component of electron velocity vanishes for the first time.

2.2 The electron dynamics

We consider two planar electrodes of infinite transversal extent which are placed at a distance d from each other. Across them, a potential difference U is applied. The z -axis is directed perpendicular to the emitter surface ($z = 0$). The external magnetic field is uniform and parallel to the emitter surface. A non-relativistic monoenergetic electron beam is supplied by the emitter with density n_0 and injection velocity v_0 perpendicular to the emitter surface with no proper magnetic field. The electrons move without collisions under self-consistent electric field and external magnetic field. They are absorbed either at the collector or at the emitter when they are turned around by the magnetic field. In presence of the transverse magnetic field, electrons move on the $\{z, x\}$ plane perpendicular to this field and have two components of a velocity: v_z and v_x . The electric field is conservative and can be calculated from the scalar potential ϕ which depends only on z -coordinate. This planar model will be adopted throughout the analysis of this thesis.

To explore the time-independent states, first, we study the motion of an electron and then find the velocity distribution $\vec{v}(z)$ within the inter-electrode gap. In

next step, we obtain a second differential equation for the potential profile $[\varphi(z)]$ utilizing the basic equations. Electrons move on $\{z, x\}$ plane perpendicular to the direction of the applied magnetic field. Their velocity \vec{v} obeys the equation

$$\vec{v} \cdot \nabla \vec{v} = -\frac{e}{m} \left(\vec{E} + \vec{v} \times \vec{B} \right). \quad (2.1)$$

Taking the z -and x -components of the above equation and using $E(z) = -d\varphi(z)/dz$, we obtain

$$v_z \frac{dv_z}{dz} = \frac{e}{m} \frac{d\varphi}{dz} - \omega v_x, \quad v_z \frac{dv_x}{dz} = \omega v_z. \quad (2.2)$$

In Eq. (2.2), Larmor frequency ω and radius λ_L are defined as

$$\omega = \frac{eB}{m} = \left(\frac{2e}{m} \right) \frac{V_0^{1/2}}{\lambda_L} [s^{-1}] \quad \text{and} \quad \lambda_L = \frac{mv_0}{eB} \approx 0.3372 \cdot 10^{-3} \frac{V_0^{1/2}}{B} [cm]$$

respectively. Here, the beam accelerating voltage $V_0 = W_0/e = mv_0^2/(2e)$ is in Volts and the magnetic field B is in Teslas; e and m represent the charge and mass of an electron. Eqs. (2.2) are also supplemented by the following conditions at the emitter:

$$v_z(0) = v_z^0 = v_0, \quad v_x(0) = v_x^0 = 0. \quad (2.3)$$

From the second equation of the system of equations (2.2) and the second boundary condition of Eq. (2.3) we have

$$v_x(z) = \omega z. \quad (2.4)$$

Eq.(2.4) indicates that v_x increases linearly when an electron moves away from the emitter. Now substituting the expression of v_x in the first equation of Eqs. (2.2) and integrating we obtain

$$(m/2)v_z^2(z) - 2e\varphi(z) + (m/2)\omega^2 z^2 = (m/2)v_0^2. \quad (2.5)$$

Here the boundary conditions at the emitter for the z -component of the electron velocity [Eq. (2.3)] and for the potential [$\varphi(0) = 0$] were used. Eq. (2.5) is the energy conservation law for the electrons moving in a self-consistent electric field and under the transverse external magnetic field. The presence of the term due to the magnetic field adds some features in the distributions of the electron velocity and density within the inter-electrode gap. The magnetic field converts a portion of the longitudinal electron energy into transverse one. As a result, the longitudinal electron energy diminishes and the potential barrier height for electrons turns out to be lower than initial energy of the electrons. Additionally, due to the magnetic field, the electrons can be turned back even at a point where $\varphi(z) > 0$.

From Eq. (2.5) we obtain

$$v_z(z) = [v_0^2 + 2(e/m)\varphi(z) - \omega^2 z^2]^{1/2}. \quad (2.6)$$

One can see that the velocity v_z does not depend on the sign of B as the square of the magnetic field enters in Eq. (2.6). In the absence of the magnetic field, the electron velocity vanishes within the inter-electrode region of the Bursian diode when the potential barrier height becomes equal to the electron energy at the emitter, and it happens at the position of the virtual cathode. In this condition, the emitted electrons are completely reflected by the potential barrier and they are sent back to the emitter, provided that the injected beam is purely mono-energetic. When there is an external magnetic field along the transverse direction, the nonnegativity condition of the radicand in (2.6) demands that, PDs $\varphi(z)$ should be confined within a region which is limited by a square parabola $p(z; \omega)$ (Fig. 2.1):

$$\varphi(z) \geq p(z; \omega) \equiv (m/2e) (\omega^2 z^2 - v_0^2). \quad (2.7)$$

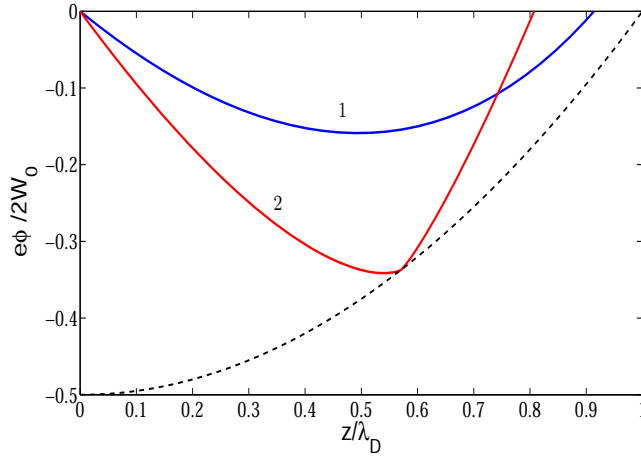


Figure 2.1: Normalized potential $e\varphi/(mv_0^2)$ as a function of normalized space z/λ_D for two $\varepsilon_0 = eE_0\lambda_D/(mv_0^2)$ values: (1) $\varepsilon_0 = 0.6$ and (2) 1.0. Dashed curve corresponds to $\varphi = p(z, \omega) = (e/2m)(\omega^2 z^2 - v_0^2)$; $\omega/\omega_0 = 1.0$; $U = 0$.

Equality sign in (2.7), i. e. the condition

$$mv_0^2/2 + e\varphi(z_H) = m\omega^2(z_H)^2/2 \quad (2.8)$$

takes place at a point where the z -component of the electron velocity vanishes and the electron is turned around by the magnetic field. For the Bursian diode without magnetic field, the turning of electrons happens at the position of the potential minimum. But in the presence of the transverse magnetic field, the event of electron turning can occur at the position which may not be the position of potential minimum. The problem is solved by two methods: with the Euler and the Lagrange formulation.

2.3 Steady-state solutions. The Euler method

In this section, we study the features of the steady-states in terms of the Eulerian variables. We set a value for the potential difference U between the electrodes. For a given value of the electric field strength at the emitter (E_0), we calculate

the velocity and electron densities, as well as the potential profile within the inter-electrode gap. The process starts from the emitter, and terminates at the moment when the value of the potential turns out to be equal to U . We take the relevant z-coordinate as the magnitude of the interelectrode distance d . Increasing E_0 gradually, we build up the dependence of E_0 on d .

We derive a differential equation for the potential and it is solved using a numerical approach with proper boundary conditions. For time-independent case, it is sufficient to use the continuity equation, the relation between the velocity and the potential [Eq. (2.6)], and the Poisson's equation. The analysis presented in this chapter is limited up to the condition when the longitudinal velocity of an emitted electron vanishes for the first time within the diode region. When there is no electron turning, i. e. the condition (2.8) does not hold anywhere, the continuity equation gives

$$n(z)v_z(z) = n_0v_0. \quad (2.9)$$

Substituting $n(z)$ from the Poisson's equation and using the relationships (2.6) and (2.9), we obtain a nonlinear differential equation for the electric potential

$$\frac{d^2\varphi}{dz^2} = \frac{e}{\epsilon_0} \frac{n_0v_0}{[v_0^2 + 2(e/m)\varphi - \omega^2z^2]^{1/2}}. \quad (2.10)$$

Next, we introduce the dimensionless quantities by using the kinetic energy of electrons at the emitter W_0 and the Debye length λ_D [58] as the basic units for the energy and length respectively

$$\lambda_D = \left[\frac{2\epsilon_0 W_0}{e^2 n_0} \right]^{1/2} \approx 0.3238 \cdot 10^{-2} \frac{V_0^{3/4}}{J_0^{1/2}} [cm],$$

$$W_0 = mv_0^2/2. \quad (2.11)$$

Here, the beam current density $J_0 = en_0v_0$ and the accelerating voltage $V_0 = W_0/e$ are taken in Amperes per square cm and Volts, respectively; the free-space permittivity $\epsilon_0 \approx 8.854 \cdot 10^{-12} C^2/Nm^2$. Then, for the dimensionless coordinate, time, velocity, potential and electric field strength we take $\zeta = z/\lambda_D$, $\tau = t\omega_0$, $u = v/v_0$, $\eta = e\varphi/(2W_0)$, $\varepsilon = eE\lambda_D/(2W_0)$; here $\omega_0 = v_0/\lambda_D$ is the plasma frequency. The dimensionless inter-electrode gap and the applied voltage between the electrodes are denoted by δ and V respectively.

Now, the equation (2.10) takes the form

$$\frac{d^2\eta}{d\zeta^2} = [1 + 2\eta - \Omega^2\zeta^2]^{-1/2}. \quad (2.12)$$

Here, the dimensionless quantity Ω is the Larmor's frequency which is written in the unit of the characteristic frequency ω_0 :

$$\Omega = \omega/\omega_0 = \lambda_D/\lambda_L \approx 9.603 V_0^{1/4} J_0^{-1/2} B. \quad (2.13)$$

In Eq.(2.13), V_0 and J_0 are taken in Volts and A/cm², and B in Teslas. The boundary conditions for (2.12) are

$$\eta(0) = 0, \quad \eta(\delta) = V. \quad (2.14)$$

Now we analyze the potential distribution (PD) in detail, i.e. we solve the Eq. (2.12) with B.C. (2.14). A diode PD is a single minimum function. We denote the value of the potential at the point of minimum (at $\zeta = \zeta_m$) by η_m . We take a certain electric field strength $\varepsilon_0 = \tilde{\varepsilon}_0$ at the emitter, and integrate the equation (2.12) from the emitter ($\zeta = 0$) towards the point of the minimum. The position and the value of the potential minimum (ζ_m, η_m) are obtained under the condition of zero electric field strength at this point. Further, we integrate Eq. (2.12) from a

point ζ_m toward the collector with the boundary conditions

$$\eta(\zeta_m) = \eta_m, \quad d\eta/d\zeta(\zeta_m) = 0. \quad (2.15)$$

The integration terminates at the point ζ where the potential becomes equal to V . This is the value of the collector voltage at the location δ .

While integrating Eq. (2.12), we use an approximation mode as follows. First we take a value of the potential at minimum (η_m) for the chosen value of ε_0 . In the region between the emitter and the location of the potential minimum, we do not take a coordinate frame, but that of a potential: $\eta_k = \eta_{k-1} + \Delta\eta_k$, $k = 1, \dots, N$, $\eta_0 = 0$. Then we multiply both sides of the equation (2.12) by $2d\eta$ and integrate it once within each layer (ζ_{k-1}, ζ_k):

$$\varepsilon_k^2 = \varepsilon_{k-1}^2 + 2 \int_{\eta_{k-1}}^{\eta_k} \frac{dw}{[1 + 2w - \Omega^2(\zeta')^2]^{1/2}}. \quad (2.16)$$

Here, $\varepsilon_k = -(d\eta/d\zeta)|_{\zeta=\zeta_k}$ and it is the electric field strength at the point $\zeta = \zeta_k$. To integrate each integral, PD is approximated with a straight line

$$\begin{aligned} \eta(\zeta) &= \eta_{k-1} - (\zeta - \zeta_{k-1})\bar{\varepsilon}_k, \\ \bar{\varepsilon}_k &= q_k\varepsilon_{k-1} + (1 - q_k)\varepsilon_k. \end{aligned} \quad (2.17)$$

In (2.17), the weights q_k lie within $(0, 1)$. In each layer, values of q_k , generally, can be different. For our purpose, we take $q_k = 0.5$. Using the approximations mentioned in Eq. (2.17), each integral becomes

$$\begin{aligned} G(\zeta_{k-1}, \eta_{k-1}, \varepsilon_{k-1}, \eta_k, \varepsilon_k) &= \int_{\eta_{k-1}}^{\eta_k} \frac{dw}{[1 + 2w - \Omega^2(\zeta')^2]^{1/2}} \\ &= \int_0^{\eta_k - \eta_{k-1}} \frac{dw}{\{(1 + 2\eta_{k-1} - \zeta_{k-1}^2\Omega^2) + 2(1 + (\zeta_{k-1}/\bar{\varepsilon}_k)\Omega^2)w - (\Omega^2/\bar{\varepsilon}_k^2)w^2\}^{1/2}} \\ &= \int_0^{\eta_k - \eta_{k-1}} \frac{dw}{(A + Bw + Cw^2)^{1/2}}. \end{aligned} \quad (2.18)$$

Here

$$\begin{aligned} A &= 1 + 2\eta_{k-1} - \zeta_{k-1}^2 \Omega^2 > 0, \\ B &= 2 \left[1 + (\zeta_{k-1}/\bar{\varepsilon}_k) \Omega^2 \right], \\ C &= -(1/\bar{\varepsilon}_k^2) \Omega^2 < 0. \end{aligned}$$

and

$$\Delta = 4AC - B^2 = -4 \left\{ 1 + [(1 + 2\eta_{k-1} + 2\zeta_{k-1}\bar{\varepsilon}_k)/\bar{\varepsilon}_k^2] \Omega^2 \right\} < 0.$$

Depending on the value of Ω , the function G (2.18) reads as

$$\begin{aligned} -\frac{1}{\Omega} \left[\arcsin \left(\frac{B - 2[(\eta_k - \eta_{k-1})/\bar{\varepsilon}_k^2] \Omega^2}{\sqrt{-\Delta}} \right) - \arcsin \left(\frac{B}{\sqrt{-\Delta}} \right) \right], \quad \Omega > 0, \\ \sqrt{1 + 2\eta_k} - \sqrt{1 + 2\eta_{k-1}}, \quad \Omega = 0. \end{aligned} \quad (2.19)$$

Thus, to obtain the PD in the region to the left of the potential minimum, within each step k , a system of the difference equations

$$\begin{aligned} \eta_k &= \eta_{k-1} + \Delta \eta_k, \\ \varepsilon_k^2 &= \varepsilon_{k-1}^2 + 2G(\zeta_{k-1}, \eta_{k-1}, \varepsilon_{k-1}, \eta_k, \varepsilon_k), \\ \bar{\varepsilon}_k &= q_k \varepsilon_{k-1} + (1 - q_k) \varepsilon_k, \\ \zeta_k &= \zeta_{k-1} - (\eta_k - \eta_{k-1})/\bar{\varepsilon}_k \end{aligned} \quad (2.20)$$

is solved under conditions as follows:

$$\eta_0 = 0, \quad \varepsilon_0 = \tilde{\varepsilon}_0, \quad \zeta_0 = 0. \quad (2.21)$$

As a result, within each step, the value of the electric field strength ε_k and coordinate ζ_k are determined. It should be noted here that, in this region, $\varepsilon_k \geq 0$.

The equation for ε_k [the 2nd equation of the Eqs. (2.20)] is the transcendental one. So, within each step k , an iteration is carried out, taking an approximate value $\varepsilon_k^{(0)}$, firstly, at the right side of the 2nd equation. Then $\varepsilon_k^{(1)}$ is calculated. From the next two equations, $\bar{\varepsilon}_k^{(1)}$ and $\zeta_k^{(1)}$ are obtained. Next, relevant parameters for the second approximation are calculated and so on.

For a particular value of k ($k = K \leq N$), the value of the right side of the 2nd equation of Eqs. (2.20) becomes negative. At this step, the iterations are carried out over η_K as ε_K becomes zero. As a result, the required value of η_m and ζ_m are determined.

When the coordinates of the potential minimum are determined, PD is calculated at the right side of the point of minimum ζ_m . Here, Eqs. (2.20) are solved with the boundary conditions (2.15). The value of the potential step is taken as $(V - \eta_m)/N$. It should be kept in mind that the electric field strength within this area is negative. The calculation is carried out until the potential η becomes equal to V . At this stage, the corresponding value of ζ is the diode gap δ . Thus, the PD is obtained for the taken value of the electric field strength at the emitter. Taking different values of ε_0 , the corresponding δ -values are calculated in this way.

Next, the value of the electric field strength at the emitter is smoothly increased, and, for each value of ε_0 , the profiles of the potential, velocity and electron density within the inter-electrode gap are evaluated. This calculations show that the very weak magnetic field ($\Omega \ll 1$) actually has no effect on the diode characteristics. Its effect arises as $\Omega \geq 0.1$. It turns out that, for the case under consideration ($V = 0$), the dependence of the velocity u_ζ on the coordinate ζ shows to form a single minimum (Fig. 2.2). The spatial dependence of u_ζ is found to be monotonic

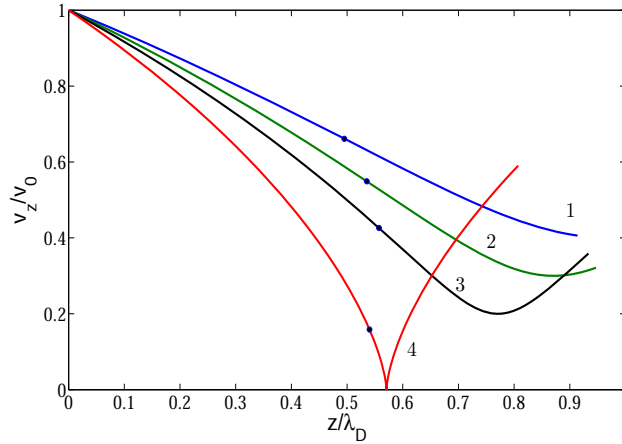


Figure 2.2: Velocity distribution in the interelectrode gap drawn for different ε_0 values: (1) $\varepsilon_0 = 0.6$, (2) 0.7, (3) 0.8, and (4) 1.0; $\Omega = 1.0$; $V = 0$. Closed circles mark position of the potential minimum.

function for small ε_0 values, and its minimum lies on the collector. As the strength of ε_0 is increased further, the location of the velocity minimum (ζ_{vm}) appears within the inter-electrode gap. With increasing ε_0 , the position of the velocity minimum begins to shift to the emitter and the minimum value of u_ζ reduces. And finally, for a certain value of $\varepsilon_0^0(\Omega)$, the minimum velocity vanishes. We name this state as “zero-point” and at this condition $\varepsilon_0 = \varepsilon_0^0$. This is demonstrated in Fig. 2.3. As we can also see that for higher values of ε_0 , the position of the velocity minimum (ζ_{vm}) approaches to the location of the potential minimum (ζ_m).

Like the case of Bursian diode without magnetic field, it is convenient to denote the steady state solutions by the points on a $\{\varepsilon_0, \delta\}$ -plane [67, 66]. At a fixed V , those lie on a continuity curve named as the branch of solutions. In Fig. 2.4 these branches are shown for a number of Ω values. Here, each curve ends at $\varepsilon_0 = \varepsilon_0^0$, i.e., when the longitudinal velocity distribution becomes tangent to the line $u_\zeta = 0$ for the first time. The $\varepsilon_0 - \delta$ parametric plots also show a region of non-unique solutions. On the right boundary of this region, there is a bifurcation

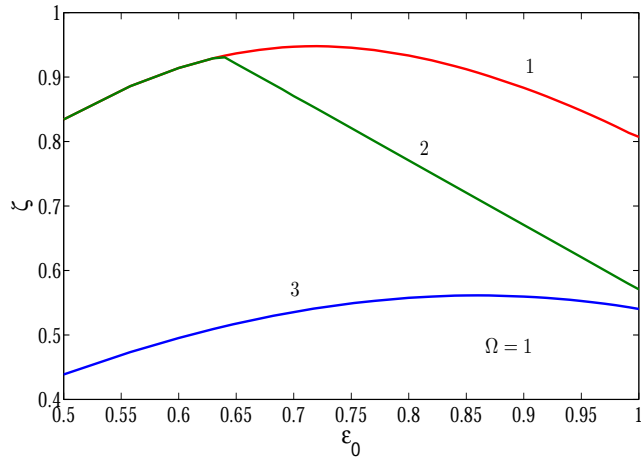


Figure 2.3: Plots of positions of (1) the collector, (2) the potential minimum, as well as (3) the velocity minimum vs ε_0 for $\Omega = 1.0$; $V = 0$.

point *SCL* (space charge limit). The left boundary point refers to the situation when u_ζ becomes zero for the first time within interelectrode gap. We denote it by an index “0” (zero-point). With increasing strength of the applied magnetic field, the width of the region of ambiguous solutions (δ_0, δ_{SCL}) narrows (Fig. 2.4) and it vanishes at $\Omega \approx 1.32$. The relevant formulas for the parameters of *SCL* and zero-point are derived using the Lagrangian variables.

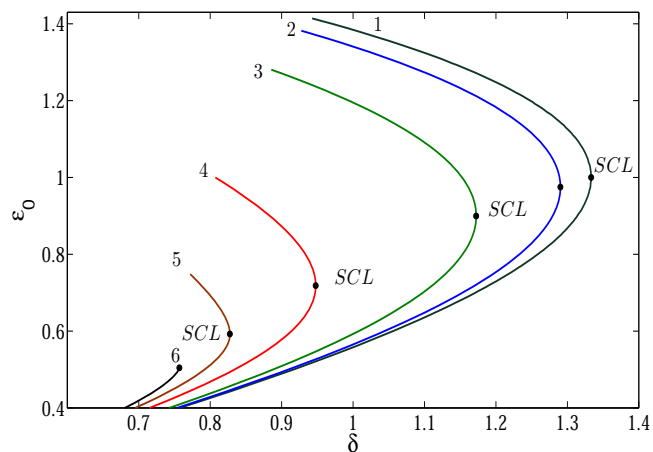


Figure 2.4: Curves $\varepsilon_0(\delta)$ drawn for various values of Ω : (1) $\Omega = 0$, (2) 0.3, (3) 0.6, (4) 1.0, (5) 1.2, and (6) 1.321; $V = 0$. In the curves $u_\zeta(\zeta) > 0$ everywhere.

2.4 Features of steady-states. The Lagrange method

Now we solve the problem using the Lagrangian variables. In 1D time-independent case, we start with the basic governing equations which are the continuity and the momentum equations along with the Poisson's equation. They are written in a dimensionless form as:

$$\begin{aligned} \frac{d}{d\zeta}(nu_\zeta) &= 0, \\ u_\zeta \frac{du_\zeta}{d\zeta} &= -\varepsilon - \Omega u_\chi, & u_\zeta \frac{du_\chi}{d\zeta} &= \Omega u_\zeta, \\ \frac{d\varepsilon}{d\zeta} &= -n. \end{aligned} \quad (2.22)$$

The boundary conditions to be used are, $n(\zeta = 0) = 1$, $u_\zeta(\zeta = 0) = 1$, $u_\chi(\zeta = 0) = 0$, electric potential, $\varphi(\zeta = 0) = 0$, and field $\varepsilon(\zeta = 0) = \varepsilon_0$ (ε_0 is used as a parameter).

To solve these nonlinear equations, we introduce the Lagrangian coordinate τ and the Lagrange transformation,

$$\zeta = \int_0^\tau u_\zeta(\tau') d\tau'.$$

Thus, $u_\zeta d/d\zeta = d/d\tau$. Eqs. (2.22) take the form

$$\begin{aligned} \frac{d}{d\tau}(nu_\zeta) &= 0, \\ \frac{du_\zeta}{d\tau} &= -\varepsilon - \Omega u_\chi, & \frac{du_\chi}{d\tau} &= \Omega u_\zeta, \\ \frac{d\varepsilon}{d\tau} &= -1. \end{aligned} \quad (2.23)$$

Combining Eqs. (2.23) we can have

$$\frac{d^2 u_\zeta}{d\tau^2} + \Omega^2 u_\zeta = 1. \quad (2.24)$$

Using the stated boundary conditions, the solutions in terms of the Lagrangian coordinate can be obtained as

$$\begin{aligned}
u_\zeta(\tau) &= \frac{1}{\Omega^2} + \left(1 - \frac{1}{\Omega^2}\right) \cos \Omega\tau - \frac{\varepsilon_0}{\Omega} \sin \Omega\tau, \\
u_\chi(\tau) &= \frac{1}{\Omega}\tau + \left(1 - \frac{1}{\Omega^2}\right) \sin \Omega\tau + \frac{\varepsilon_0}{\Omega}(\cos \Omega\tau - 1), \\
n &= \frac{1}{u_\zeta}, \\
\varepsilon(\tau) &= -\tau + \varepsilon_0.
\end{aligned} \tag{2.25}$$

The relation between the Eulerian variable ζ and the Lagrangian one τ can be derived in following form

$$\zeta = \frac{1}{\Omega^2}\tau + \frac{1}{\Omega} \left(1 - \frac{1}{\Omega^2}\right) \sin \Omega\tau + \frac{\varepsilon_0}{\Omega^2}(\cos \Omega\tau - 1). \tag{2.26}$$

The electric potential is suitable to express as

$$\eta(\tau) = \frac{1}{2} [u_\zeta^2(\tau) + \Omega^2\zeta^2(\tau) - 1]. \tag{2.27}$$

Here the energy conservation law (2.5) was used. At the collector position [$\zeta = \delta$, $\eta(\delta) = V$] we have

$$\begin{aligned}
\delta &= \frac{1}{\Omega^2}T + \frac{1}{\Omega} \left(1 - \frac{1}{\Omega^2}\right) \sin \Omega T + \frac{1}{\Omega^2}\varepsilon_0 (\cos \Omega T - 1), \\
V &= \frac{1}{2} [u_\zeta^2(T) + \Omega^2\delta^2 - 1], \\
u_\zeta(T) &= \frac{1}{\Omega^2} + \left[1 - \frac{1}{\Omega^2}\right] \cos \Omega T - \frac{1}{\Omega}\varepsilon_0 \sin \Omega T.
\end{aligned} \tag{2.28}$$

Here T is the time-of-flight of an electron to travel between the electrodes.

Using Eqs (2.25)–(2.27), one can determine the spatial variations of the electron velocity, density, electric field and potential within the inter-electrode space. For some given values of Ω and ε_0 , the dependencies are built up by gradually increasing τ , and terminated at the moment when the potential η [Eq. (2.27)] takes

the value V (collector potential). At this situation, corresponding values of ζ and τ respectively give the inter-electrode gap δ and the time T when an electron arrives at the collector surface.

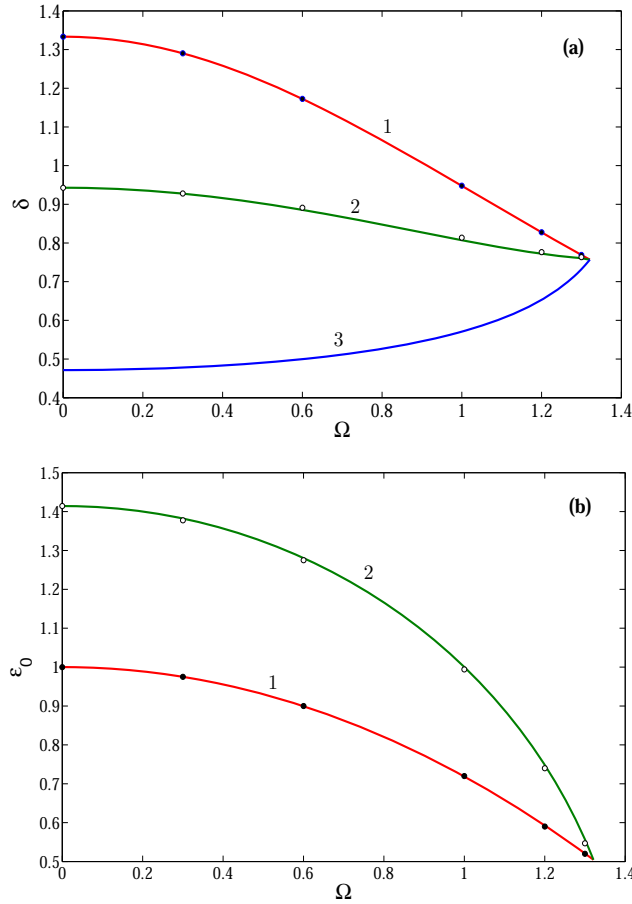


Figure 2.5: Dependences (1) δ_{SCL} , (2) δ_0 , and (3) ζ_0 (a) and (1) $\varepsilon_{0,SCL}$ and (2) ε_0^0 (b) as functions of Ω . The lines denote the calculation involving the Lagrange method, and circles – the Euler one. $V = 0$.

For a particular value of ε_0^0 , a situation appears when the longitudinal velocity of the electron vanishes for the first time. This point is denoted by “0”. At larger values of ε_0 , the electrons are turned back by the magnetic field and they fly toward the emitter. To find the coordinates of the zero velocity point we use the conditions $u_\zeta(\tau) = 0$ and $du_\zeta(\tau)/d\tau = 0$. Using Eqs. (2.25), we obtain two

equations to determine ε_0^0 and τ_0 (τ_0 determines the moment when u_ζ vanishes):

$$\begin{aligned} (1 - \Omega^2) \cos(\Omega\tau) + \varepsilon_0 \Omega \sin(\Omega\tau) &= 1, \\ -(1 - \Omega^2) \sin(\Omega\tau) + \varepsilon_0 \Omega \cos(\Omega\tau) &= 0. \end{aligned} \quad (2.29)$$

Solving these equations, we find

$$\begin{aligned} \varepsilon_0^0 &= \frac{1}{\Omega} [1 - (1 - \Omega^2)^2]^{1/2} = \sqrt{2 - \Omega^2}, \\ \sin(\Omega\tau_0) &= \Omega\sqrt{2 - \Omega^2}, \quad \cos(\Omega\tau_0) = 1 - \Omega^2. \end{aligned} \quad (2.30)$$

Substituting the terms from (2.30) into Eq. (2.26), we can find the point ζ_0 where u_ζ vanishes. Depending on the value of Ω , the function $\zeta_0(\Omega)$ reads

$$\begin{aligned} \Omega^{-3} \left[\arcsin \left(\Omega\sqrt{2 - \Omega^2} \right) - \Omega\sqrt{2 - \Omega^2} \right], & \text{ if } \Omega \leq 1, \\ \Omega^{-3} \left[\pi - \arcsin \left(\Omega\sqrt{2 - \Omega^2} \right) - \Omega\sqrt{2 - \Omega^2} \right], & \text{ if } \Omega > 1. \end{aligned} \quad (2.31)$$

Note that with no magnetic field, $\varepsilon_0^0 = \sqrt{2}$, and the relevant value of ζ_0 is $\sqrt{2}/3$. The dependence of ζ_0 on Ω is shown in Fig. 2.5a (line 3). To obtain the dependence of δ_0 on Ω corresponding to zero-point solutions, we need to calculate the function $T_0(\Omega)$ from the equation

$$u_\zeta^2(T_0, \Omega) + \Omega^2 \delta^2(T_0, \Omega) - (1 + 2V) = 0, \quad (2.32)$$

which is obtained from the 2nd relationship of (2.28). The relevant variations of $\delta(T_0, \Omega)$ and $u_\zeta(T_0, \Omega)$ are determined from the 1st and 3rd equations of (2.28), and $\varepsilon_0^0(\Omega)$ is determined from (2.30) [note that at $\tau = T_0$, $\delta = \delta_0$]. The curve $\delta_0(\Omega)$ is shown in Fig. 2.5a (line 2). Fig. 2.5b shows the dependence ε_0^0 on Ω .

We can say from the Fig. 2.4 that, at *SCL* point, the condition $d\delta/d\varepsilon_0 = 0$ has

to hold. We can calculate this derivative as a complex function from Eqs (2.28):

$$\begin{aligned}
\frac{d\delta}{d\varepsilon_0} &= \frac{\partial\delta}{\partial\varepsilon_0} + \frac{\partial\delta}{\partial T} \frac{dT}{d\varepsilon_0} = \frac{\partial\delta}{\partial\varepsilon_0} - \frac{\partial\delta}{\partial T} \frac{(\partial V/\partial\varepsilon_0)}{(\partial V/\partial T)} \\
&= \frac{\partial\delta}{\partial\varepsilon_0} - \left(u_\zeta \frac{\partial u_\zeta}{\partial\varepsilon_0} + \Omega^2 \delta \frac{\partial\delta}{\partial\varepsilon_0} \right) / \left(\frac{\partial u_\zeta}{\partial T} + \Omega^2 \delta \right) \\
&= \left(\frac{\partial\delta}{\partial\varepsilon_0} \frac{\partial u_\zeta}{\partial T} - u_\zeta \frac{\partial u_\zeta}{\partial\varepsilon_0} \right) / \left(\frac{\partial u_\zeta}{\partial T} + \Omega^2 \delta \right). \tag{2.33}
\end{aligned}$$

Calculating partial derivatives in (2.33) and reducing the similar terms in the numerator, we obtain

$$\frac{1}{\Omega} \sin \Omega T - \frac{\varepsilon_0}{\Omega^2} (1 - \cos \Omega T) = 0. \tag{2.34}$$

Transferring to half-index argument in trigonometric functions, Eq (2.34) is reduced to an equation as below

$$\frac{2}{\Omega} \sin \frac{\Omega T}{2} \left(\cos \frac{\Omega T}{2} - \frac{\varepsilon_0}{\Omega} \sin \frac{\Omega T}{2} \right) = 0. \tag{2.35}$$

It also gives the relationship of T with ε_0 at SCL :

$$T_{SCL} = \frac{2}{\Omega} \arctan \frac{\Omega}{\varepsilon_{0,SCL}}. \tag{2.36}$$

Substituting T_{SCL} into the first equation of (2.28), we obtain δ_{SCL} :

$$\delta_{SCL} = \frac{2}{\Omega^2} \left(\frac{1}{\Omega} \arctan \frac{\Omega}{\varepsilon_{0,SCL}} - \frac{\varepsilon_{0,SCL}}{\varepsilon_{0,SCL}^2 + \Omega^2} \right). \tag{2.37}$$

Now, we need to calculate the value of ε_0 at the SCL point. First, the expression of u_ζ at the collector is found, then, the law of energy conservation, i.e. the second equation in (2.28) is utilized. Substituting T_{SCL} into the 3rd equation of (2.28), we obtain

$$u_\zeta = \frac{2}{\Omega^2 + \varepsilon_0^2} - 1. \tag{2.38}$$

When we substitute u_ζ into the 2nd equation of (2.28), we get a transcendental equation to calculate the desired form of $\varepsilon_{0,SCL}$:

$$\left(\frac{2}{\varepsilon_{0,SCL}^2 + \Omega^2} - 1 \right)^2 + \frac{4}{\Omega^2} \left(\frac{1}{\Omega} \arctan \frac{\Omega}{\varepsilon_{0,SCL}} - \frac{\varepsilon_{0,SCL}}{\varepsilon_{0,SCL}^2 + \Omega^2} \right)^2 = 1 + 2V. \quad (2.39)$$

In fact, relationships (2.37) and (2.39) represent together the maximum value

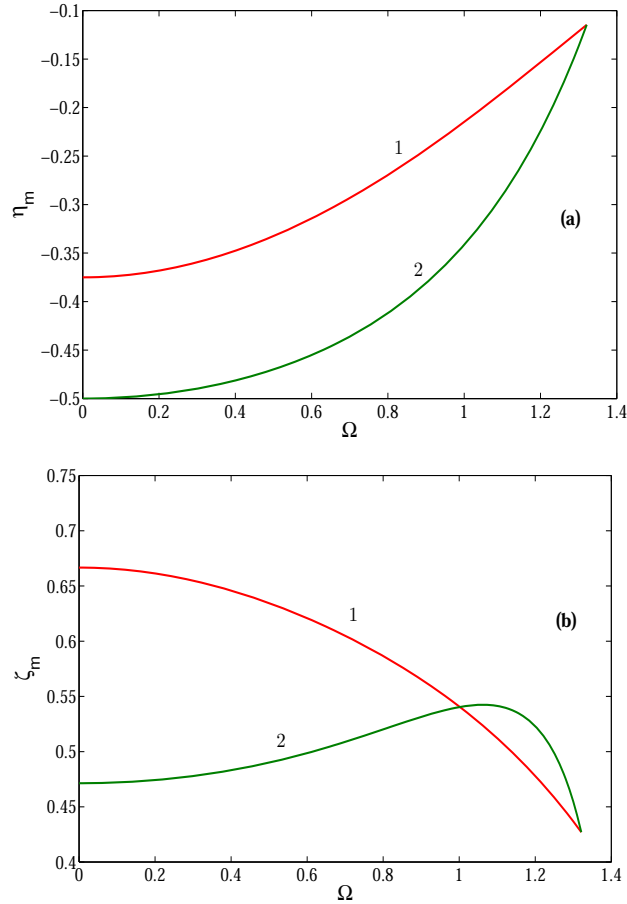


Figure 2.6: Plots of the minimum potential η_m (a) and its position ζ_m (b) for the PDs, relating to (1) *SCL* and (2) 0 points, vs Ω ; $V = 0$.

of the current that can pass through the diode at steady state with a uniform magnetic field along the transverse direction (as $J_{max} \sim \delta_{SCL}^2$).

Fig. 2.5 shows that δ_{SCL} and δ_0 decrease as Ω increases. At a certain value Ω (say Ω_0), the 0 and *SCL* points merge together. The value of Ω_0 is determined

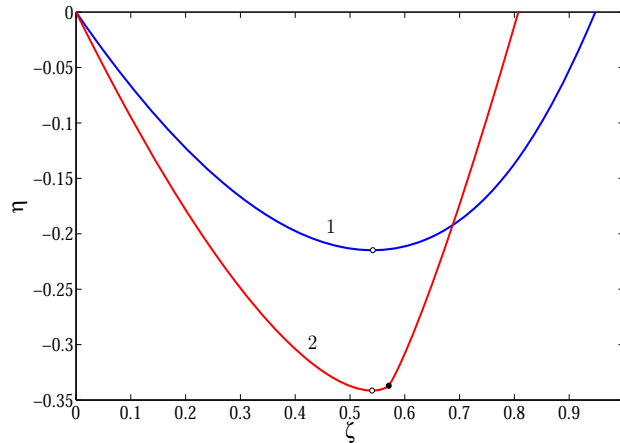


Figure 2.7: The PDs, relating to (1) *SCL* ($\varepsilon_0 \approx 0.7185$) and (2) 0 ($\varepsilon_0 \approx 1.0$) points, for $\Omega = 1$; $V = 0$. The open circles mark positions of the potential minimum, closed circle shows the place where a velocity vanishes.

from an equation which results when we substitute the expression of ε_0^0 from the 1st equation of (2.30) into (2.39):

$$\frac{2}{\Omega} \left(\frac{1}{\Omega} \arctan \frac{\Omega}{\sqrt{2 - \Omega^2}} - \frac{\sqrt{2 - \Omega^2}}{2} \right) = \sqrt{1 + 2V}. \quad (2.40)$$

For $V = 0$, we can get $\Omega_0 \approx 1.3212$, $\varepsilon_0^0 \approx 0.5042$, and $\delta_0 \approx 0.7569$. In Fig. 2.5, the lines are terminated at $\Omega = \Omega_0$, where the *SCL* point coincides with the zero-point.

Fig. 2.5a demonstrates the dependencies of δ_{SCL} , δ_0 and ζ_0 with respect to Ω . The solid lines are obtained by the Lagrange method and the Eulerian approach gives the circles. We can see that both results agree well with each other.

Fig. 2.6 depicts the dependencies of minimum value of the potential and its position on Ω for the solutions corresponding to the *SCL* and zero-points. They are calculated from the Eqs. (2.26) and (2.27) at $\tau = \varepsilon_0$ (the time when ε vanishes). It is interesting to note that the position of the minimum potential shows a nonmonotonic behaviour for the zero-point. Fig. 2.7 shows the PDs relating to the points *SCL* and 0, for $\Omega = 1$. One can see that velocity vanishes to the right of the potential minimum.

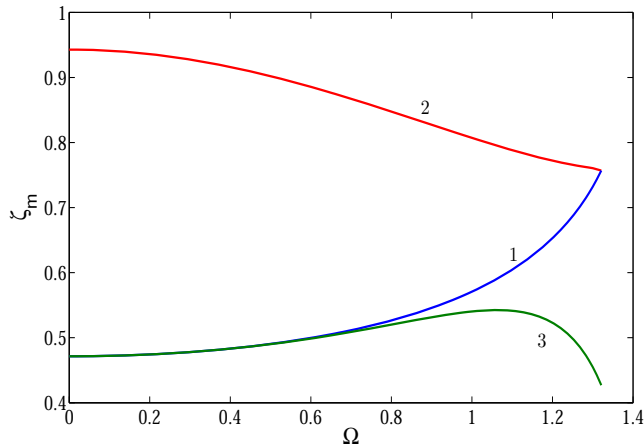


Figure 2.8: Plots of positions of the point where a velocity vanishes (curve 1) as well as the collector (2) and the potential minimum (3) positions vs Ω . $V = 0$.

Fig. 2.8 exhibits the dependence of the position where the longitudinal velocity of the electron vanishes (ζ_0) (line 1) on Ω . In this figure, the variations of the gap value (line 2) and the position of the potential minimum (line 3) are presented, too. It is seen that the velocity vanishes practically at the point of the potential minimum for $\Omega < 0.6$. For higher values of Ω , the position of zero velocity (ζ_0) approaches to the collector, and at last it falls on the collector at $\Omega = \Omega_0$ for which the zero-point merges with the *SCL* one.

As the zero-point falls on the collector position at $\Omega = \Omega_0$, it stays there as Ω is increased further. However, now the condition $du_\zeta(\tau)/d\tau = 0$ turns out to be untrue. The condition when the *SCL* and zero-points coincide together and both of them lie on the collector, can be determined from the Eqs. (2.32) with $u_\zeta = 0$:

$$\delta_{SCL}(\Omega; V) = \frac{\sqrt{1 + 2V}}{\Omega}. \quad (2.41)$$

2.5 Summary

The investigation presented in this chapter shows that in a Bursian diode with a transverse magnetic field, the potential distributions remain the single minimum functions, but the height of the minimum turns out to be lower than the initial kinetic energy of the electrons. The steady state solutions are pictured through the ε_0, δ -diagram. There is a region on this ε_0, δ -diagram where the solutions are non-unique (the region between *SCL* and “zero-point”). Strong effect of the magnetic field occurs when the Larmor radius becomes comparable with the Bursian threshold. In this case the region of non-uniqueness vanishes.

The magnetic field also results to the displacement of (ε_0, δ) -diagram. The *SCL* points are displaced to the left, and at its right, solutions without electron turning are absent. Hence, the magnetic field can be used to design a fast electronic switches based on the current interception mechanism of the Bursian diode. Such a device can operate as follows. Imagine that the initial state of a Bursian diode lies very close to the *SCL* point. Here, the relevant current passing through the diode is nearly equal to the maximum value ($J_{max} \sim \delta_{SCL}^2$). When magnetic field is switched on, the relevant (ε_0, δ) -curve is displaced to the left, and the steady state with a net current for given δ disappears. As a result, a state-transition occurs in the Bursian diode for which the system switches to a final state with a negligible current. For weak magnetic field, very small current may pass through the diode because of the incomplete current cut-off. However, for $\Omega > 1$, the current is totally cut off and this corresponds to the total interception of the current. When the magnetic field is turned on, the diode returns to its initial state with a net current.

Chapter 3

Stability analysis of the steady state solutions of Bursian Diode in presence of transverse magnetic field

The stability properties of the steady state solutions of a Bursian diode in presence of constant transverse magnetic field have been studied in this chapter. Employing first order perturbation theory, a relevant dispersion relation has been derived for the time dependent states. It is found that the steady state solutions which lie on branch I (C normal branch) of “ $\varepsilon_0 - \delta$ ” curve are stable and the solutions which belong to branch II (C overlap branch) are unstable with respect to small aperiodic perturbations. The width of the unstable branch gradually decreases as the magnitude of external magnetic field is increased.

3.1 Introduction

In the absence of external magnetic field, the steady state solutions of different kind of vacuum diode systems (like Bursian diode, Pierce diode etc.) and their stability properties have been investigated theoretically by several authors [44, 57, 72, 79, 86, 91, 92, 93, 94, 113, 135, 66, 147, 148, 149, 150]. Theoretical studies suggest that all steady state solutions of a vacuum diode can be visualized as three distinct branches of “ $\varepsilon_0 - \delta$ ” parametric plot, where ε_0 and δ are the electric field strength at emitter and the diode gap respectively. These branches were termed as “C normal branch”, “C overlap branch” and “virtual cathode branch” (the branch corresponding to partial electron reflection). Stability of these three branches was analyzed by introducing an apparatus of “collector potential vs emitter electric field” diagram (η, ε -diagram)[148] as well as deriving a dispersion relation with the help of perturbative approach [72, 94]. It was shown that one of these branches (C overlap branch) is unstable and the other two branches are stable under small aperiodic perturbation [67, 113, 135, 66, 150].

In the previous chapter, the stationary states of a Bursian diode are investigated when there is an external magnetic field along the transverse direction. This chapter contains the stability analysis of those steady-state solutions. The regime within which no electrons are turned around by the external transverse magnetic field is taken under consideration only. The results show that there is a prominent effect of the magnetic field on the stability properties of the steady state solutions.

3.2 Steady State Solutions

We adopt the same planar model for the Bursian diode which is discussed in the previous chapter. The beam accelerating voltage $V_0 = W_0/e = mv_0^2/(2e)$ is in Volts and the magnetic field B is in Teslas; e and m are electron charge and mass. The relevant Larmor frequency and radius are $\omega = eB/m$ and $\lambda_L = mv_0/(eB)$ respectively. Basic governing equations for time dependent states are the continuity equation, the momentum equation and the Poisson's equation :

$$\begin{aligned} \frac{\partial n}{\partial t} + \nabla \cdot (n\vec{v}) &= 0, \\ \left(\frac{\partial}{\partial t} + \vec{v} \cdot \nabla \right) \vec{v} &= -\frac{e}{m} \left(\vec{E} + \vec{v} \times \vec{B} \right), \\ \nabla \cdot \vec{E} &= -\frac{ne}{\epsilon_0}. \end{aligned} \quad (3.1)$$

To rewrite the above equations in terms of dimensionless quantities, we use kinetic energy of the electrons [$W_0 = (1/2)mv_0^2$] and beam Debye length [$\lambda_D = \{(2\epsilon_0 W_0)/(e^2 n_0)\}^{1/2}$] as the basic units for energy and length respectively. For dimensionless coordinates, time, velocity, potential and electric field strength we have $(\zeta, \chi) = (z, x)/\lambda_D$, $t = t\omega_0$, $u = v/v_0$, $\eta = e\varphi/(2W_0)$, $\varepsilon = eE\lambda_D/(2W_0)$; here $\omega_0 = v_0/\lambda_D$ is the characteristic frequency. Expressing Eq. (3.1) in terms of the components along ζ and χ directions, now we obtain

$$\begin{aligned} \frac{\partial n}{\partial t} + \frac{\partial(nu_\zeta)}{\partial \zeta} &= 0, \\ \left(\frac{\partial}{\partial t} + u_\zeta \frac{\partial}{\partial \zeta} \right) u_\zeta &= -\varepsilon - \Omega u_\chi, \\ \left(\frac{\partial}{\partial t} + u_\zeta \frac{\partial}{\partial \zeta} \right) u_\chi &= \Omega u_\zeta, \\ \frac{\partial \varepsilon}{\partial \zeta} &= -n. \end{aligned} \quad (3.2)$$

In Eq. (3.2), normalized Larmor frequency Ω is given by $\Omega = (eB)/(m\omega_0)$. Let us fix the value of potential difference between two electrodes at V , the inter-electrode distance δ , the Larmor frequency Ω , and the emitter electric field strength ε_0 . Boundary conditions to be used are as follows, $n(\zeta = 0, t) = 1$, $u_\zeta(\zeta = 0, t) = 1$, $u_\chi(\zeta = 0, t) = 0$, $\eta(\zeta = 0, t) = 0$ and $\eta(\zeta = \delta, t) = V$.

To study the system of time dependent equations (3.2) using Lagrangian description, we introduce a “stream function”, [72, 92, 93, 94, 135, 150] $t_0(\zeta, t)$, which satisfies the following conditions: $\partial_\zeta t_0 = -n$ and $\partial_t t_0 = nu_\zeta$ (the notation ∂_ζ denotes partial derivative of first order with respect to ζ). Physically, t_0 represents the time of injection of an electron, i. e., $\zeta(t = t_0) = 0$. It can be easily checked that $(d/dt)t_0 \equiv \partial_t t_0 + u_\zeta \partial_\zeta t_0 = 0$. Hence, “ t_0 ” remains constant along the path of an electron.

When we switch the basis from Eulerian (ζ, t) to Lagrangian (t_0, t) , the differential operators are transformed as $\partial_\zeta \equiv -n\partial_{t_0}$ and $\partial_t \equiv \partial_t + nu_\zeta \partial_{t_0}$. Hence, last three equations of the set of equations (3.1) take the form,

$$\partial_t u_\zeta = -\varepsilon(t_0, t) - \Omega u_\chi, \quad (3.3)$$

$$\partial_t u_\chi = \Omega u_\zeta, \quad (3.4)$$

$$\partial_{t_0} \varepsilon(t_0, t) = 1. \quad (3.5)$$

Equation (3.5) gives

$$\varepsilon(t_0, t) = -(t - t_0) + \varepsilon_0(t). \quad (3.6)$$

Using the fact that $u_\zeta = \partial_t \zeta$, we get from Eqs. (3.3) and (3.4)

$$\frac{\partial^2 \zeta}{\partial t^2} + \Omega^2 \zeta = -\varepsilon(t_0, t). \quad (3.7)$$

In steady state, electric field strength at emitter (ε_0) is time-independent and the other quantities depend only on $t-t_0 = \tau$. Thus, at steady state, $\varepsilon(t_0, t) = -\tau + \varepsilon_0$, $\partial_t \rightarrow \partial_\tau$ and $\partial_{t_0} \rightarrow -\partial_\tau$. Consequently, Eq. (3.7) becomes

$$\frac{\partial^2 \zeta}{\partial \tau^2} + \Omega^2 \zeta = -\tau + \varepsilon_0. \quad (3.8)$$

Solving Eq. (3.8), we can have the steady state solutions for ζ , η and u_ζ as [151]

$$\begin{aligned} \zeta(\tau) &= \frac{1}{\Omega^2} \tau + \frac{1}{\Omega} \left(1 - \frac{1}{\Omega^2} \right) \sin \Omega \tau + \frac{1}{\Omega^2} \varepsilon_0 (\cos \Omega \tau - 1), \\ \eta(\tau) &= \frac{1}{2} [u_\zeta^2(\tau) + \Omega^2 \delta^2 - 1], \\ u_\zeta(\tau) &= \frac{1}{\Omega^2} + \left[1 - \frac{1}{\Omega^2} \right] \cos \Omega \tau - \frac{1}{\Omega} \varepsilon_0 \sin \Omega \tau. \end{aligned} \quad (3.9)$$

For given values of Ω and ε_0 , we can evaluate the profiles of the electron velocity, density, potential and electric field within the inter-electrode space by gradually increasing τ . At the moment when (say, at $\tau = T$) the potential η takes the value V (collector potential), ζ takes the value δ . Thus, at $\tau = T$ an electron arrives at the collector surface.

At the collector position ($\zeta = \delta$, $\eta(\delta) = V$) we have

$$\begin{aligned} \delta &= \frac{1}{\Omega^2} T + \frac{1}{\Omega} \left(1 - \frac{1}{\Omega^2} \right) \sin \Omega T + \frac{1}{\Omega^2} \varepsilon_0 (\cos \Omega T - 1), \\ V &= \frac{1}{2} [u_\zeta^2(T) + \Omega^2 \delta^2 - 1], \\ u_\zeta(T) &= \frac{1}{\Omega^2} + \left[1 - \frac{1}{\Omega^2} \right] \cos \Omega T - \frac{1}{\Omega} \varepsilon_0 \sin \Omega T. \end{aligned} \quad (3.10)$$

Here T is the transit time of an electron between electrodes.

It was shown in earlier works [67, 66] that, for a fixed V , the steady state solutions of a Bursian diode can be represented by the points on a “ $\varepsilon_0 - \delta$ ” continuity curve. In Fig. 3.1, these curves are shown for $V = 0$ and for a number of Ω values. In previous chapter, it is already discussed that each curve ends at such a value of

ε_0 (say, ε_0^0), when the longitudinal velocity, u_ζ becomes zero for the first time, i.e., at “zero-point”. On the right boundary of each curve, we have point SCL which

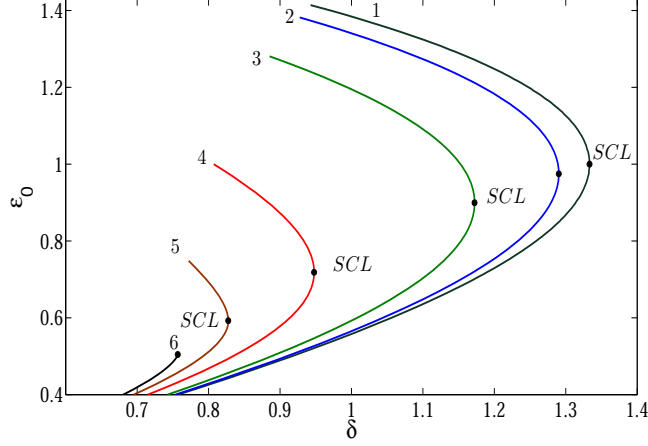


Figure 3.1: Curves $\varepsilon_0(\delta)$ drawn for various values of Ω : (1) $\Omega = 0$, (2) 0.3, (3) 0.6, (4) 1.0, (5) 1.2, and (6) 1.321; $V = 0$. In the curves $u_\zeta(\zeta) > 0$ everywhere.

corresponds to the steady state solutions when current passing through the diode gap is maximum. Each curve is consist of two branches of solutions. Branch I (C normal branch) covers the the steady state solutions for $\varepsilon_0 \leq \varepsilon_{0,SCL}$ and branch II (C overlap branch) corresponds to the steady state solution for $\varepsilon_{0,SCL} < \varepsilon_0 \leq \varepsilon_0^0$. As we increase the strength of magnetic field, the width of the region between endpoint and SCL (δ_0, δ_{SCL}) narrows and it vanishes when $\Omega \approx 1.32$.

At the SCL point we can have a relationship [see previous chapter] of T and δ with ε_0 as [151]:

$$T_{SCL} = \frac{2}{\Omega} \arctan \frac{\Omega}{\varepsilon_{0,SCL}},$$

$$\delta_{SCL} = \frac{2}{\Omega^2} \left(\frac{1}{\Omega} \arctan \frac{\Omega}{\varepsilon_{0,SCL}} - \frac{\varepsilon_{0,SCL}}{\varepsilon_{0,SCL}^2 + \Omega^2} \right). \quad (3.11)$$

Eliminating ε_0 from Eq. (3.10) for SCL point, we can find a relationship of T_{SCL} with δ_{SCL}

$$\Omega^3 \delta_{SCL} - \Omega T_{SCL} + \sin \Omega T_{SCL} = 0. \quad (3.12)$$

For the relevant u_ζ we obtain

$$u_{\zeta,SCL} = \frac{2}{\Omega^2 + \varepsilon_{0,SCL}^2} - 1. \quad (3.13)$$

The value of desired $\varepsilon_{0,SCL}$ can be found from the equation:

$$\left(\frac{2}{\varepsilon_{0,SCL}^2 + \Omega^2} - 1 \right)^2 + \frac{4}{\Omega^2} \left(\frac{1}{\Omega} \arctan \frac{\Omega}{\varepsilon_{0,SCL}} - \frac{\varepsilon_{0,SCL}}{\varepsilon_{0,SCL}^2 + \Omega^2} \right)^2 = 1 + 2V. \quad (3.14)$$

Now we need to study the stability properties of these steady state branches shown in Fig. 3.1.

3.3 Stability of the steady states with respect to Aperiodic Perturbation

Firstly, we determine whether the steady state solutions are aperiodically stable or not. We use the (η, ε) -diagram technique [63] for this purpose. This diagram permits one (i) to find all time-independent states which are consistent with the given boundary condition for the potential, as well as for the specific δ -values and (ii) to determine whether these states are stable or not with respect to the aperiodic (non-oscillatory) perturbations.

To construct the (η, ε) -diagram we use the emitter field strength ε_0 as a parameter. For each value of ε_0 , we develop the dependence of the potential η on the coordinate ζ [from Eqs. (3.9)] by gradually increasing τ and then we find the potential η at the position of the collector δ when τ takes the value T . Varying ε_0 , we complete the (η, ε) -diagram, i. e., the dependence of $\eta(\delta)$ on ε_0 . Now we intersect this curve by the load line $\eta = V$ which corresponds to the boundary condition at the collector. Points of the intersection denote the time independent states of

the diode corresponding to the given δ -value and the fixed collector potential V . The state that corresponds to the negative slope is stable against small aperiodic perturbations and the state which corresponds to the positive slope of the diagram is unstable [150]. We should note that, an instability is developed in the diodic systems due to the positive feed back process through the external circuit of the diode.

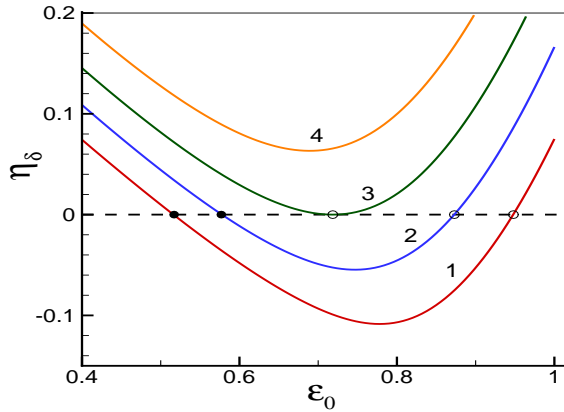


Figure 3.2: The η, ε -diagram for $\Omega = 1.0$ and various values of δ : (1) $\delta = 0.85$, (2) 0.90 , (3) $\delta_{SCL} = 0.947747$, (4) 1.00 ; $V = 0$. Open circle corresponds to an unstable steady state, closed circle – to an aperiodic stable one.

Fig. 3.2 demonstrates exemplarily the η, ε -diagram for $\Omega = 1$ and for several values of δ . Comparing these curves with the curves shown in Fig. 3.1 corresponding to the same Ω , we see that η, ε -diagram does determine all the time independent states of the diode. We can also see that the slope of the diagram is negative for $\varepsilon_0 < \varepsilon_{0,SCL}$, it vanishes at $\varepsilon_0 = \varepsilon_{0,SCL}$, and it is positive for $\varepsilon_{0,SCL} < \varepsilon_0 < \varepsilon_0^0$. Thus, we can conclude that the states which correspond to lower segments of the curves from Fig. 3.1 are stable against small aperiodic perturbations, and those corresponding to the upper segments are unstable.

However, aperiodically stable states can still be oscillatory unstable. In order

to complete our analysis on stability properties of the diode states, we derive the dispersion equation and investigate its properties in following sections.

3.4 The Dispersion equation

We assume that a Bursian diode is functioning in a steady state defined by the Eq. (3.9). The electric field at the emitter is now perturbed and it acquires a time dependence. Accordingly, this perturbation will modify the steady state solutions. The perturbation ansatz is assumed as [72, 150]

$$\begin{aligned}\tilde{\varepsilon}_0(t) &= \varepsilon_0 + \varepsilon_1 \exp(\sigma t), \\ \tilde{\zeta} &= \zeta(\tau) + \zeta_1(\tau) \exp(\sigma t), \\ \tilde{T} &= T + T_1 \exp(\sigma t).\end{aligned}\tag{3.15}$$

Here, ε_0 , $\zeta(\tau)$ and T are the zero-th order terms representing equilibrium solutions [see Eqs. (3.9) and (3.10)], and, ε_1 , T_1 and ζ_1 are the first order perturbed quantities. Therefore, for electric field, one can write upto first order, $\varepsilon = \varepsilon^{(0)} + \varepsilon^{(1)}$, where $\varepsilon^{(0)} = -\tau + \varepsilon_0$ and $\varepsilon^{(1)} = \varepsilon_1 \exp(\sigma t)$. Now, $\tilde{\zeta}(\tau, t)$ should obey the equation

$$\frac{\partial^2 \tilde{\zeta}}{\partial t^2} + \Omega^2 \tilde{\zeta} = -\varepsilon(\tau, t).\tag{3.16}$$

At first order we can get from Eq. (3.15)

$$\frac{\partial^2 \zeta_1}{\partial \tau^2} + 2\sigma \frac{\partial \zeta_1}{\partial \tau} + (\sigma^2 + \Omega^2) \zeta_1 = -\varepsilon_1.\tag{3.17}$$

Using the initial condition, $\zeta_1(\tau = 0) = 0$ and $\partial_\tau \zeta_1(\tau = 0) = 0$, one can readily have

$$\zeta_1 = \frac{\varepsilon_1}{\sigma^2 + \Omega^2} \left[e^{-\sigma\tau} \left\{ \cos \Omega\tau + \frac{\sigma}{\Omega} \sin \Omega\tau \right\} - 1 \right].\tag{3.18}$$

When the emitter electric field is perturbed, as a result of it, the path of the electron trajectory gets modified from the equilibrium solution and it further leads to the modification of the transit time $\tilde{T} = T + T_1 \exp(\sigma t)$ from the equilibrium value T . In first order, from the condition $\tilde{\zeta}(\tilde{T}) = \delta$, we can get

$$T_1 = -\frac{\zeta_1(T_0)}{[2V + 1 - \Omega^2 \delta^2]^{1/2}}. \quad (3.19)$$

To derive Eq. (3.19), we have used the second equation of (3.10). We can get back the corresponding expressions for ζ_1 and T_1 for the state without magnetic field, if we put $\Omega = 0$ in Eq. (3.18) and (3.19) [72]. If collector potential is set at V , then

$$V = -\int_0^\delta \varepsilon(\zeta) d\zeta = -\int_0^{\tilde{T}} \varepsilon(\tau) u_\zeta(\tau) d\tau. \quad (3.20)$$

With the help of Eqs. (3.18) and (3.19), we can have a relation from Eq. (3.20) in first order

$$\int_0^T \zeta_1 d\tau + \varepsilon_1 \delta = 0. \quad (3.21)$$

Substituting the expression of ζ_1 from Eq. (3.18) into Eq. (3.21), we can have the dispersion relation of the form

$$F(\sigma; \delta, T) = -e^{-\sigma T} \left[2\sigma \cos \Omega T + \frac{\sigma^2 - \Omega^2}{\Omega} \sin \Omega T \right] + \delta(\sigma^2 + \Omega^2)^2 + 2\sigma - (\sigma^2 + \Omega^2)T = 0. \quad (3.22)$$

It is interesting to note that this equation coincides with the dispersion relation (67), obtained in Ref. [26] for the Pierce diode, when we replace the Larmor frequency Ω^2 in place of the neutralization parameter γ , which equals to the ratio of the constant ion background density to the emitter electron density. However, relations between T , δ and ε_0 turn out to be different for both diodes. If we set

$\Omega = 0$ in Eq. (3.22), we get

$$-e^{-\sigma T} [2 + \sigma T] + \delta \sigma^3 + 2 - \sigma T = 0. \quad (3.23)$$

It is the dispersion relation for the case when there is no external magnetic field [72].

3.5 Stability Analysis

Let us now study the eigen-frequencies $\sigma(\delta, V) = \gamma(\delta, V) + i\omega(\delta, V)$ of the dispersion relation (3.22). We should note that there is a countable number of eigen-modes for each and every value of the parameters V and δ ; moreover, the main eigen-mode (one that grows at the fastest rate when the solution is unstable or is damped at the slowest rate when the solution is stable) turns out to be an aperiodic mode. For a fixed parameter value V , the curves of $\gamma(\delta, V)$ or $\omega(\delta, V)$ are named as branches of instability.

At first, let us consider the aperiodic branches of instability (*A*-branches). They are determined by the roots of Eq. (3.22) for real σ 's ($\omega = 0$ and $\sigma = \gamma$):

$$\begin{aligned} & \exp(-\gamma T) \left[2\gamma \cos \Omega T + \frac{\gamma^2 - \Omega^2}{\Omega} \sin \Omega T \right] \\ & - (\Omega^2 + \gamma^2)^2 \delta + (\Omega^2 + \gamma^2) T - 2\gamma = 0. \end{aligned} \quad (3.24)$$

For $\gamma = 0$, Eq. (3.24) gives

$$\Omega^3 \delta - \Omega T + \sin \Omega T = 0. \quad (3.25)$$

Comparing (3.25) with (3.12), we can infer that the aperiodic growth rate vanishes just at *SCL* point. The branches end at 0 points. At this stage [151] $\varepsilon_0^0 = \sqrt{2 - \Omega^2}$

and

$$\begin{aligned} \delta_0 &= \frac{1}{\Omega^2} T_0 + \frac{1}{\Omega} \left(1 - \frac{1}{\Omega^2} \right) \sin \Omega T_0 + \frac{1}{\Omega^2} \sqrt{2 - \Omega^2} (\cos \Omega T_0 - 1), \\ u_\zeta^2(T_0) + \Omega^2 \delta_0^2 - (1 + 2V) &= 0, \\ u_\zeta(T_0) &= \frac{1}{\Omega^2} + \left[1 - \frac{1}{\Omega^2} \right] \cos \Omega T_0 - \frac{1}{\Omega} \sqrt{2 - \Omega^2} \sin \Omega T_0. \end{aligned} \quad (3.26)$$

The function $T_0(\Omega)$ can be calculated from the second equation, and δ_0 from the first equation of Eq. (3.26).

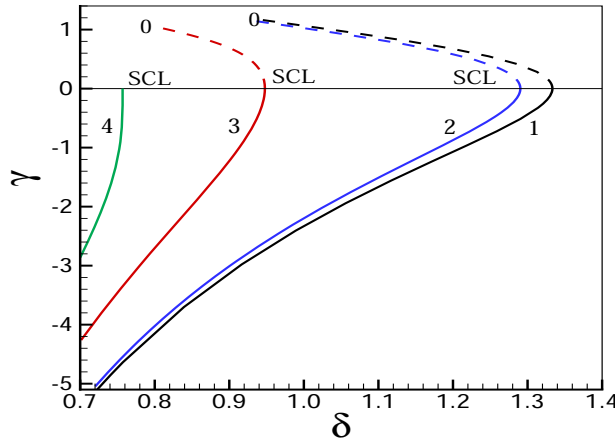


Figure 3.3: Growth rate γ vs gap δ for various values of Ω : (1) $\Omega = 0$, (2) 0.3, (3) 1.0, (4) 1.32; $V = 0$.

Fig. 3.3 exhibits A -branches for various values of Ω . It is seen that the growth rate at such a branch is negative for $\varepsilon_0 < \varepsilon_{0,SCL}$. It signifies that corresponding steady-state solutions are stable relative to the small aperiodic perturbations. Then it vanishes at $\varepsilon_0 = \varepsilon_{0,SCL}$, and it becomes positive for $\varepsilon_{0,SCL} < \varepsilon_0 < \varepsilon_0^0$, i. e., corresponding steady-state solutions are unstable for this region. This picture is similar to the Fig. 3.3 presented in [66], where the stability properties of steady-state solutions were studied for a Bursian diode with no magnetic field.

Now the oscillatory branches of instability (O -branches) are determined by the complex roots of Eq. (3.22). Let us prove that these branches can not cross the

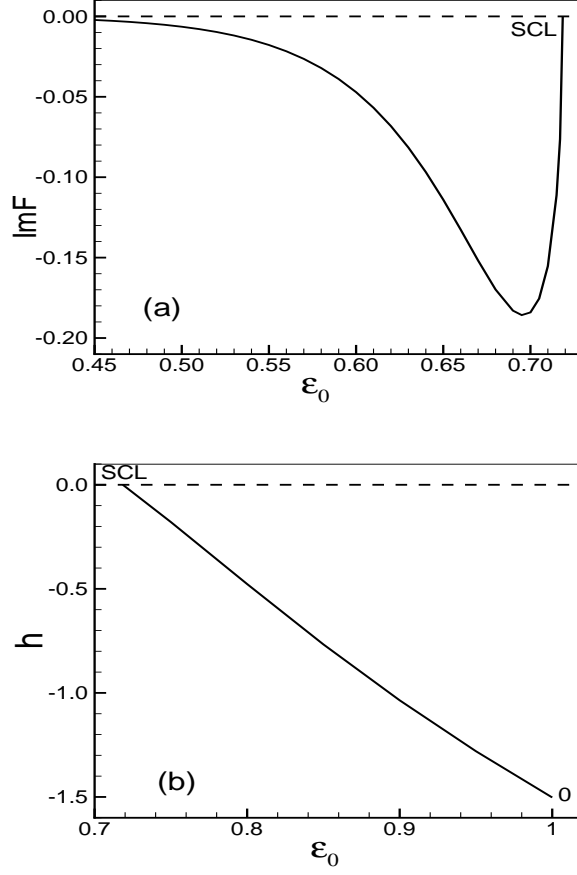


Figure 3.4: (a) Imaginary part of the dispersion equation (3.22) vs ε_0 for the branch II of the steady state solutions at $\gamma = 0$; (b) the radicand of Eq. (3.29) vs ε_0 for the branch I of the steady state solutions. Positions of *SCL* and 0 point are marked. $\Omega = 1.0$. $V = 0$.

axis $\gamma = 0$. Substituting $\sigma = \gamma + i\omega$ into Eq. (3.22) and separating the real and the imaginary parts, we get

$$\begin{aligned}
& \exp(-\gamma T) \left(2\gamma \cos \Omega T \cos \omega T + 2\omega \cos \Omega T \sin \omega T \right. \\
& \left. + \frac{\gamma^2 - \omega^2 - \Omega^2}{\Omega} \sin \Omega T \cos \omega T + 2\frac{\gamma\omega}{\Omega} \sin \Omega T \sin \omega T \right) \\
& - \left[(\gamma^2 - \omega^2 + \Omega^2)^2 - 4\gamma^2\omega^2 \right] \delta + (\gamma^2 - \omega^2 + \Omega^2) T - 2\gamma = 0, \\
& \exp(-\gamma T) \left(2\omega \cos \Omega T \cos \omega T - 2\gamma \cos \Omega T \sin \omega T + \right. \\
& \left. + 2\frac{\gamma\omega}{\Omega} \sin \Omega T \cos \omega T - \frac{\gamma^2 - \omega^2 - \Omega^2}{\Omega} \sin \Omega T \sin \omega T \right) \\
& - 4\gamma\omega (\gamma^2 - \omega^2 + \Omega^2) \delta + 2\gamma\omega T - 2\omega = 0. \tag{3.27}
\end{aligned}$$

This system of equations must be supplemented by the relations given in Eq. (3.10)

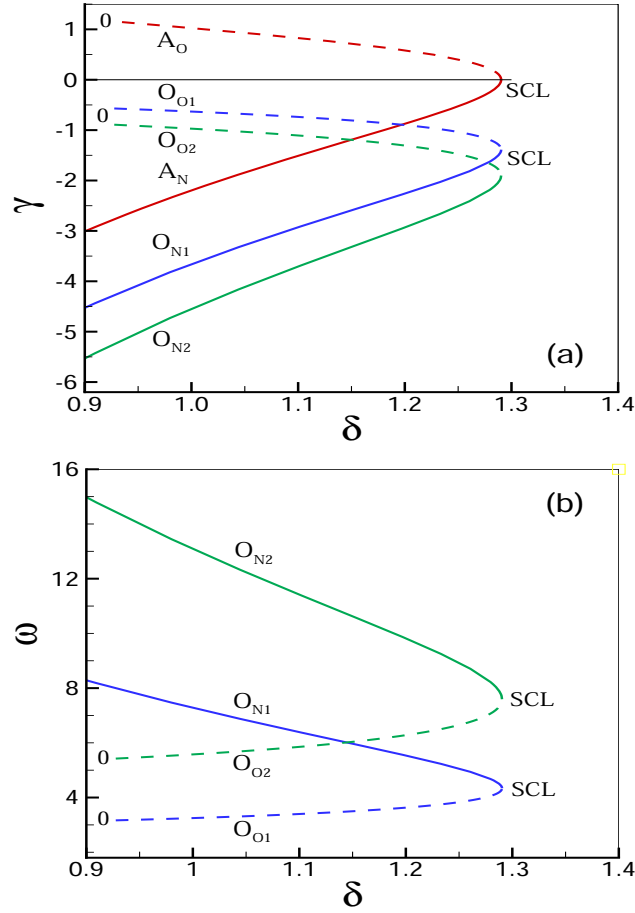


Figure 3.5: Dispersion curves for branches I and II of steady state solutions: the solid curves correspond to branch I, and the dashed curves, to branch II. Curves A are aperiodic branches, and curves O are oscillatory branches. (a) Growth rate γ and (b) frequency ω . Positions of SCL and 0 point are marked. $\Omega = 0.3$. $V = 0$.

which connect T with ε_0 and δ .

For $\gamma = 0$, we can have from Eq. (3.27)

$$\begin{aligned}
 2\omega \cos \Omega T \sin \omega T - \frac{\omega^2 + \Omega^2}{\Omega} \sin \Omega T \cos \omega T \\
 &= (\omega^2 - \Omega^2)^2 \delta + (\omega^2 - \Omega^2) T, \\
 2\omega \cos \Omega T \cos \omega T + \frac{\omega^2 + \Omega^2}{\Omega} \sin \Omega T \sin \omega T &= 2\omega.
 \end{aligned} \tag{3.28}$$

When both equations of (3.28) are squared and then added, we find

$$\begin{aligned}
4\omega^2 \cos^2 \Omega T + \frac{(\omega^2 + \Omega^2)^2}{\Omega^2} \sin^2 \Omega T &= \left[(\omega^2 - \Omega^2)^2 \delta + (\omega^2 - \Omega^2) T \right]^2 + 4\omega^2, \\
\left[\frac{(\omega^2 + \Omega^2)^2}{\Omega^2} - 4\omega^2 \right] \sin^2 \Omega T &= \left[(\omega^2 - \Omega^2)^2 \delta + (\omega^2 - \Omega^2) T \right]^2, \\
\left[(\omega^2 - \Omega^2) \delta + T \right]^2 - \frac{\sin^2 \Omega T}{\Omega^2} &= 0. \quad (3.29)
\end{aligned}$$

Eq. (3.29) leads us to

$$\frac{\omega}{\Omega} = \left(\frac{\Omega^3 \delta - \Omega T + \sin \Omega T}{\Omega^3 \delta} \right)^{1/2}. \quad (3.30)$$

However, we should keep in mind that “spurious” roots may occur as Eq. (3.28) is squared. Therefore, each time we need to check the validity of the solution (3.30) by substituting them into Eq. (3.28). Besides, we should note that for the negative value of the radicand in (3.30), solution for ω can not exist.

Equation (3.12) implies that the radicand of (3.30) will vanish at SCL. It happens because of the fact that, at the *SCL* point the eigen-value $\sigma = 0$. In Fig. 3.4, imaginary part of the dispersion function $\{Im(F)\}$ and the radicand of Eq. (3.30) $\{h = \Omega^3 \delta - \Omega T + \sin \Omega T\}$ are built for $\Omega = 1.0$ ($\varepsilon_0^0 = 1.0$ and $\varepsilon_{0,SCL} = 0.7185$). Fig. 3.4b shows that h is negative for $\varepsilon_0 > \varepsilon_{0,SCL}$. On the other hand, Fig. 3.4a demonstrates that, for $\varepsilon_0 < \varepsilon_{0,SCL}$, the solution (3.30) does not obey the second equation of (3.28). Same results are obtained for any other values of Ω . Thus, we can assert that an oscillatory branch can not cross the line $\gamma = 0$.

In Fig. 3.5 and Fig. 3.6, oscillatory dispersion branches ($\omega \neq 0$) are built for $\Omega = 0.3$ and $\Omega = 1$ respectively. For a fixed value of V , each curve corresponds to a particular eigen-mode. The symbol “ O_N ” represents the oscillatory C normal branch or branch I ($\varepsilon_0 < \varepsilon_{0,SCL}$) and “ O_O ” refers to the oscillatory C overlap branch or branch II ($\varepsilon_{0,SCL} < \varepsilon_0 < \varepsilon_0^0$). The suffix indices indicate the numbers of relevant

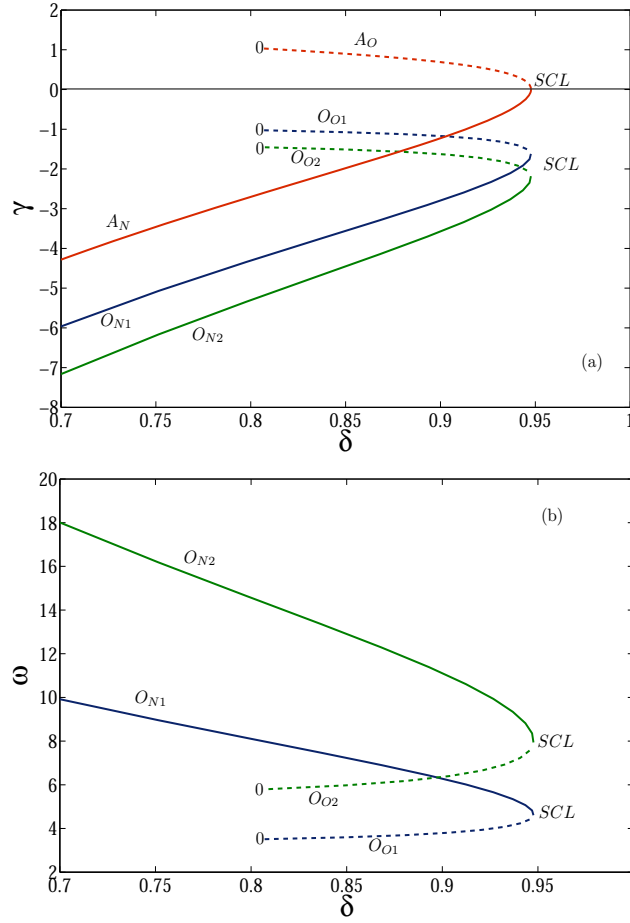


Figure 3.6: Dispersion curves for branches I and II of steady state solutions: the solid curves correspond to branch I, and the dashed curves, to branch II. Curves A are aperiodic branches, and curves O are oscillatory branches. (a) Growth rate γ and (b) frequency ω . Positions of SCL and 0 point are marked. $\Omega = 1$. $V = 0$.

dispersion branches. Two oscillatory branches are shown in Fig. 3.5 and Fig. 3.6 for two different values of Ω . The solid curves correspond to the oscillatory C overlap branch, and the dashed curves correspond to the oscillatory C normal branch. It is clear from Fig. 3.5a and Fig. 3.6a that these branches have negative growth rates. For higher numbers of oscillatory branches, the magnitude of negative growth rates and frequency becomes higher. The characteristics of the dispersion branches for the diode with transverse magnetic field are similar to the Bursian diode with no magnetic field [67]. As an effect of the nonzero magnetic field, the width of the

unstable region is diminished when the strength of the external magnetic field is increased.

3.6 Summary

The results can be summarized as follows. We have studied the stability properties of the steady state solutions of a Bursian diode in presence of constant transverse magnetic field. Our analysis is valid up to the limit where the longitudinal velocity of an electron vanishes for the first time within the inter-electrode region. With the help of the Lagrangian description, the steady state solutions of the Bursian diode are obtained and they are shown to belong to two distinct branches of “ $\varepsilon_0 - \delta$ ” diagram. The dispersion relation is obtained from the time dependent basic equations using first order perturbation theory. Utilizing this dispersion relation, aperiodic and oscillatory branches for the fixed value of V and δ are developed. It is shown that the solutions corresponding to branch I ($\varepsilon \leq \varepsilon_{0,SCL}$) are always stable, and those of branch II ($\varepsilon_{0,SCL} < \varepsilon_0 \leq \varepsilon_0^0$) are unstable with respect to the small aperiodic perturbation. When the strength of the magnetic field is increased, the width of the unstable region (branch II) gradually decreases and vanishes at $\Omega \approx 1.32$. The method of “ $\eta - \varepsilon$ ” diagram leads us to same results.

Chapter 4

Stationary states of a Bursian diode in presence of transverse magnetic field representing partial or total electron reflection

In this chapter, the steady-states of a planar vacuum diode are investigated in the presence of an external transverse magnetic field when the emitted electrons are reflected back to the emitter by the virtual cathode. With the help of a numerical scheme, the features of the steady-state solutions are explored in the Eulerian frame. On the other hand, exact analytical formulas for the potential and velocity profiles have been derived with the Lagrangian description.

4.1 Introduction

The results of the previous studies on the Bursian diodes show that a class of steady-state solutions exists which corresponds to the electron reflections from the virtual cathode [66, 67, 69, 134, 135, 138, 148, 152]. Generally, the potential distribution within the diode gap region is a single minimum function and this potential minimum serves as a potential barrier to the electron flow [55, 58, 113, 133, 136, 137, 146]. In the absence of magnetic field, the situation of electron reflection appears when kinetic energy of the emitted electron becomes equal to the potential energy at the position of minimum potential [66, 148]. If the velocity distribution function of the emitted electron beam is a δ -function, all the electrons are reflected back to the emitter by the potential barrier (virtual cathode). But in reality, the electrons are always injected from the emitter with a small velocity spread. So, in practical situations, there will be always a few number of electrons which can overcome the potential barrier with a small but nonzero velocity [67].

In first chapter, assuming the emitted electrons to be purely monoenergetic, we have studied the effect of the transverse magnetic field on the steady-state solutions of the Bursian diode up to the limit, when the longitudinal component of the electron velocity becomes zero within inter-electrode region for the first time. It is also explained from the energy conservation principle that, for the case of “zero-point” solution, at the position of zero electron-velocity, potential profile approaches to a threshold value. At this condition, electrons are completely turned around by the magnetic field when they are emitted from the emitter in monoenergetic way. But, if there is a small velocity spread in the emitted electron beam, they can be

reflected back partially or completely depending on the value of the applied magnetic field. In this present work, we report the partial or complete reflection of the electrons in a Bursian diode in presence of transverse magnetic field. The problem has been solved with two techniques: the Euler and the Lagrange formalism. For our purpose, we shall follow the same model and unit system which are described in chapter two and three.

4.2 Complete electron-reflection: The Euler method

As it was shown in second chapter, the potential distributions, $\eta(\zeta)$ which is consistent with the distributions of the electrons, should be confined within a region limited by a square parabola $p(\zeta; \omega)$ (Fig. 4.1):

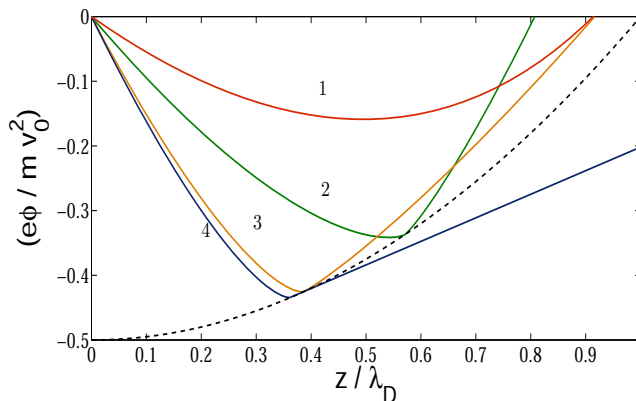


Figure 4.1: Normalized potential $e\varphi/(mv_0^2)$ as a function of normalized space $\zeta = z/\lambda_D$ for various values of $\varepsilon_0 = eE_0\lambda_D/(mv_0^2)$: (1) $\varepsilon_0 = 0.6$ (no electrons are turned due to a magnetic field), (2) 1.0 and (3) 1.61 (a portion of the injected electrons is turned due to a magnetic field), and (4) 1.7321 (all electrons are turned due to a magnetic field). Dashed curve corresponds to $\varphi = p(z, \omega) = (e/2m)(\omega^2 z^2 - v_0^2)$; $\omega/\omega_0 = 1.0$; $U = 0$.

$$\eta(\zeta) \geq p(\zeta; \Omega) \equiv \frac{1}{2} (\Omega^2 \zeta^2 - 1). \quad (4.1)$$

We now consider the case when there is a point ζ_H within the inter-electrode gap where the electrons are completely turned back and move toward emitter under

certain emitter electric field strength. At this point, the longitudinal component of the velocity u_ζ vanishes, so for the potential at this point, we can have a relationship

$$1 + 2\eta_H - \Omega^2 \zeta_H^2 = 0. \quad (4.2)$$

Here $\eta_H = \eta(\zeta_H)$. To the left of the point ζ_H , the PDs lie within a parabolic region $p(\zeta; \Omega)$ [Eq. (4.1)]. It is clear that, for any point where $\zeta \leq \zeta_H$, the velocity of electron returning toward emitter differs in sign only from that of its first passage at this point. So, the electron density at any point in this region is twice the density for the electrons with velocities $u_\zeta(\zeta) > 0$. Within the region $\zeta \leq \zeta_H$, the PD obeys the differential equation

$$\frac{d^2\eta}{d\zeta^2} = 2 [1 + 2\eta - \Omega^2 \zeta^2]^{-1/2}. \quad (4.3)$$

The boundary conditions for the potential at the electrodes are

$$\eta(0) = 0, \quad \eta(\delta) = V. \quad (4.4)$$

As derived in second chapter, the differential equation (4.3) reduces to a system of difference equations. The potential profile is evaluated first to the left of the potential minimum, and the coordinates of the potential minimum are calculated. The calculation in this region is carried out via a numerical scheme shown in chapter two. A value of the potential at the minimum η_m is taken. Its true value is obtained in the course of calculation. In a region between the emitter and the location of the potential minimum, a potential frame is taken: $\eta_k = \eta_{k-1} + \Delta\eta_k$, $k = 1, \dots, N$, $\eta_0 = 0$. Within each layer (ζ_{k-1}, ζ_k) the PD is approximated with a

straight line. The system of difference equations

$$\begin{aligned}
\eta_k &= \eta_{k-1} + \Delta\eta_k, \\
\varepsilon_k^2 &= \varepsilon_{k-1}^2 + 2\beta G(\zeta_{k-1}, \eta_{k-1}, \varepsilon_{k-1}, \eta_k, \varepsilon_k; \Omega), \\
\bar{\varepsilon}_k &= q_k \varepsilon_{k-1} + (1 - q_k) \varepsilon_k, \\
\zeta_k &= \zeta_{k-1} - (\eta_k - \eta_{k-1}) / \bar{\varepsilon}_k
\end{aligned} \tag{4.5}$$

is solved taking $\beta = 2$ and under the conditions as follows:

$$\eta_0 = 0, \quad \varepsilon_0 = \tilde{\varepsilon}_0, \quad \zeta_0 = 0. \tag{4.6}$$

Depending on the value of Ω , the function G in (4.5) reads as

$$\begin{aligned}
-\frac{|\bar{\varepsilon}_k|}{\Omega} \left[\sin^{-1} \left(\frac{B - 2[(\eta_k - \eta_{k-1})/\bar{\varepsilon}_k^2]\Omega^2}{\sqrt{-\Delta}} \right) - \sin^{-1} \left(\frac{B}{\sqrt{-\Delta}} \right) \right], \quad \Omega > 0, \\
\sqrt{1 + 2\eta_k} - \sqrt{1 + 2\eta_{k-1}}, \quad \Omega = 0.
\end{aligned} \tag{4.7}$$

Here

$$\begin{aligned}
A &= 1 + 2\eta_{k-1} - \zeta_{k-1}^2 \Omega^2 > 0, \\
B &= 2 \left[1 + (\zeta_{k-1}/\bar{\varepsilon}_k) \Omega^2 \right], \\
C &= -(1/\bar{\varepsilon}_k^2) \Omega^2 < 0, \\
\Delta &= 4AC - B^2 = -4 \left\{ 1 + [(1 + 2\eta_{k-1} + 2\zeta_{k-1}\bar{\varepsilon}_k)/\bar{\varepsilon}_k^2] \Omega^2 \right\} < 0.
\end{aligned} \tag{4.8}$$

Then, PD is calculated to the right of the point of minimum. For a certain value of the index k (say, K), sign of the radicand in the formula for velocity (4.2) is negative. At this step, the iteration over η_K is carried out till the radicand vanishes. At this point ζ_K takes the value ζ_H .

To the right of the point ζ_H , there are no electrons as they are completely reflected back by the magnetic field. The electric field strength at this point turns

out to be negative. To the right of this point, the potential grows linearly as space coordinate increases:

$$\eta = \eta_H - \varepsilon_H(\zeta - \zeta_H). \quad (4.9)$$

In this region, $\varepsilon_H = \varepsilon(\zeta_H) < 0$. For a fixed value of V (potential difference between the electrodes), we get the value of the inter-electrode gap from Eq. (4.9):

$$\delta = \zeta_H - (V - \eta_H)/\varepsilon_H. \quad (4.10)$$

We should note that, for the case of complete reflection, at first the PD gradually approaches a point (ζ_H, η_H) which is lying on the parabola (4.1). Then, it leaves this region and goes directly towards a point referring to the collector location (line 4 in Fig. 4.1).

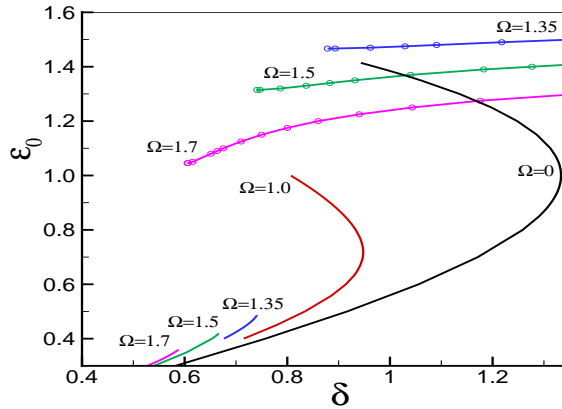


Figure 4.2: The “ $\varepsilon_0 - \delta$ ” curves are drawn for various values of Ω : (1) $\Omega = 0$, (2) 1.0, (3) 1.35, (4) 1.5 and (5) 1.7; $V = 0$. Two regimes are only included: no electrons are turned by magnetic field, and all electrons are turned (marked by open circles).

In Fig. 4.2, the dependencies of ε_0 on δ are shown for the two following cases, when there is no reflection of electrons and when the electrons are completely reflected by the magnetic field (marked by circles). For $\Omega = 1.0$, the second part of the branch (corresponding to complete reflection) begins with $\delta \approx 2.5$. Therefore,

it does not appear in this figure. At $\Omega \rightarrow 0$, this part of the branch goes to infinity. The first part of the branch contains a right bifurcation point, which was termed as “SCL” and it ends at a “zero-point” [see chapter two]. When all of the electrons are turned by the magnetic field, the current on the collector is zero and it corresponds to the second part of the solution branch.

4.3 Partial electron-reflection: The Euler method

In earlier works, [66, 67, 148] for the case of Bursian diode with no magnetic field, the region of solutions regarding the partial electron reflection was explored. Considering nearly monoenergetic electron beam with a small velocity spread, a whole class of steady-state solutions was derived and the potential profiles corresponding to the partial reflection of electrons were shown. These are the PD with the virtual cathode (VC). The VC-height equals electron energy at the emitter position. The existence of such solutions was also approved experimentally [138]. To describe this class of solutions, the literature includes a reflection coefficient r which describes the eventual “split” of the electron beam in terms of the reflected part from VC and those overcoming it [35, 148].

In chapter two it was shown that, in presence of the transverse magnetic field, the ζ -component of electron velocity decreases with space coordinate ζ and becomes a tangent to a line $u_\zeta = 0$ at a point where u_ζ vanishes. Then u_ζ begins to increase. Thus, zero velocity position is actually a point type. As physical situations demand, taking into consideration a small velocity spreading within the beam, we can assume that all the electrons would not be turned around by the magnetic field at the point ζ_r (the point where u_ζ vanishes). A portion of such

electrons can overcome this point with velocities little higher than zero and flow toward collector. To involve “electron beam splitting” at a point ζ_r , we also introduce reflection coefficient r [35, 148]. In this situation, there are two flows in the region between the emitter and the point ζ_r : the direct and the reverse flow. Since at any point ζ the velocities of direct and reverse particles coincide absolutely, the densities of the direct and reverse particles become $1/u_\zeta$ and r/u_ζ , respectively. Thus, in this region, the total density of the electrons is $(1+r)/u_\zeta$. To the right of the point ζ_r , there is the direct electron flow with a weight $1-r$.

When a portion of the injected electrons is turned around, all PDs remain within a region limited by a parabola $p(\zeta; \Omega)$ [Eq. (4.1)], and the function $\eta(\zeta)$ becomes a tangent to this parabola at the point of reflection ζ_r (see curves 2, 3 and the dashed curve in Fig. 4.1). In this situation, the product of the density and the longitudinal component of electron velocity (coming from the continuity equation at steady state) at a point ζ should be modified as

$$n(\zeta)u_\zeta(\zeta) = H(\zeta; \zeta_r, r) \equiv (1+r)\Theta(\zeta_r - \zeta) + (1-r)\Theta(\zeta - \zeta_r). \quad (4.11)$$

Here, splitting of the electron beam at the turning point ζ_r is taken into consideration. As a result, instead of Eq. (4.3), the equation for PD becomes

$$\frac{d^2\eta}{d\zeta^2} = \frac{H(\zeta; \zeta_r, r)}{[1 + 2\eta - \Omega^2\zeta^2]^{1/2}}. \quad (4.12)$$

One can see that, now in Eq. (4.12) an extra parameter r arises. Its value is determined through the course of the calculations. Solution algorithm is as follows. At a given value $\varepsilon_0 = \tilde{\varepsilon}_0$, a value of the coefficient r is taken. First, Eq. (4.12) is integrated on a path from the emitter position to the location of potential minimum

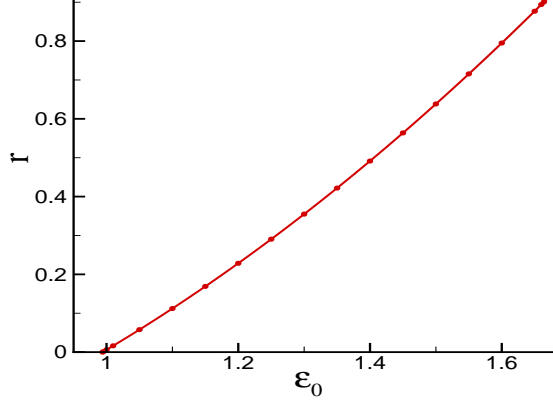


Figure 4.3: Coefficient r vs ϵ_0 for $\Omega = 1.0$; $V = 0$.

with the boundary conditions

$$\eta(\zeta = 0) = 0, \quad \frac{d}{d\zeta}[\eta(\zeta = 0)] = -\tilde{\epsilon}_0. \quad (4.13)$$

The position (ζ_m) and the value (η_m) of the potential minimum are determined from the zero electric field condition. Further, Eq. (4.12) is integrated with the boundary conditions

$$\eta(\zeta = \zeta_m) = \eta_m, \quad \frac{d}{d\zeta}[\eta(\zeta = \zeta_m)] = 0, \quad (4.14)$$

from the point ζ_m to the point ζ_r , where electron velocity u_ζ vanishes. Now, iterating over a parameter r , we obtain that for some value of r , u_ζ turns out to be a tangent to the straight line $u_\zeta = 0$. As a result, we obtain the relation between coefficient r and ϵ_0 and we determine ζ_r , ϵ_r and η_r . And at last, Eq. (4.12) is integrated from a point ζ_r to the collector and δ is determined.

On the path from the emitter ($\zeta = 0$) to the electron turning point (ζ_r), Eq. (4.12) reduces to the system of difference equations (4.5) with $\beta = 1 + r$ and $\Delta\eta_k = \eta_m/N$. To the right of the turning point, there is also a system of equations as shown in Eq. (4.5) with $\beta = 1 - r$ and $\Delta\eta_k = (V - \eta_r)/N$.

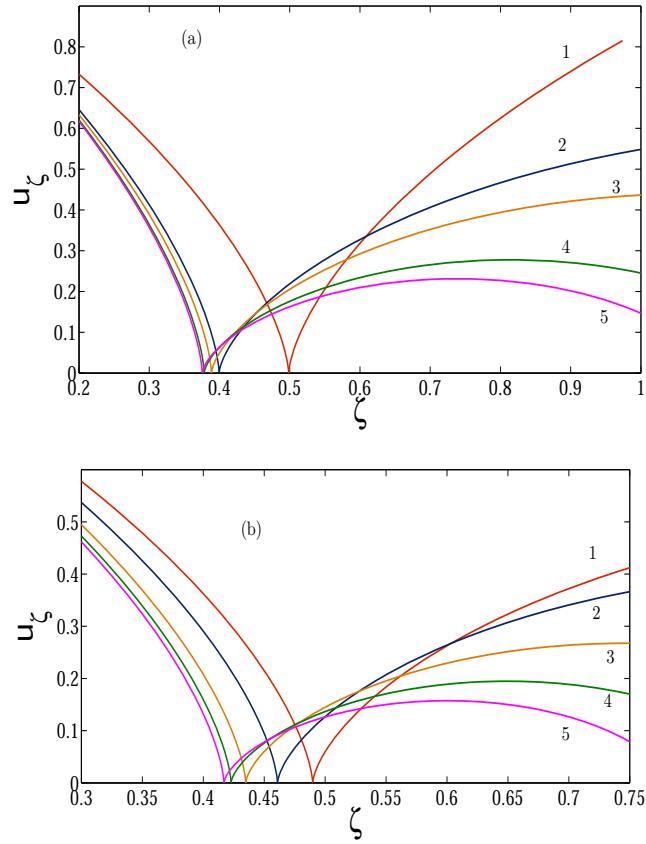


Figure 4.4: Velocity profile within the interelectrode gap drawn for different ε_0 values: Fig. (a): $\Omega = 1$; (1) $\varepsilon_0 = 1.20$, (2) 1.55, (3) 1.60, (4) 1.65, and (5) 1.664; Fig. (b): $\Omega = 1.35$; (1) $\varepsilon_0 = 1.10$, (2) 1.20, (3) 1.30, (4) 1.35, and (5) 1.375. $V = 0$.

In the course of these calculations, ε_0 is increased gradually and for some certain value of it (say, $\varepsilon_0 = \varepsilon_0^0$), electron velocity u_ζ vanishes first time. At this moment, we have $r = 0$. When ε_0 is increased further, the coefficient r grows too. The dependence of r on ε_0 is obtained in the process of the calculation, and it is shown in Fig. 4.3 for $\Omega = 1.0$. Fig. 4.4 exhibits the velocity profile $u_\zeta(\zeta)$ for a number of ε_0 values. It is seen that, these curves really are the tangents to the line $u_\zeta = 0$.

In Fig. 4.5, dependence of ε_0 on δ is shown for several Ω values. In this figure, the solutions corresponding to the “partial” reflection of electrons are also taken

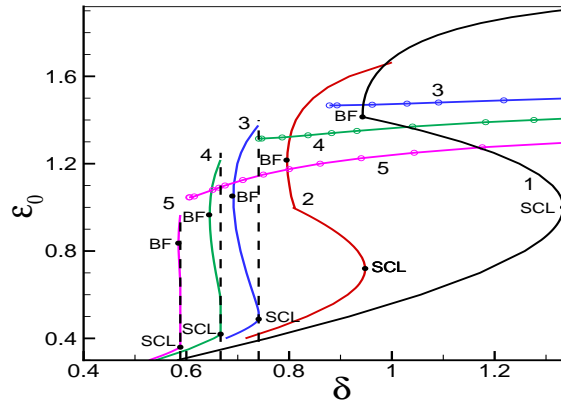


Figure 4.5: The “ $\varepsilon_0 - \delta$ ” curves are drawn for various values of Ω : (1) $\Omega = 0$, (2) 1.0, (3) 1.35, (4) 1.5, and (5) 1.7; $V = 0$. The regions with partial electron turning are included here. Dashed vertical lines corresponds to a dependence $\delta = 1/\Omega$.

into consideration. Fig. 4.5 shows that two bifurcation points arise in each curve : SCL and BF . This feature was also reported for the case of electron reflection in classical Bursian diode with no magnetic field [35, 69, 67]. Fig. 4.5 also shows that the BF point does not lie on the reflection threshold (zero point) and the reflection coefficient $r > 0$ at this point. For example, at a point BF , we have $\varepsilon_0 \approx 1.2$, $r \approx 0.23$ for $\Omega = 1.0$, and $\varepsilon_0 \approx 1.0$, $r \approx 0.418$ for $\Omega = 1.35$. It is also evident from Fig. 4.5 that the region of hysteresis (the region between SCL and BF) gets narrowed as magnetic field increases. This area disappears practically at $\Omega \approx 1.7$. Thus, a rather strong magnetic field (when Larmor radius is approximately equal to δ_{SCL}) leads to the hysteresis disappearance. This effect arises due to the fact that the presence of the transverse magnetic field modifies the electron trajectories and introduces velocity spread in the injected electron beam so that its distribution function acquires a non beam-like nature. Analogous phenomenon takes place when we simply introduce spreading in velocity distribution function of emitted electrons (see, e. g., [67, 152]).

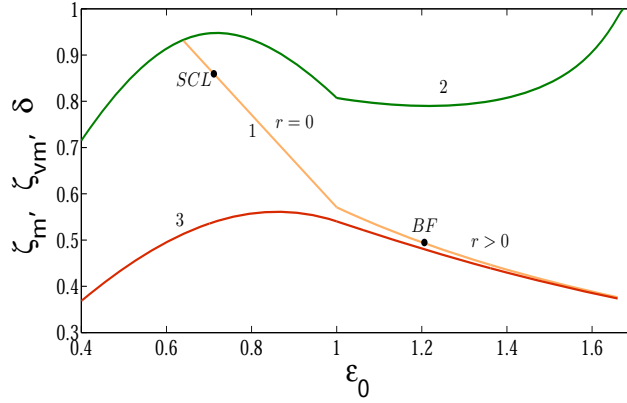


Figure 4.6: The dependence of the position of velocity minimum (curve 1), collector position (curve 2) and the position of potential minimum (curve 3) on ε_0 , for $\Omega = 1$ and $V = 0$. Closed circles refer to the bifurcation points.

Again, we return to Fig. 4.5. At $\Omega \approx 1.32$, a state is reached when the zero point and the point *SCL* merge with each other at the collector position. With the further increase of ε_0 (and consequently the coefficient r), zero point continues to stay on the collector and (ε_0, δ) -diagram goes almost vertically. At $\Omega = 1.7$, the vertical section of this diagram turns out to be rather large.

The variation of the location of minimum electron velocity (ζ_{vm}) on ε_0 for $\Omega = 1.0$ is presented in Fig. 4.6. At first, this point lies on the collector (δ), then, with the increase of ε_0 , it begins to approach to the point of potential minimum (ζ_m). It should be noted that, for $\Omega < 1.32$, the turning point arises within the inter-electrode gap for the first time (e.g., in Fig. 4.6 it is the knee point of the curve 1 between $r = 0$ and $r > 1$). At $\Omega = 1.32$, this knee point appears at the collector position and takes the value δ_{SCL} . At this stage, for the relevant gap value, we can have a relationship $\delta = (1 + 2V)^{1/2}/\Omega$. Basically, at $\Omega = 1.32$, the transition to the regime with electron reflection does occur at the point *SCL*.

Our results also reveals that, with the increase of ε_0 (and respectively r), a

moment appears when the electron velocity u_ζ turns out to be zero again, i. e., the electrons face another turning point (see Fig. 4.7). At this very moment, the reflection coefficient does not reach its limiting value 1. For example, we have $\varepsilon_0 \approx 1.664$, $r \approx 0.9007$ for $\Omega = 1.0$, and $\varepsilon_0 \approx 0.965$, $r \approx 0.91819$ for $\Omega = 1.7$.

Apparently, with the further increase of ε_0 , the number of turning point would increase. In addition, the distance between the turning points and the value of the velocity maximum in each turn would decrease. At $r \rightarrow 1$, the number of turning points would go to infinity. This phenomena is further studied in the following section.

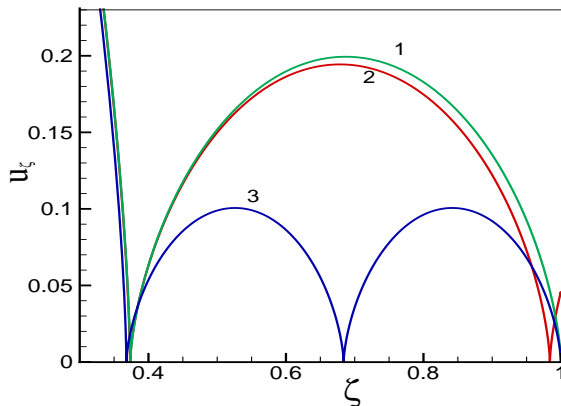


Figure 4.7: Velocity profile within the interelectrode gap drawn for case of several turning-about points: (1) $\varepsilon_0 = 1.673499$ ($r = 0.9003$), (2) $\varepsilon_0 = 1.675$ – second turning-about point lies within the gap, (3) $\varepsilon_0 = 1.7027$ ($r = 0.949697$) – third turning-about point lies on the collector. $\Omega = 1$, $V = 0$.

4.4 Partial electron-reflection: The Lagrange method

In this section, we solve the problem using the Lagrange variables. In 1D time-independent case, we start with the basic governing equations which are the continuity and the momentum equations along with the Poisson's equation. When they are written in terms of the dimensionless quantities, we get

$$\begin{aligned}
nu_\zeta &= H(\zeta; \zeta_r, r), \\
u_\zeta \frac{du_\zeta}{d\zeta} &= -\varepsilon - \Omega u_\chi, \quad u_\zeta \frac{du_\chi}{d\zeta} = \Omega u_\zeta, \\
\frac{d\varepsilon}{d\zeta} &= -n.
\end{aligned} \tag{4.15}$$

Here, the function $H(\zeta; \zeta_r, r)$ is determined by Eq. (4.11). The boundary conditions to be used are, $n(\zeta = 0) = 1$, $u_\zeta(\zeta = 0) = 1$, $u_\chi(\zeta = 0) = 0$, electric potential, $\eta(\zeta = 0) = 0$, and field $\varepsilon(\zeta = 0) = \varepsilon_0$. Here, ε_0 serves as a parameter.

To solve these set of non-linear equations, we introduce the Lagrangian coordinate τ and the Lagrange transformation,

$$\zeta = \int_0^\tau u_\zeta(\tau') d\tau'.$$

Thus, $u_\zeta d/d\zeta = d/d\tau$. Eqs. (4.15) take the form

$$\begin{aligned}
nu_\zeta &= H(\zeta; \zeta_r, r), \\
\frac{du_\zeta}{d\tau} &= -\varepsilon - \Omega u_\chi, \quad \frac{du_\chi}{d\tau} = \Omega u_\zeta, \\
\frac{d\varepsilon}{d\tau} &= -H(\zeta; \zeta_r, r).
\end{aligned} \tag{4.16}$$

Here, we ought to take into account that the electron flow splits at the point ζ_r where

$$u_\zeta(\tau = \tau_r) = 0. \tag{4.17}$$

Combining Eqs. (4.16) we obtain

$$\frac{d^2 u_\zeta}{d\tau^2} + \Omega^2 u_\zeta = H(\tau; \tau_r, r). \tag{4.18}$$

Using the stated boundary conditions, solution in terms of the Lagrange coordinate to the left of the point ζ_r can be found as

$$u_\zeta(\tau) = \frac{1+r}{\Omega^2} + \left(1 - \frac{1+r}{\Omega^2}\right) \cos \Omega\tau - \frac{\varepsilon_0}{\Omega} \sin \Omega\tau. \tag{4.19}$$

The relation between the Euler variable ζ and the Lagrange one τ for $\tau < \tau_r$ can be obtained as,

$$\zeta = \frac{1+r}{\Omega^2}\tau + \frac{1}{\Omega} \left(1 - \frac{1+r}{\Omega^2}\right) \sin \Omega\tau + \frac{\varepsilon_0}{\Omega^2}(\cos \Omega\tau - 1). \quad (4.20)$$

If the electrons are not turned back at all, then $r = 0$ and the formulas (4.19) and (4.20) coincide with the relevant formulas given in second chapter.

To calculate the time τ_r when an electron is turned at the point ζ_r , as well as to get a relation between r and ε_0 we have two conditions

$$u_\zeta(\tau = \tau_r) = 0, \quad \frac{du_\zeta}{d\tau}(\tau = \tau_r) = 0. \quad (4.21)$$

From Eq. (4.19) and conditions (4.21), we obtain two equations to determine τ_r , as well as a relation between r and ε_0 :

$$\begin{aligned} (1+r-\Omega^2)\cos\Omega\tau_r + \varepsilon_0\Omega\sin\Omega\tau_r &= 1+r, \\ (1+r-\Omega^2)\sin\Omega\tau_r - \varepsilon_0\Omega\cos\Omega\tau_r &= 0. \end{aligned} \quad (4.22)$$

From Eq. (4.22) we find

$$\begin{aligned} r &= \frac{\varepsilon_0^2 + \Omega^2}{2} - 1, \quad \varepsilon_0 = \sqrt{2(1+r) - \Omega^2}, \\ \sin\Omega\tau_r &= \frac{\Omega}{1+r} \sqrt{2(1+r) - \Omega^2}, \quad \cos\Omega\tau_r = 1 - \frac{\Omega^2}{1+r}. \end{aligned} \quad (4.23)$$

Eqs. (4.23) allow us to calculate maximum ε_0 , corresponding to the solutions with partial electron turning, for any magnetic field strength:

$$\varepsilon_{0,max}(\Omega) = \sqrt{4 - \Omega^2}. \quad (4.24)$$

This maximum is attained at $r = 1$. From the 3rd and 4th equations of (4.23), we find time τ_r when the electron velocity vanishes. Depending on the values of Ω

and r , the function $\tau_r(\Omega, r)$ reads

$$\frac{1}{\Omega} \sin^{-1} \frac{\Omega \sqrt{2(1+r) - \Omega^2}}{1+r}, \quad \text{if } \Omega \leq \sqrt{1+r},$$

$$\frac{1}{\Omega} \left(\pi - \sin^{-1} \frac{\Omega \sqrt{2(1+r) - \Omega^2}}{1+r} \right), \quad \text{if } \Omega > \sqrt{1+r}. \quad (4.25)$$

Now, substituting (4.25) into Eq. (4.20), we find the position where the electron velocity vanishes

$$\zeta_r = \frac{1}{\Omega^2} \left[(1+r)\tau_r - \sqrt{2(1+r) - \Omega^2} \right]. \quad (4.26)$$

To deduce the parameters of an electron trajectory within the region locating to the right of ζ_r , we need to solve the Eq. (4.18) with the initial conditions (4.21).

Thus, for $\zeta > \zeta_r$, we can have

$$u_\zeta = \frac{1-r}{\Omega^2} [1 - \cos \Omega(\tau - \tau_r)],$$

$$\zeta = \zeta_r + \frac{1-r}{\Omega^2} (\tau - \tau_r) - \frac{1-r}{\Omega^3} \sin \Omega(\tau - \tau_r). \quad (4.27)$$

The electric potential is suitable to write in the form

$$\eta(\tau) = \frac{1}{2} [u_\zeta^2(\tau) + \Omega^2 \zeta^2(\tau) - 1], \quad (4.28)$$

which follows from the energy conservation law. At the collector, we have

$$\delta = \zeta_r(\Omega, r) + \frac{1-r}{\Omega^2} (T - \tau_r) - \frac{1-r}{\Omega^3} \sin \Omega(T - \tau_r),$$

$$V = \frac{1}{2} [u_\zeta^2(T; \Omega, r) + \Omega^2 \delta^2 - 1],$$

$$u_\zeta(T; \Omega, r) = \frac{1-r}{\Omega^2} [1 - \cos \Omega(T - \tau_r)]. \quad (4.29)$$

Here, T is the time of flight for the electrons to travel between the electrodes.

Utilizing Eqs. (4.29), one can calculate the potential profile for any ε_0 -value and build the dependence of ε_0 on δ in the region, $\zeta > \zeta_r$. For this purpose, we increase

the parameter r , starting from $r = 0$ ($\varepsilon_0 = \varepsilon_0^0 = \sqrt{2 - \Omega^2}$). This point corresponds to the solution for which the turning point arises for the first time. We can see from Fig. 4.5, that at first, δ decreases and this curve goes to the left. However, at a certain value of r , the $\varepsilon_0 - \delta$ curve turns and goes to the right. This bifurcation point is named as the BF point.

A condition $d\delta/dr = 0$ has to hold at the BF point. We can calculate this derivative as a complex function by using Eqs. (4.29):

$$\frac{d\delta}{dr} = \frac{\left[\frac{\partial\delta}{\partial r} \frac{\partial u_\zeta}{\partial(T-\tau_r)} - u_\zeta \frac{\partial u_\zeta}{\partial r} \right]}{\left[\Omega^2 \delta + \frac{\partial u_\zeta}{\partial(T-\tau_r)} \right]} = 0. \quad (4.30)$$

For particular terms we obtain

$$\begin{aligned} \frac{\partial u_\zeta}{\partial(T-\tau_r)} &= \frac{1-r}{\Omega} \sin \Omega(T-\tau_r), \\ \frac{\partial u_\zeta}{\partial r} &= -\frac{1}{\Omega^2} [1 - \cos \Omega(T-\tau_r)], \\ \frac{\partial \zeta_r}{\partial r} &= \frac{1}{\Omega^3} \left[\Omega \tau_r - \frac{2\Omega}{\sqrt{2(1+r) - \Omega^2}} \right], \\ \frac{\partial \delta}{\partial r} &= \frac{\partial \zeta_r}{\partial r} - \frac{1}{\Omega^2} (T-\tau_r) + \frac{1}{\Omega^3} \sin \Omega(T-\tau_r). \end{aligned} \quad (4.31)$$

Substituting the related terms from Eqs. (4.31) into Eq. (4.30) and multiplying the result by Ω^4 we obtain

$$\begin{aligned} &\left\{ \Omega \tau_r - 2\Omega [2(1+r) - \Omega^2]^{-1/2} - \Omega(T-\tau_r) + \sin \Omega(T-\tau_r) \right\} \times \\ &\quad \times \sin \Omega(T-\tau_r) + [1 - \cos \Omega(T-\tau_r)]^2 = 0. \end{aligned} \quad (4.32)$$

Here, τ_r is determined by Eq. (4.25). After transforming the trigonometrical functions to half arguments, Eq. (4.32) breaks into two equations:

$$\left[\Omega \tau_r - \frac{2\Omega}{\sqrt{2(1+r) - \Omega^2}} - \Omega(T - \tau_r) + \sin \Omega(T - \tau_r) \right] \times \\ \times \cos \frac{\Omega(T - \tau_r)}{2} + 2 \left[\sin \frac{\Omega(T - \tau_r)}{2} \right]^3 = 0 \quad (4.33)$$

and

$$\sin \frac{\Omega(T - \tau_r)}{2} = 0. \quad (4.34)$$

In order to calculate the parameters corresponding to the BF point, we have to use Eq. (4.33). This gives the first equation relating $(T - \tau_r)$ and r . The second equation relating $(T - \tau_r)$ and r is

$$u_\zeta^2(T - \tau_r, r; \Omega) + \Omega^2 \delta^2(T - \tau_r, r; \Omega) - (1 + 2V) = 0. \quad (4.35)$$

From the system of equations (4.33) and (4.35), we can calculate $(T - \tau_r)_{BF}$ and r_{BF} . When we substitute them into Eqs. (4.23) and (4.29), we obtain the values of $\varepsilon_{0,BF}$ and δ_{BF} for the BF point.

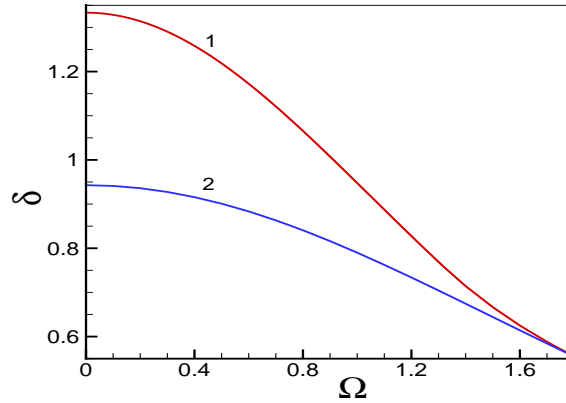


Figure 4.8: The position of the SCL and BF points vs Ω : (1) δ_{SCL} , (2) δ_{BF} ; $V = 0$.

Fig. 4.8 demonstrates the variation of δ_{BF} with respect to Ω . Here, the dependence of δ_{SCL} on Ω is also shown. It is seen that the region of hysteresis narrows with the increase of Ω . At $\Omega \approx 1.7$ hysteresis disappears practically.

As it was revealed in previous section, at a certain value of $r(\varepsilon_0)$, electron velocity u_ζ can vanish for the second time to the right of the point ζ_r . At first this occurs at the collector. Actually, the first equation of (4.27) shows that, depending on the values of ε_0 and Ω , electron velocity can vanish for several times. Corresponding time and relevant positions are determined by the formulas

$$\begin{aligned}\tau_i &= \tau_r + \frac{2\pi}{\Omega}i, \\ \zeta_i &= \zeta_r(r; \Omega) + \frac{2\pi}{\Omega^3}(1-r)i.\end{aligned}\quad (4.36)$$

Here, $\zeta_r(r; \Omega)$ is determined by Eq. (4.25) and Eq. (4.26) and i takes the positive integer values (i. e., $i = 1, 2, \dots$). When this event occurs at the collector ($T = \tau_i$), the second equation of (4.29) shows that the value of the inter-electrode gap is independent of the time (τ_i) when electron velocity vanishes. Moreover, this particular value of the inter-electrode gap turns out to be maximum for the regime where only a portion of the injected electrons is turned about by the magnetic field. We denote this gap value by δ_{max} :

$$\delta_{max} = \frac{\sqrt{1+2V}}{\Omega}.\quad (4.37)$$

Fig. 4.9 (a) shows the dependence of δ_{max} on Ω . The relation to calculate the values of the parameter r corresponding to δ_{max} can be obtained from Eqs. (4.36) and (4.37) by taking $\zeta_i = \delta_{max}$:

$$\frac{1}{\Omega^2} \left[(1+r)(\Omega\tau_r) - \Omega\sqrt{2(1+r) - \Omega^2} + 2\pi i(1-r) \right] = \sqrt{1+2V}.\quad (4.38)$$

We denote the value of r obtained from Eq. (4.38) for $i = 1$ by r_1 . Fig. 4.9(b) exhibits the dependence of r_1 on Ω . One can see that $r_1(\Omega)$ turns out to be more than 0.87 for the whole range of Ω .

Now, we investigate the case when the electron longitudinal velocity vanishes repeatedly, in detail. For a certain value of r (say, $r = r_i$), derived from Eq. (4.38), we need to calculate u_ζ , ζ and η from Eqs. (4.27) and (4.28). During the calculation of velocity and potential profiles, starting with the zero value, the value of τ is varied up to the instant when η becomes equal to V . For each value of r we calculate ε_0 and δ . Fig. 4.10(a) represents how r varies with δ . A fragment of the $\varepsilon_0 - \delta$ -plot is shown in Fig. 10(b) in the neighborhood of δ_{max} . We can see that both curves are many-valued over a certain range of the δ 's, and have many bifurcation points. Each right bifurcation point corresponds to $u_\zeta(\delta) = 0$, and at these points all values of δ takes the same value δ_{max} . The relevant values of r can be calculated from Eq. (4.38) for different values of index i . The values of the coefficient r for the left bifurcation points are calculated from Eqs. (4.33) and (4.35). Then they can be used to find relevant parameters, ε_0 and δ accordingly from Eqs. (4.23) and (4.29). Thus, we have revealed the existence of new bifurcation points and the ambiguity of the solutions in the vicinity of δ_{max} .

4.5 Total electron-reflection: The Lagrange method

In this case, we assume that under a certain emitter electric field strength there is a point ζ_H within the inter-electrode gap from where all the electrons are turned back toward the emitter. At this point the longitudinal component of the velocity u_ζ vanishes, and for the PD, the relationship (4.2) takes place. To the left of the

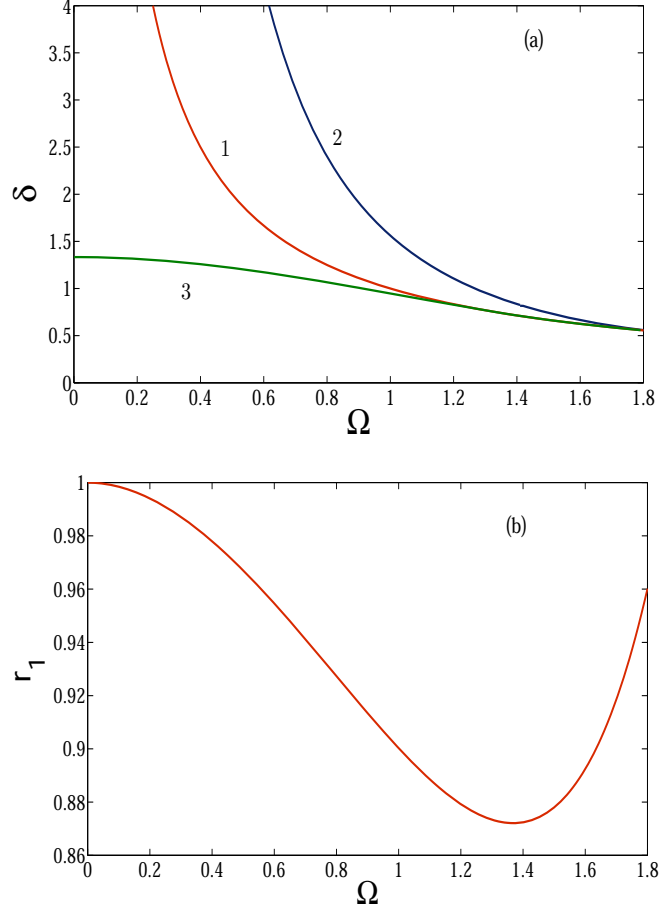


Figure 4.9: Fig. (a): Variation of δ_{max} (curve 1), $\delta_{min}(1)$ (curve 2), and δ_{SCL} (curve 3) with Ω ; Fig. (b) coefficient r_1 vs Ω ; $V = 0$.

turning point ζ_H , the relevant profiles of ζ , u_ζ and η are determined by the Eqs. (4.19), (4.20) and

$$\eta = \frac{1}{2} [u_\zeta^2(\tau; \Omega, r) + \Omega^2 \zeta^2 - 1], \quad (4.39)$$

with $r = 1$. To the right of this point PDs are determined by Eqs. (4.9), (4.10) with

$$\begin{aligned} \eta_H &= \frac{1}{2} [\Omega^2 \zeta_H^2 - 1], \\ \zeta_H &= \frac{2}{\Omega^2} \tau_H + \frac{1}{\Omega} \left(1 - \frac{2}{\Omega^2}\right) \sin \Omega \tau_H + \frac{\varepsilon_0}{\Omega^2} (\cos \Omega \tau_H - 1), \\ \varepsilon_H &= -2\tau_H + \varepsilon_0. \end{aligned} \quad (4.40)$$

The value of τ_H is determined from the condition $u_\zeta(\tau_H) = 0$:

$$\frac{2}{\Omega^2} + \left(1 - \frac{2}{\Omega^2}\right) \cos \Omega\tau_H - \frac{\varepsilon_0}{\Omega} \sin \Omega\tau_H = 0. \quad (4.41)$$

Depending on the value of Ω , τ_H reads

$$\begin{aligned} \frac{1}{\Omega} \left[\sin^{-1} \frac{2}{\sqrt{(2-\Omega^2)^2 + \varepsilon_0^2 \Omega^2}} - \sin^{-1} \frac{2-\Omega^2}{\sqrt{(2-\Omega^2)^2 + \varepsilon_0^2 \Omega^2}} \right], \quad \Omega < \sqrt{2}, \\ \frac{1}{\Omega} \left[\sin^{-1} \frac{2}{\sqrt{(2-\Omega^2)^2 + \varepsilon_0^2 \Omega^2}} + \sin^{-1} \frac{\Omega^2 - 2}{\sqrt{(2-\Omega^2)^2 + \varepsilon_0^2 \Omega^2}} \right], \quad \Omega > \sqrt{2}, \end{aligned} \quad (4.42)$$

or,

$$\begin{aligned} \frac{1}{\Omega} \sin^{-1} \frac{2\varepsilon_0 - (2-\Omega^2)\sqrt{\varepsilon_0^2 - 4 + \Omega^2}}{(2-\Omega^2)^2 + \varepsilon_0^2 \Omega^2} \Omega, \quad \Omega < \sqrt{2}, \\ \frac{1}{\Omega} \left[\pi - \sin^{-1} \frac{2\varepsilon_0 + (\Omega^2 - 2)\sqrt{\varepsilon_0^2 - 4 + \Omega^2}}{(2-\Omega^2)^2 + \varepsilon_0^2 \Omega^2} \Omega \right], \quad \Omega > \sqrt{2}. \end{aligned} \quad (4.43)$$

The dependence of δ on ε_0 for a set of Ω -values is marked in Fig. 4.5 by open circles. At the left boundary of the region corresponding to $r = 1$ we have

$$\begin{aligned} \varepsilon_{0,min} &= \sqrt{4 - \Omega^2}, \\ \zeta_{H,min} &= \frac{1}{\Omega^2} \left(2\tau_{H,min} - \sqrt{4 - \Omega^2} \right), \\ \eta_{H,min} &= \frac{1}{2} \left[\frac{1}{\Omega^2} \left(2\tau_{H,min} - \sqrt{4 - \Omega^2} \right)^2 - 1 \right], \\ \varepsilon_{H,min} &= - \left(2\tau_{H,min} - \sqrt{4 - \Omega^2} \right). \end{aligned} \quad (4.44)$$

Here depending on the value of Ω , $\tau_{H,min}$ reads

$$\begin{aligned} \frac{1}{\Omega} \sin^{-1} \frac{\sqrt{4 - \Omega^2}}{2} \Omega, \quad \Omega < \sqrt{2}, \\ \frac{1}{\Omega} \left(\pi - \sin^{-1} \frac{\sqrt{4 - \Omega^2}}{2} \Omega \right), \quad \Omega > \sqrt{2}. \end{aligned} \quad (4.45)$$

Making use of Eqs. (4.40), (4.41), (4.44) and (4.45), from (4.10) we find minimum gap value $\delta_{min}(1)$, corresponding to $r = 1$:

$$\delta_{min}(1) = \frac{1}{2} \left[\zeta_{H,min} + \frac{1 + 2V}{\Omega^2 \zeta_{H,min}} \right]. \quad (4.46)$$

As an example, for $\Omega = 1$, we can have $\tau_{H,min} = \pi/3 \approx 1.0472$, $\zeta_{H,min} = 0.3623$, $\varepsilon_{H,min} = -0.3623$, $\eta_{H,min} = -0.4344$ and $\delta_{min}(1) = 1.5611$. Fig. 4.9(a) shows the dependence of $\delta_{min}(1)$ on Ω (curve 2). We can see that the distance between $\delta_{min}(1)$ and δ_{max} decreases with the increase of Ω .

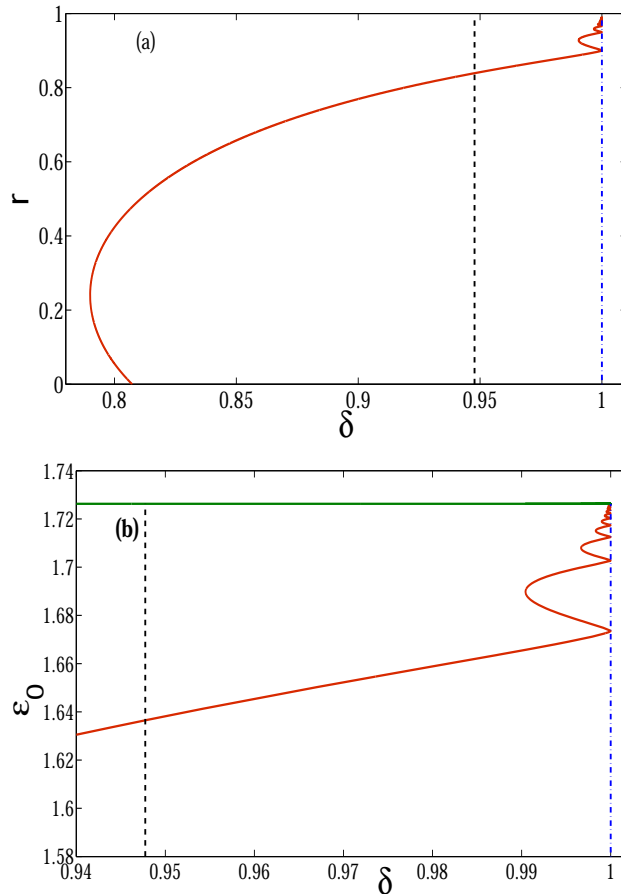


Figure 4.10: Fig. (a) r and (b) ε_0 vs δ . Vertical dashed line corresponds to position of the *SCL* point, dashed-dotted line is for δ_{max} , and horizontal solid line is for $r = 1.0$. $\Omega = 1.0$, $V = 0$.

It is seen from Fig. 4.9(a), that the steady-state solutions are absent within the region $\delta_{max} < \delta < \delta_{min}(1)$. This paradox arises owing to the fact that the velocity distribution function of the emitted electron is taken as a δ -function for this analysis. Such a function describes very well the solutions for $r < 1$. However, when $r \rightarrow 1$ we need to keep in mind that in reality, there is always a small amount

of the electrons with $v_z > v_0$. To take into account this fact we can, for example, choose the velocity distribution function of the emitted electrons in a form

$$f_0(v_z) = \frac{n_0}{v_0} A(\alpha) \exp \{-\alpha (v_z^2/v_0^2 - 1)\} \Theta(v_z - v_0),$$

$$A(\alpha) = \frac{2\sqrt{\alpha}}{\sqrt{\pi} \text{exers}(\alpha)}. \quad (4.47)$$

Here, $\alpha = v_0^2/(2kT/m) \gg 1$ with T being an effective “temperature”; $\text{exers}(\alpha) = \exp(\alpha)(1 - \text{erf}\sqrt{\alpha})$ with $\text{erf}(\alpha)$ being the error integral. The characteristic velocity v_0 is determined from the equation $v_0 = J_0/(en_0)[1/\{\sqrt{\pi\alpha} \text{exers}(\alpha)\}]$ and the kinetic energy of electrons at the emitter can be written as, $W_0 = (mv_0^2/2)[1/\{\sqrt{\pi\alpha} \text{exers}(\alpha)\} + 1/(2\alpha)]$. We should note that for $\alpha \gg 1$, v_0 and W_0 differ slightly from the corresponding values associated with the monoenergetic beam.

4.6 Summary

In this chapter we have shown that, in the presence of a transverse magnetic field in a Bursian diode, a fraction of the emitted electrons can be turned back (partially or totally) toward the emitter and, as a result of it, the diode current decreases. To study this behaviour, a reflection coefficient r has been introduced. This coefficient takes the value zero for the solution without electron turning and one for complete electron turning. The situation of partial electron turning appears when $0 < r < 1$. Two characteristic-points (*SCL* and *BF*) of ε_0, δ -curve serve as the boundaries of a region of non-unique solutions. However, with the increase of the magnetic field, this region of non-uniqueness disappears slowly and it occurs when the Larmor radius becomes comparable to the Bursian threshold.

However, unlike the classical Bursian diode, the (ε_0, δ) -diagram demonstrates a

new zig-zag region. This region contains the solutions for which the longitudinal velocity of the injected electrons vanishes for several times within the inter-electrode space. Here the coefficient r , which controls the amount of the electrons to be turned back by the magnetic field, is more than about 0.9. When $r \rightarrow 1$, the period and the amplitude of the velocity oscillations tend to zero.

A primary model can be suggested to design a fast electronic switches based on Bursian diode. The working mechanism of this electronic switch involves a transition between the states of the normal C branch (the section of “ $\varepsilon_0 - \delta$ ” curve for $\delta < \delta_{SCL}$, $\varepsilon_0 < \varepsilon_{SCL}$) and the B branch (the section of “ $\varepsilon_0 - \delta$ ” curve for $\delta > \delta_{BF}$, $\varepsilon_0 > \varepsilon_{SCL}$). This B branch was absent in the results discussed in chapter two, as electron reflection was not taken into account in that case. We can see from Eq.(4.37), that if Ω exceeds $\sqrt{1 + 2V}/\delta_{SCL}(0)$, the current turns out to be zero after switching, i. e., current cut-off is complete. Whereas, at $\Omega < \sqrt{1 + 2V}/\delta_{SCL}(0)$ the state corresponds to the regime with an incomplete current cut-off.

Chapter 5

Stationary states of a relativistic Bursian diode in the presence of a transverse magnetic field

The previous chapters were devoted to study the steady-state properties of a non-relativistic Bursian diode. In this chapter, a comprehensive study on the steady states of a planar vacuum diode driven by a cold relativistic electron beam in the presence of an external transverse magnetic field is presented. The regimes, where no electrons are turned around by the external magnetic field and where they are reflected back to the emitter by the magnetic field, are both considered in a generalized way. The dependencies of the characteristic bifurcation points and the transmitted current on the Larmor frequency as well as on the relativistic factor are explored.

5.1 Introduction

The physics of the relativistic electron beam driven vacuum diodes is of fundamental interest due to a number of important applications like plasma heating, inertial fusion etc. Most importantly, they are also widely used as the generators of powerful microwave radiation (vircator, reditron, reflecting triode) which are tunable over a wide frequency range. The generation of the microwave radiation in these high power devices generally happens when the electron beam energy is converted into the electric field oscillations [153, 154, 155]. The operation of a vircator as a microwave generator is based on the oscillations of the virtual cathode (VC) in the electron beam when diode current crosses a critical value (space charge limit) [138, 156, 157, 158]. The origin of the space charge limited current in the diode like systems and the formation of the VC have been studied extensively both in non-relativistic [66, 148, 150, 158, 159] and relativistic cases [69, 160, 161, 162, 163, 164, 165]. Recently, Lin and Chuu considered the quasi-stationary states of a relativistic planar diode [166] and Lopez et al. calculated limiting emission current in a relativistic diode under the condition of magnetic insulation [167]. It should be mentioned that the copious beams of the relativistic electrons occur also in the pulsar magnetospheres [168].

In high power relativistic diodes, the strong inherent magnetic field (generated due to the very high current density of the relativistic electron beam) affects the motion of the charge particles. It was also reported that in the presence of strong magnetic field, the oscillation amplitude and the output power of the microwave generator decrease [118]. Several authors have diagnosed the effect of the external magnetic field on the space charge limiting current in relativistic electron beam and

studied the output power of the electromagnetic radiation in recent years [169, 170]. Harmov *et. al.* have shown that the value of the space charge limiting (critical) current decreases as the strength of the external magnetic field is increased, and there is an optimal value of the magnetic field induction at which the critical value of the diode current is minimum for the onset of the virtual cathode oscillations in the electron beam. Whereas, Kurkin *et. al.* have pointed out that the output power of the vircator shows several maxima when it is plotted with respect to the external magnetic field. They also explained that the characteristics of the power behaviour depend on the conditions of the virtual cathode formation in the presence of the external transverse magnetic field and the REB self-magnetic fields.

This chapter explores the impact of the external transverse magnetic field on the steady states of a planar vacuum diode when a cold relativistic beam of electrons is injected by the emitter surface.

5.2 The electron dynamics

To study a relativistic Bursian diode in the presence of the transverse magnetic field, we use the planar model which is explained before (see second chapter). In this case, a relativistic monoenergetic electron flow is supplied by the emitter with density n_0 and injection velocity v_0 perpendicular to the emitter surface. The velocity of the electrons \vec{v} obeys the equation

$$\vec{v} \cdot \nabla \vec{p} = -e\vec{E} - \frac{e}{c}\vec{v} \times \vec{B}. \quad (5.1)$$

In Eq. (5.1), the relativistic momentum \vec{p} is determined as

$$\vec{p} = \gamma m \vec{v} \quad (5.2)$$

with the relativistic Lorentz factor being

$$\gamma = (1 - v^2/c^2)^{-1/2}, \quad v^2 = v_z^2 + v_x^2. \quad (5.3)$$

Using the relation $E(z) = -d\varphi(z)/dz$ and from Eq. (5.1) we obtain

$$v_z \frac{dp_z}{dz} = e \frac{d\varphi}{dz} - \omega m v_x, \quad v_z \frac{dp_x}{dz} = \omega m v_z. \quad (5.4)$$

Here e and m are the charge and the rest mass of the electron respectively, and the Larmor frequency $\omega = eB/(mc)$. To solve Eq. (5.4), we add following boundary conditions at the emitter:

$$\begin{aligned} v_z(0) = v_z^0 = v_0, \quad v_x(0) = v_x^0 = 0, \quad \varphi(0) = 0, \\ \gamma(0) = \gamma_0 \equiv (1 - v_0^2/c^2)^{-1/2}. \end{aligned} \quad (5.5)$$

Firstly, we obtain explicit expressions for the velocity components. From the second equation of the system of equations (5.4), the second boundary condition of Eq. (5.5), and Eq. (5.2), the x -component of the electron velocity can be obtained as

$$v_x(z) = p_x/(m\gamma) = \omega z/\gamma. \quad (5.6)$$

Using this expression of v_x , we can find v_z from Eq. (5.3) :

$$v_z(z) = \frac{c}{\gamma} \sqrt{\gamma^2 - 1 - \frac{\omega^2}{c^2} z^2}. \quad (5.7)$$

Now to get a relation between the the factor γ and φ , we substitute $v_x(z)$ and $v_z(z)$ from Eqs. (5.6) and (5.7) in the first equation of the system of equations (5.4). From Eqs. (5.4) we find

$$\begin{aligned} (\gamma - 1)mc^2 - e\varphi(z) &= (\gamma_0 - 1)mc^2, \\ \text{or } \gamma &= \gamma_0 + e\varphi/(mc^2). \end{aligned} \quad (5.8)$$

Here the boundary conditions for γ and for the potential φ at the emitter [Eq. (5.5)] are used. The first equation of Eqs. (5.8) is the energy conservation law for the relativistic electrons moving in the presence of the self-consistent electric field and the transverse external magnetic field. The term $(\gamma_0 - 1)mc^2$ residing on the right hand side of the first equation of Eqs. (5.8) is the kinetic energy of the electrons at the emitter.

When we substitute γ from Eq. (5.8) into Eqs. (5.6) and (5.7), we have explicit expression for $v_x(z)$ and $v_z(z)$:

$$\begin{aligned} v_x(z) &= \frac{\omega z}{\gamma_0 + e\varphi/(mc^2)}, \\ v_z(z) &= \frac{c\sqrt{[\gamma_0 + e\varphi/(mc^2)]^2 - 1 - (\omega^2/c^2)z^2}}{\gamma_0 + e\varphi/(mc^2)}. \end{aligned} \quad (5.9)$$

In a nonrelativistic limit ($\gamma_0 \rightarrow 1$, $v_0^2/c^2 \ll 1$), we get

$$\begin{aligned} v_x(z) &= \omega z, \\ v_z(z) &= \sqrt{v_0^2 + 2(e/m)\varphi(z) - \omega^2 z^2}. \end{aligned}$$

The presence of the transverse magnetic field brings some new features in the electron velocity and density distributions within the inter-electrode gap (as compared with Ref. [69]). As the magnetic field converts a portion of the longitudinal electron energy into the transverse one, the longitudinal electron energy diminishes and the potential barrier height for the electrons turns out to be lower than the initial energy of the electrons. Additionally, due to the presence of the transverse magnetic field, now the electrons can be turned back even at a point where $\varphi(z) > 0$.

One can see that the velocity v_z does not depend on the sign of B as Eq. (5.9) carries the square of the magnetic field. When the magnetic field is not present in

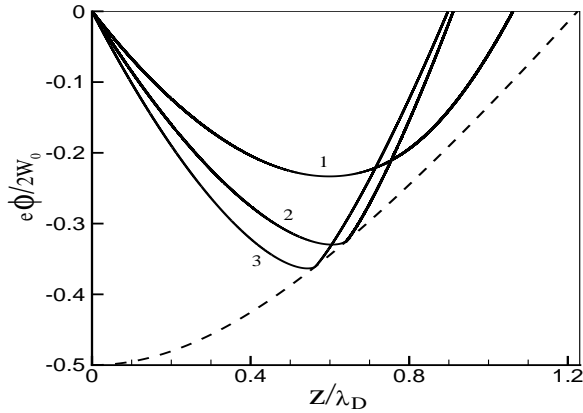


Figure 5.1: Normalized potential $e\varphi/(2W_b)$ is plotted as a function of normalized space $\zeta = z/\lambda_D$ for various values of $\varepsilon_0 = eE_0\lambda_D/(2W_b)$: (1) $\varepsilon_0 = 0.72$ (no electrons are turned due to the magnetic field), (2) 0.9029 and (3) 1.0793 [for (2) and (3), there is a point within the diode gap in which the longitudinal velocity vanishes for the first time]. Dashed curve corresponds to $\varphi = p(z, \omega) = (mc^2/e) \left(\sqrt{1 + (\omega^2/c^2)z^2} - \gamma_0 \right)$; $\gamma_0 = 2$; $\omega/\omega_0 = 1.0$; $U = 0$.

the Bursian diode, the velocity of the emitted electron vanishes if only the potential barrier height becomes equal to the electron energy at the emitter, and it happens at the position of the potential minimum (virtual cathode). Here a portion of the emitted electrons is reflected by the potential barrier towards the emitter. When there is a magnetic field in the transverse direction, the non-negativity condition of the radicand in Eq. (5.9) shows that PDs $\varphi(z)$ should be restricted within a region limited by the curve $p(z; \omega)$, to be consistent with the distributions of the electrons (Fig. 5.1):

$$\varphi(z) \geq p(z; \omega) \equiv (mc^2/e) \left(\sqrt{1 + (\omega^2/c^2)z^2} - \gamma_0 \right). \quad (5.10)$$

Equality sign in (5.10), i. e. a condition

$$e\varphi(z_r) + \gamma_0 mc^2 = mc^2 \sqrt{1 + (\omega^2/c^2)z_r^2} \quad (5.11)$$

appears at a point z_r where the z -component of the electron velocity vanishes and the electron is turned around by the magnetic field. We can check that, unlike the

case where the external magnetic field was absent, the electron turning does not occur at the point of the potential minimum in the presence of the magnetic field in transverse direction. In the following sections, the problem is approached by two techniques: with the Euler and the Lagrange formulation.

5.3 Steady-state solutions. The Euler method

In this section, we study the features of the steady state solutions by using the Eulerian variables. We approach this problem in a similar way as it was solved for the Bursian diode in the absence of magnetic field [69]. We set a value for the potential difference U between the electrodes. For a given value of the electric field strength E_0 at the emitter end, we calculate the velocity and the electron density, as well as the potential distribution (PD) within the inter-electrode gap. The process starts from the emitter, and terminates at the moment when the value of the potential turns out to be equal to U . The relevant z -coordinate implies the distance of any point within inter-electrode region from the emitter. Increasing gradually E_0 , we build the dependence of E_0 on diode gap (d).

In time-independent case, it is sufficient to use the continuity equation, the relation between the longitudinal velocity and the potential [Eq. (5.9)], and the Poisson's equation. When no electrons are turned back by the magnetic field, i. e., when the equality condition (5.11) does not hold anywhere, the continuity equation gives

$$en(z)v_z(z) = en_0v_0 \equiv j_b. \quad (5.12)$$

Substituting the above expression of $n(z)$ into the Poisson's equation and using

the relationship (5.9), we obtain a nonlinear differential equation for the potential

$$\frac{d^2\varphi}{dz^2} = \frac{e}{\epsilon_0}n = \frac{j_b}{\epsilon_0 c} \frac{\gamma_0 + e\varphi/(mc^2)}{\{[(\gamma_0 + e\varphi/(mc^2))^2 - 1 - (\omega^2/c^2)z^2]^{1/2}}. \quad (5.13)$$

Here, the free-space permittivity $\epsilon_0 \approx 8.854 \cdot 10^{-12} C^2/Nm^2$.

Next we introduce dimensionless quantities by using the kinetic energy of the electrons at the emitter (W_b) and the Debye length (λ_D) for the energy and length units respectively:

$$W_b = (\gamma_0 - 1)mc^2, \quad \lambda_D = \left(\frac{2\epsilon_0 W_b}{e^2 n_0} \right)^{1/2}. \quad (5.14)$$

As we follow the Ref. [69], we can see that it is convenient to use the current density j_b and the accelerating voltage $V_b = W_b/e$ as the basic units instead of the density n_0 and the energy W_b . Thus,

$$\begin{aligned} \lambda_D &= \left(\frac{2\epsilon_0 e V_b v_0}{e j_b} \right)^{1/2} = \left(\frac{2\epsilon_0 m c^3}{e j_b} \right)^{1/2} F(V_b), \\ F(V_b) &= \left(\frac{e V_b}{m c^2} \right)^{3/4} \left(\frac{e V_b}{m c^2} + 2 \right)^{1/4} \left(\frac{e V_b}{m c^2} + 1 \right)^{-1/2}. \end{aligned} \quad (5.15)$$

When j_b is expressed in Amperes per square centimeters, we obtain

$$\lambda_D \approx 0.5205 \times 10^2 F(V_b) j_b^{-1/2} [cm]. \quad (5.16)$$

Expressing V_b in Volts, we find for the function $F(V_b)$

$$F(V_b) \approx \frac{(1.9570 \times 10^{-6} V_b)^{3/4} (2 + 1.9570 \times 10^{-6} V_b)^{1/4}}{(1 + 1.9570 \times 10^{-6} V_b)^{1/2}}. \quad (5.17)$$

and the relativistic factor at the emitter is found to be $\gamma_0 = 1 + (e/mc^2)V_b = 1 + 1.9570 \times 10^{-6} V_b$. Thus, for a given accelerating voltage V_b and a beam current density j_b , one can determine the Debye length from Eqs. (5.16) and (5.17) and calculate γ_0 .

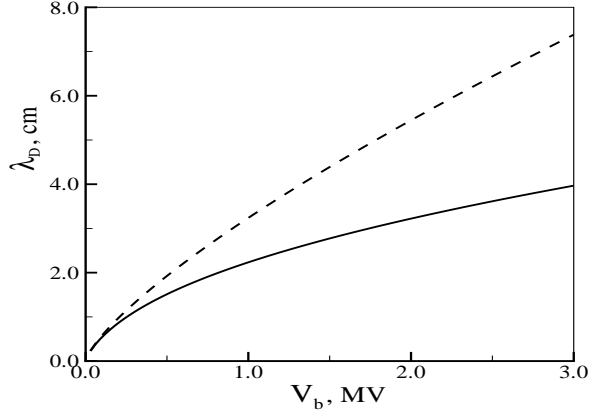


Figure 5.2: Debye length λ_D vs V_b for $j_b = 1\text{kA/cm}^2$. The relativistic and non-relativistic Debye lengths are represented by the solid and dashed lines respectively [69].

In Fig. 5.2, the value of j_b has been chosen to be 1kA/cm^2 and we can see that the relativistic and non-relativistic Debye lengths practically coincide with each other as long as $V_b < 0.1\text{MV}$. However, for large V_b , the non-relativistic Debye length differs significantly from the relativistic one.

For the dimensionless coordinate, time, velocity, potential and electric field strength we have $(\zeta, \chi) = (z, x)/\lambda_D$, $\tau = t\omega_0$, $(u_\zeta, u_\chi) = (v_z, v_x)/\sqrt{2W_b/m}$, $\eta = e\varphi/(2W_b)$, $\varepsilon = eE\lambda_D/(2W_b)$; here $\omega_0 = [e^2n_0/(m\epsilon_0)]^{1/2}$ is the characteristic frequency. The dimensionless forms of the inter-electrode gap and the applied voltage between the electrodes are denoted by δ and V respectively.

Now the equation (5.13) takes the form

$$\frac{d^2\eta}{d\zeta^2} = \frac{(\gamma_0^2 - 1)^{1/2}}{\gamma_0} \frac{2(\gamma_0 - 1)\eta + \gamma_0}{\{[2(\gamma_0 - 1)\eta + \gamma_0]^2 - 1 - 2(\gamma_0 - 1)\Omega^2\zeta^2\}^{1/2}}. \quad (5.18)$$

Here the dimensionless Larmor's frequency Ω is expressed in units of the frequency ω_0 :

$$\Omega = \frac{\omega}{\omega_0} = \frac{\lambda_D}{\lambda_L}, \quad \lambda_L = \frac{mc\sqrt{2W_b/m}}{eB}. \quad (5.19)$$

The boundary conditions for Eq. (5.18) are

$$\eta(0) = 0, \quad \eta(\delta) = V. \quad (5.20)$$

In the non-relativistic case, the steady-state solutions are determined by two parameters: δ and V . Whereas, in the relativistic situation, there is an additional third parameter, which is the emitter's relativistic factor γ_0 . The normalized potential distribution $\eta(\zeta)$ should be confined within the boundary defined by

$$\eta_c = \frac{1}{2(\gamma_0 - 1)} \left[\sqrt{1 + 2(\gamma_0 - 1)\Omega^2\zeta^2} - \gamma_0 \right].$$

We should note that Eq. (5.8) gives the relation between the relativistic factor γ and the potential η :

$$\gamma = 2(\gamma_0 - 1)\eta + \gamma_0. \quad (5.21)$$

Therefore, we can obtain a differential equation for γ from Eq. (5.18):

$$\frac{d^2\gamma}{d\zeta^2} = \frac{(\gamma_0^2 - 1)^{1/2}}{\gamma_0} \frac{\gamma}{\sqrt{\gamma^2 - 1 - 2(\gamma_0 - 1)\Omega^2\zeta^2}} \quad (5.22)$$

with boundary conditions

$$\gamma(0) = \gamma_0, \quad \gamma(\delta) = 2(\gamma_0 - 1)V + \gamma_0. \quad (5.23)$$

From Eqs. (5.6) and (5.7), we obtain

$$u_x = \frac{\Omega\zeta}{\gamma}, \quad u_\zeta = \frac{1}{\sqrt{2(\gamma_0 - 1)}} \frac{1}{\gamma} \sqrt{\gamma^2 - 1 - 2(\gamma_0 - 1)\Omega^2\zeta^2}. \quad (5.24)$$

Eqs. (5.24) also give

$$p^2 = p_\zeta^2 + p_x^2 = \frac{\gamma^2 - 1}{2(\gamma_0 - 1)}. \quad (5.25)$$

Next we solve the Eq. (5.18) to find the space dependencies of γ and η with the help of B.C. (5.20). A diode PD is a single minimum function. We denote the

potential at the point of minimum $\zeta = \zeta_m$ by η_m . We take a particular value of the electric field strength $\varepsilon_0 = \tilde{\varepsilon}_0$ at the emitter, and integrate the equation (5.18) from the emitter ($\zeta = 0$) towards the point of the minimum. The position and the value of the potential minimum (ζ_m, η_m) are obtained under the condition of zero electric field strength. Further, we integrate Eq. (5.18) from the point ζ_m towards the collector with the boundary conditions

$$\eta(\zeta_m) = \eta_m, \quad d\eta/d\zeta(\zeta_m) = 0. \quad (5.26)$$

While integrating Eq. (5.18), we use an approximation method which is described in previous chapters. We take a guess-value of the potential at minimum: η_m . The true value of it will be determined in the process of the calculations. In a region between the emitter and the location of the potential minimum, we take the potential frame (instead of coordinate frame): $\eta_k = \eta_{k-1} + \Delta\eta_k$, $k = 1, \dots, N$, $\eta_0 = 0$. Then we multiply both sides of Eq. (5.18) by $2d\eta$ and integrate it once over the potential within each layer (ζ_{k-1}, ζ_k) :

$$\varepsilon_k^2 = \varepsilon_{k-1}^2 + 2 \frac{\sqrt{\gamma_0^2 - 1}}{\gamma_0} \int_{\eta_{k-1}}^{\eta_k} \frac{[2(\gamma_0 - 1)w + \gamma_0]dw}{\{[2(\gamma_0 - 1)w + \gamma_0]^2 - 1 - 2(\gamma_0 - 1)\Omega^2(\zeta')^2\}^{1/2}}. \quad (5.27)$$

Here, $\varepsilon_k = -(d\eta/d\zeta)|_{\zeta=\zeta_k}$ is the electric field strength at a point $\zeta = \zeta_k$. After simplification, Eq. (5.27) takes the form

$$\varepsilon_k^2 = \varepsilon_{k-1}^2 + \frac{\sqrt{2(\gamma_0 + 1)}}{\gamma_0} \int_{\eta_{k-1}}^{\eta_k} \frac{[2(\gamma_0 - 1)w + \gamma_0]dw}{[2(\gamma_0 - 1)w^2 + 2\gamma_0w + (\gamma_0 + 1)/2 - \Omega^2(\zeta')^2]^{1/2}}. \quad (5.28)$$

While integrating the integral of Eq. (5.28), PD is approximated with a straight

line

$$\begin{aligned}\eta(\zeta) &= \eta_{k-1} - (\zeta - \zeta_{k-1})\overline{\varepsilon}_k, \\ \overline{\varepsilon}_k &= q_k\varepsilon_{k-1} + (1 - q_k)\varepsilon_k.\end{aligned}\tag{5.29}$$

In Eq. (5.29), the weights q_k lie within $(0, 1)$. In each layer, values of q_k , generally, can be different. In our calculation, we take $q_k = 0.5$. The relevant mathematics which have been used to calculate the integral in Eq. (5.28) are deduced in the Appendix.

Thus to obtain the PD in the region to the left of the potential minimum, within each step k , a system of the difference equations

$$\begin{aligned}\eta_k &= \eta_{k-1} + \Delta\eta_k, \\ \varepsilon_k &= \pm \left\{ \varepsilon_{k-1}^2 + \beta [\sqrt{2(\gamma_0 + 1)}/\gamma_0] G(\zeta_{k-1}, \eta_{k-1}, \varepsilon_{k-1}, \eta_k, \varepsilon_k) \right\}^{1/2}, \\ \overline{\varepsilon}_k &= q_k\varepsilon_{k-1} + (1 - q_k)\varepsilon_k, \\ \zeta_k &= \zeta_{k-1} - (\eta_k - \eta_{k-1})/\overline{\varepsilon}_k\end{aligned}\tag{5.30}$$

is solved under the conditions :

$$\eta_0 = 0, \quad \varepsilon_0 = \tilde{\varepsilon}_0, \quad \zeta_0 = 0.\tag{5.31}$$

Note that here we have artificially introduced a factor β which is equal to 1 for the case of no electron turning. We shall widely use this factor in following sections. Within each step, a value of the electric field strength ε_k and coordinate ζ_k are determined. It should be noted here that in this region, $\varepsilon_k \geq 0$.

The equation for ε_k [the 2nd equation of the system of Eqs. (5.30)] is the transcendental one. So, within each step k , an iteration is carried out. Taking an approximate value of $\varepsilon_k^{(0)}$, firstly, at the right side of the 2nd equation, $\varepsilon_k^{(1)}$ is calculated. From the next two equations, $\overline{\varepsilon}_k^{(1)}$ and $\zeta_k^{(1)}$ are obtained. Then, the relevant

parameters for the second approximation are calculated and so on. Under certain value of k ($k = K \leq N$), the radicand in the second equation of the system of equations (5.30) becomes negative. At this step, the iterations are carried out over η_K as ε_K becomes zero. As a result, the required values of the potential and the position of the potential minimum (η_m and ζ_m) are determined.

When the coordinates of the potential minimum are determined, the PD is calculated to the right of the point of minimum ζ_m . Eqs. (5.30) are solved with the boundary conditions (5.26). The value of the potential step is taken as $(V - \eta_m)/N$. It should be kept in mind that the electric field strength is now negative in this region. The calculation is completed when the potential takes the value V and at this situation, the value of ζ becomes δ . Thus, the PD related to the chosen value of the electric field strength at the emitter is obtained. In addition, for each value of ε_0 , the inter-electrode gap value δ is calculated.

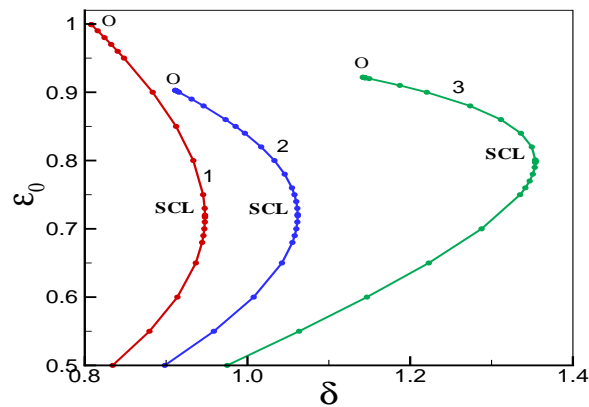


Figure 5.3: The $\varepsilon_0(\delta)$ curves are drawn for various values of γ_0 : (1) $\gamma_0 = 1$, (2) 2, (3) 10; $\Omega = 1$. $V = 0$. The regime where no electrons are turned by the magnetic field.

5.3.1 Regime of no electron-reflection

Unlike the non-relativistic case, we have an additional parameter which is the emitter's relativistic factor γ_0 for the relativistic Bursian diode. Now we analyse how the diode characteristics depend on this parameter. First we fix the magnetic field value (i. e. the parameter Ω). During the calculations, the value of the emitter's electric field strength is smoothly increased, and, for each value of ε_0 , the profiles of the potential, velocity, and density within the inter-electrode gap are calculated. The nature of these dependencies are similar to the non-relativistic case. For the case under consideration ($V = 0$), the diode PD is found to be a single minimum function. The dependence of the velocity $u_\zeta(\zeta)$ on the space coordinate shows that u_ζ also has a single minimum on space. This dependence is a monotonic function for small values of ε_0 , and its minimum lies on the collector at first. As ε_0 is increased, the position of the velocity minimum (ζ_{vm}) appears within the inter-electrode gap. When the value of the ε_0 is increased further, the location of the velocity minimum begins to shift towards the emitter and the minimum value of the velocity ($u_{\zeta,min}$) reduces. At a particular value of the emitter electric field strength [$\varepsilon_0 = \varepsilon_0^0(\gamma_0, \Omega)$], the value of $u_{\zeta,min}$ vanishes and for $\varepsilon_0 \geq \varepsilon_0^0$, the electrons are turned back by the magnetic field towards the emitter.

Like the non-relativistic case, it is convenient to represent the steady state solutions by the points of the $\{\varepsilon_0, \delta\}$ -curves. For a fixed V , those points lie on a continuity curve which is named as the branch of solutions. In Fig. 5.3 these branches are shown for a number of γ_0 values and $\Omega = 1$. Here the calculation ends at such a value of ε_0 when the longitudinal velocity profile touches the line $u_\zeta = 0$ for the first time. The dependence of ε_0 on δ has a region of non-unique

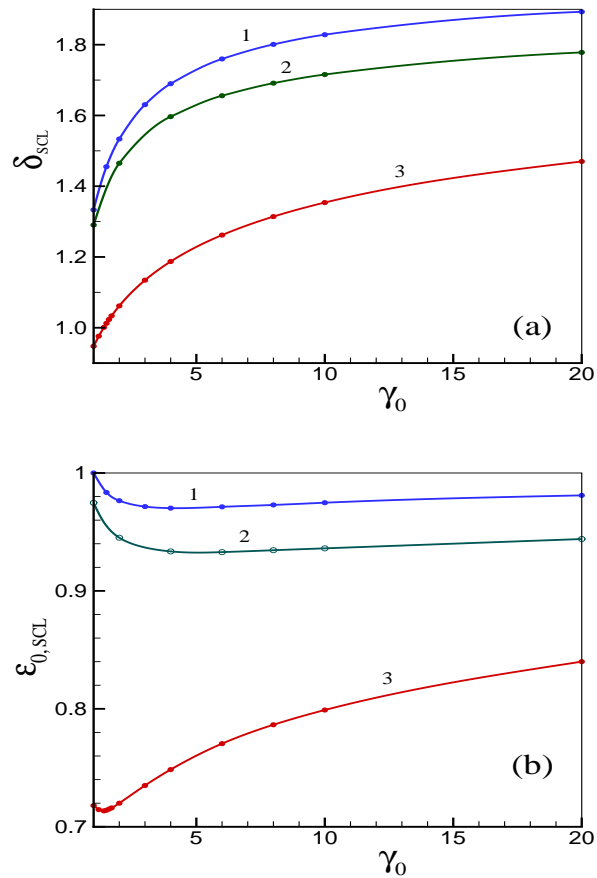


Figure 5.4: The dependencies (a) $\delta_{SCL}(\gamma_0)$ and (b) $\varepsilon_{0,SCL}(\gamma_0)$ are drawn for various values of Ω : (1) $\Omega = 0$, (2) 0.3 and (3) 1.0; $V = 0$.

solutions. To the right boundary of this region, there is a bifurcation point SCL . The end point at the left of this region refers to a situation when there is a point within the diode gap where the velocity u_ζ becomes zero for the first time. We denote it by an index “0”. With the increasing value of the relativistic factor γ_0 , the width of the region of the ambiguous solutions (the region between δ_0 and δ_{SCL}) increases (Fig. 5.3).

Fig. 5.4 demonstrates the variations of δ_{SCL} and $\varepsilon_{0,SCL}$ with γ_0 for different values of Ω . We can see the non-monotonic behaviour of the curve $\varepsilon_{0,SCL}(\gamma_0)$ around the region of small γ_0 's and it is likely to be inherent characteristic of the

relativistic diodes [69]. The dependencies of δ_{SCL} , δ_0 , $\varepsilon_{0,SCL}$ and $\varepsilon_{0,0}$ on γ_0 are shown in Fig. 5.5 for $\Omega = 1$.

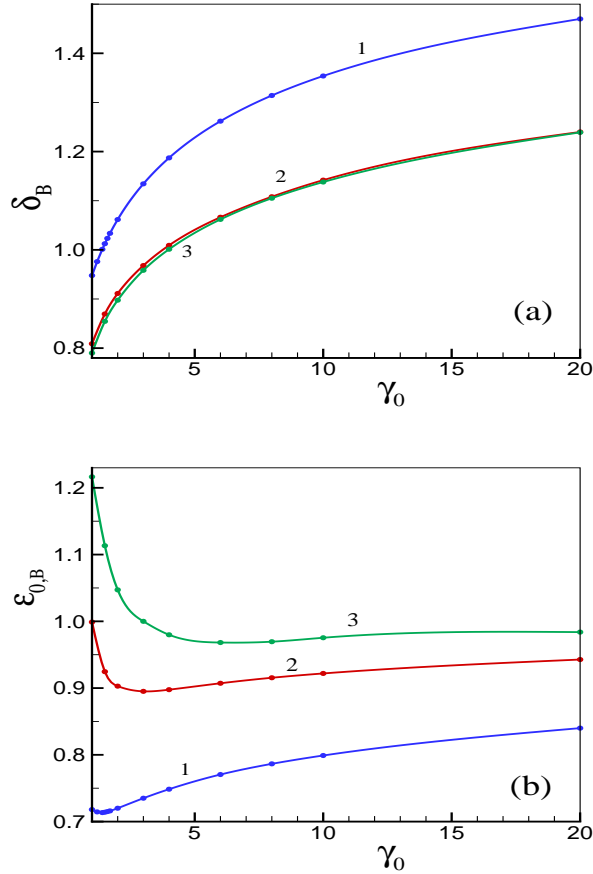


Figure 5.5: The dependencies (a) $\delta(\gamma_0)$ and (b) $\varepsilon_0(\gamma_0)$ are shown for (1) “SCL”, (2) “0” and (3) “BF” points; $\Omega = 1$. $V = 0$.

5.3.2 Regime of electron reflection

In the presence of the magnetic field, the ζ -component of the electron velocity decreases with space coordinate ζ and becomes a tangent to the line $u_\zeta = 0$ at a point where u_ζ vanishes. Then u_ζ begins to increase. Thus, we can say that the nature of the zero velocity position is point type. This feature was also observed in the non-relativistic case. As physical situations demand, taking into consideration

a small velocity spreading within the beam, we can assume that all electrons would not be turned around by the magnetic field at a point ζ_r where u_ζ vanishes. A portion of such electrons can overcome this point with velocities little higher than zero and flow toward collector. To involve “electron beam splitting” at a point ζ_r , we introduce a reflection coefficient r . In this situation, there are two flows in the region between the emitter and the point ζ_r : the direct and the reverse flow. Since at any point ζ ($\zeta < \zeta_r$), the velocities of the direct and reverse particles coincide absolutely, the densities of the direct and reverse particles become $1/u_\zeta$ and r/u_ζ , respectively. Thus, in this region, the total density of the electrons is $(1+r)/u_\zeta$. To the right of the point ζ_r , there is the direct electron flow with a weight $1-r$.

When a portion of the injected electrons is turned back, all PDs remain within a region limited by the curve $p(\zeta; \Omega)$ [as shown in (5.10)], and the function $\eta(\zeta)$ turns out to be a tangent to this curve at the point of reflection ζ_r (see curves 2, 3 and the dashed curve in Fig. 5.1).

Now we can continue our calculations for the region with $r > 0$. We utilize Eqs. (5.30) with the factor $\beta = 1+r$ to the left of the turning point ζ_r and $\beta = 1-r$ to the right of this point. The value of the extra parameter r is determined in the course of solving these equations. Solution algorithm is as follows. At a given value of ε_0 (say, $\varepsilon_0 = \tilde{\varepsilon}_0$), a particular value of the coefficient r is taken. First, Eqs. (5.30) are solved on a path from the emitter position to the location of the potential minimum with the boundary conditions (5.31). The position (ζ_m) and the value of the potential minimum (η_m) are determined from the zero electric field condition. Beyond the point of the potential minimum, Eqs. (5.30) are solved with

the boundary conditions

$$\eta_n = \eta_m, \quad \varepsilon_n = 0, \quad \zeta_n = \zeta_m \quad (5.32)$$

from the point ζ_m to the point ζ_r , where the electron velocity u_ζ vanishes. Now, iterating over a parameter r , we obtain that for some value of r , u_ζ turns out to be tangent to the straight line $u_\zeta = 0$. At this situation, we note the values of r and ε_0 and determine the relevant quantities like ζ_r , ε_r and η_r . At last, Eqs. (5.30) are solved from the point ζ_r to the collector position and δ is determined.

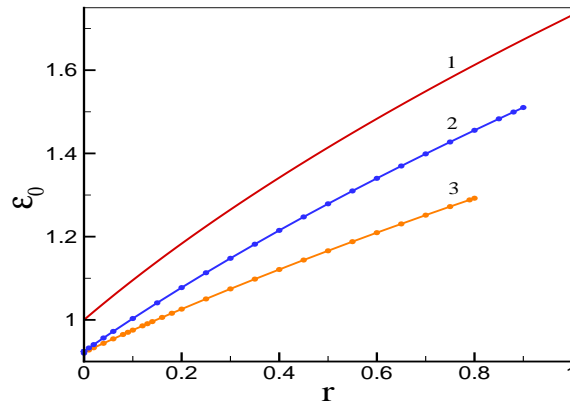


Figure 5.6: The ε_0 vs r curves are drawn for various values of γ_0 : (1) $\gamma_0 = 1$, (2) 1.5, (3) 10; $\Omega = 1$. $V = 0$.

In the course of these calculations, we increase gradually ε_0 starting from the value ε_0^0 , which corresponds to the state when the situation of zero electron velocity ($u_\zeta = 0$) arises for first time. At this moment, we have $r = 0$. When ε_0 is increased further, the coefficient r grows too. The dependence of r on ε_0 is obtained in the process of calculation, and it is shown in Fig. 5.6 for several values of γ_0 and $\Omega = 1.0$.

In Fig. 5.7, the dependence of ε_0 on δ is shown for several γ_0 values ($\Omega = 1$). In this figure, the solutions corresponding to the “partial” reflection of electrons are

also taken into consideration. Like the non-relativistic case, one can see that there are two bifurcation points in Fig. 5.7, which are *SCL* and *BF* points. Fig. 5.7 also shows that the *BF* point does not lie on the reflection threshold (zero point) and the reflection coefficient $r > 0$ at this point. It is also evident from Fig. 5.7 that the region of hysteresis (the region between δ_{SCL} and δ_{BF}) is enlarged and the region between δ_{BF} and δ_0 is narrowed, as the value of relativistic factor γ_0 increases. The *BF*-point and zero point merge together at large γ_0 values. These phenomena are clearly evident from Fig. 5.5.

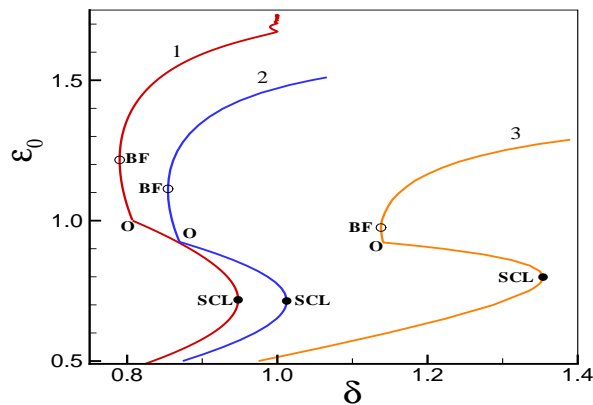


Figure 5.7: The $\varepsilon_0(\delta)$ curves are drawn for various values of γ_0 : (1) $\gamma_0 = 1$, (2) 1.5, (3) 10. $\Omega = 1$. $V = 0$. Solid circles correspond to the *SCL* points, hollow circles refer to the *BF* points and zero-points are marked by “0”.

As it was shown in Fig. 5.6, for a definite value of Ω , the value of r increases with ε_0 . When r is very close to the value 1, a moment may appear when the velocity u_ζ turns out to be zero again, i. e., the electrons may face another turning point. The situation of multiple turning points was also observed in the non-relativistic diode (see chapter four). It was reported that, at this very moment, the coefficient r does not reach its limiting value 1 but it is very close to it. Apparently, when ε_0 is increased further, the number of turning points increases and theoretically, for

$r = 1$, it becomes infinity. This fact is clearly evident from the curve 1 in Fig. 5.7 [this curve belongs to non-relativistic diode ($\gamma_0 = 1$)]. In relativistic situation, we also expect to have similar type of feature. It will be detailed in the next section.

5.4 Features of the steady-states. The Lagrange method

Now we solve the problem, using the Lagrangian variables. For 1D time-independent case we start with the basic governing equations which are the continuity and the momentum equations along with the Poisson's equation. They are written in dimensionless form as:

$$\begin{aligned} nu_\zeta &= H(\zeta; \zeta_r, r), \\ u_\zeta \frac{dp_\zeta}{d\zeta} &= -\varepsilon - \Omega u_x, \quad u_\zeta \frac{dp_x}{d\zeta} = \Omega u_\zeta, \\ \varepsilon &= -\frac{d\eta}{d\zeta}, \quad \frac{d\varepsilon}{d\zeta} = -n. \end{aligned} \quad (5.33)$$

Here $H(\zeta; \zeta_r, r) = (1+r)\Theta(\zeta_r - \zeta) + (1-r)\Theta(\zeta - \zeta_r)$, ζ_r is the point where an electron is turned around, r is the reflection coefficient; the function $\Theta(x) = 1$ at $x > 0$ and 0 at $x < 0$. The boundary conditions to be used are, density $n(\zeta = 0) = 1$, components of velocity $u_\zeta(\zeta = 0) = u_0 \equiv \sqrt{\gamma_0 + 1}/(\sqrt{2}\gamma_0)$, $u_x(\zeta = 0) = 0$, relativistic factor $\gamma(\zeta = 0) = \gamma_0$, electric potential, $\eta(\zeta = 0) = 0$, and electric field $\varepsilon(\zeta = 0) = \varepsilon_0$.

To solve these nonlinear equations, we introduce the Lagrangian coordinate τ and the Lagrange transformation,

$$\zeta = \int_0^\tau u_\zeta(\tau') d\tau'.$$

Thus, $u_\zeta d/d\zeta = d/d\tau$. Eqs. (5.33) take the form

$$\begin{aligned} nu_\zeta &= H(\zeta; \zeta_r, r), \\ \frac{dp_\zeta}{d\tau} &= -\varepsilon - \Omega u_\chi, \quad \frac{dp_\chi}{d\tau} = \Omega u_\zeta, \\ \frac{d\eta}{d\tau} &= -u_\zeta \varepsilon, \quad \frac{d\varepsilon}{d\tau} = -u_0 H(\zeta; \zeta_r, r). \end{aligned} \quad (5.34)$$

Besides, we have the conservation law of energy (5.21) and the relations (5.24) for the velocity components.

The last equation of (5.34) gives the evolution of the electric field strength

$$\begin{aligned} \varepsilon &= \varepsilon_0 - u_0(1+r)\tau, \quad \text{if } \zeta < \zeta_r, \\ \varepsilon &= \varepsilon_r - u_0(1-r)(\tau - \tau_r), \quad \text{if } \zeta > \zeta_r. \end{aligned} \quad (5.35)$$

Here τ_r is the time when an emitted electron is turned back and $\varepsilon_r = \varepsilon(\tau_r) = \varepsilon_0 - u_0(1+r)\tau_r$.

Next we have solved the system of coupled differential equations (5.34) numerically. The algorithm used is as follows: First we fixed the values of Ω , γ_0 and applied potential V . For the case of no electron turning, we have taken $r = 0$, $H = 1$ and $\varepsilon = \varepsilon_0 - u_0\tau$. For a fixed value of ε_0 , we have gradually increased the value of τ from zero and calculated the variations of ζ , u_ζ , u_χ and η with respect to τ . The ζ -dependencies of the velocity components $[u_\zeta(\zeta), u_\chi(\zeta)]$ and potential $[\eta(\zeta)]$ are evaluated through the dependence of ζ on τ . The value of τ is increased up to the moment when η takes the value V . At this stage, $\tau = T$ and $\zeta = \delta$, where T is the time of flight required for an electron to cross the inter-electrode region and δ is the inter-electrode distance in dimensionless form.

The longitudinal velocity profile $[u_\zeta(\zeta)]$ is found to form a minimum ($u_{\zeta,m}$) within diode region. With the increasing value of the ε_0 , $u_{\zeta,m}$ starts to decrease

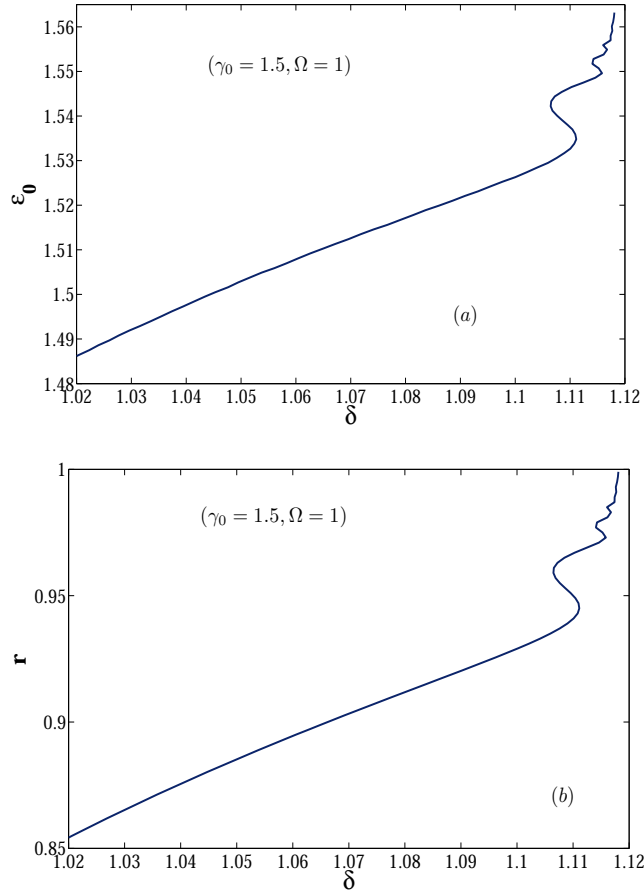


Figure 5.8: The dependencies (a) $\varepsilon_0(\delta)$ and (b) $r(\delta)$ are plotted for $\gamma_0 = 1.5$, $\Omega = 1$ and $V = 0$ in the vicinity of $r \rightarrow 1$.

and finally a situation comes when $u_{\zeta,m} = 0$, i.e., at this moment the longitudinal velocity of an electron emitted with a velocity u_0 , becomes zero within the inter-electrode region for the first time. The corresponding position of zero longitudinal velocity is calculated and denoted as ζ_r . This is the onset of the electron reflection.

If we increase the emitter-electric field strength at further, the value of r starts to increase too. For the case of partial electron reflection, r can take any value between zero and one, depending on the strength of applied magnetic field and emitter-electric field strength. For total reflection of electrons r is 1. To inspect the dependence of ε_0 on r , we have taken a fixed value of r and gradually varied the

value of ε_0 . For each value of ε_0 , the potential distribution $[\eta(\zeta)]$ and the velocity

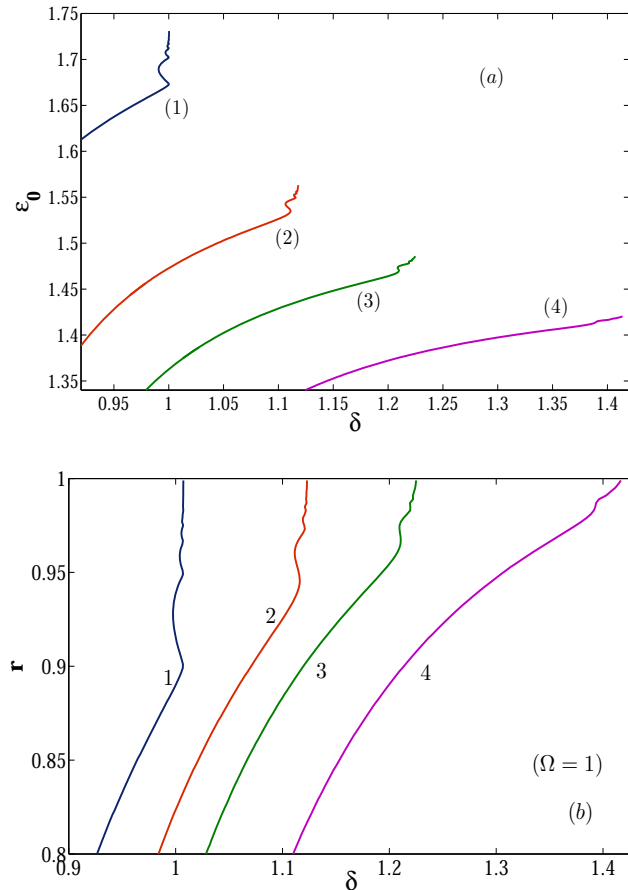


Figure 5.9: The dependencies (a) $\varepsilon_0(\delta)$ and (b) $r(\delta)$ are plotted in the vicinity of $r \rightarrow 1$, for a number of γ_0 values: (1) $\gamma_0 = 1$ (blue), (2) $\gamma_0 = 1.5$ (red), (3) $\gamma_0 = 2$ (green) and (4) $\gamma_0 = 3$ (magenta); $\Omega = 1$ and $V = 0$.

profile $[u_\zeta(\zeta)]$ are developed. The minimum value of the longitudinal component of the electron velocity ($u_{\zeta,m}$) is also calculated in each case. When for some particular value of ε_0 , $u_{\zeta,m}$ vanishes, we checked whether it is tangent to the line $u_\zeta(\zeta) = 0$ at the point of velocity minimum. If this condition holds, the value of the parameter ε_0 is marked and we assign $\tau = \tau_r$, $\zeta = \zeta_r$ and $\eta = \eta_r$. Otherwise we continue to vary ε_0 .

Once we get the turning point ζ_r , we solve the equations (5.34) for the right side

of the point ζ_r with proper boundary conditions [$u_\zeta(\tau = \tau_r) = 0$, $p_\zeta(\tau = \tau_r) = 0$ and $\eta_\zeta(\tau = \tau_r) = \eta_r$]. We increased τ starting from $\tau = \tau_r$ and started to calculate the necessary quantities. It continues up to the moment when η takes the value V . At this moment, $\zeta = \delta$. Thus, for some fixed value of r , we can have the corresponding values of ε_0 and δ . We should mention that the results obtained by the Lagrange formulation coincide with those found by the Eulerian technique.

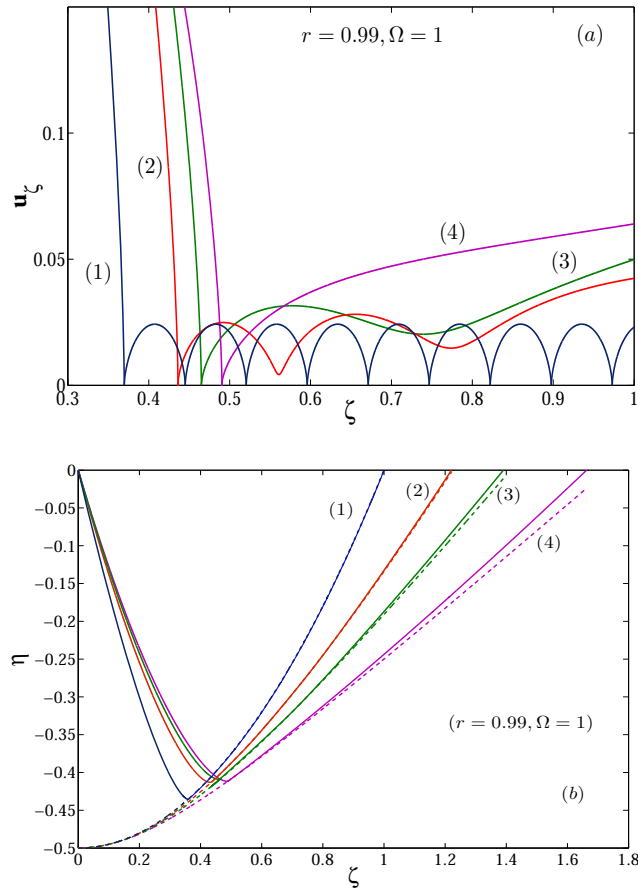


Figure 5.10: The profile of (a) velocity [$u_\zeta(\zeta)$] and (b) potential [$\eta(\zeta)$] for a number of γ_0 values: (1) $\gamma_0 = 1$ (blue), (2) $\gamma_0 = 2$ (red), (3) $\gamma_0 = 3$ (green) and (4) $\gamma_0 = 5$ (magenta); $r = 0.99, \Omega = 1$ and $V = 0$. The dashed curves in Fig. 10(b) refer to the corresponding η_c for each case.

For the case of the non-relativistic Bursian diode with uniform transverse magnetic field, an oscillatory region has been spotted in the (ε_0, δ) -diagram, as the

reflection coefficient r approaches to the value 1 (see, e.g., curve 1 in Fig. 5.7). The reason of this oscillatory region lies behind the fact that depending on the strength of the transverse magnetic field, the longitudinal component of the electron velocity can vanish for several times. As the system steps into relativistic regime, the oscillatory region disappears gradually. In our relativistic case, the oscillatory regions are also observed for relatively small values of γ_0 , when r is very close to 1. In Fig. 5.8(a) and Fig. 5.8(b), this oscillatory region is shown for $\gamma_0 = 1.5$ and $\Omega = 1$. In Fig. 5.9, the oscillatory regions are shown for $\Omega = 1$ and several γ_0 values in the vicinity of $r \rightarrow 1$. It is found that for higher values of γ_0 , the width of the oscillatory region gradually decreases. As we can see from Fig. 5.9, the oscillatory region practically disappears for $\gamma_0 \geq 3$. The physical reason behind this can be explained as follows: the presence of the transverse magnetic field starts to convert some portion of the longitudinal kinetic energy of the emitted electrons into transverse one and at zero point, for some particular strength of it, longitudinal kinetic energy becomes zero. At this position, the longitudinal velocity of the electrons becomes zero for the first time and this is the first turning point. If the strength of the external magnetic field is increased further, the electrons may suffer multiple turning points. But when the value of γ_0 is raised, the longitudinal kinetic energy of the emitted electrons increases too, reducing the possibility of having zero longitudinal velocity for multiple times within the diode gap. In Fig. 5.10(a), the velocity profile is plotted for $\Omega = 1$, $r = 0.99$ and various γ_0 values. We can see that for $\gamma_0 = 1$, the longitudinal velocity component u_ζ vanishes for many times. At first turning point, $\zeta = \zeta_r$. The velocity profiles for $\gamma_0 = 2, 3, 5$ carry a zero velocity position at $\zeta = \zeta_r$, as well as few nonzero

local velocity minima for $\zeta > \zeta_r$. The magnitudes of the velocities at these local minima increase with the increasing γ_0 values. When γ_0 is increased further, the local velocity minima disappear. Thus we can infer that, for higher γ_0 values, the tendency of multiple zero longitudinal velocities reduces. Corresponding potential distributions are plotted in Fig. 5.10(b).

5.5 Summary

In this chapter, we have studied the characteristics of the space charge limited flow for a relativistic electron beam driven Bursian diode, in the presence of a transverse magnetic field. Depending on the values of the applied magnetic field and the electric field strength at emitter, either the emitted electrons can cross the potential barrier and reach the collector surface or a fraction of them is reflected back to the emitter by the magnetic field. Both of these situations are treated separately with the help of the Eulerian and the Lagrangian descriptions.

In the relativistic vacuum diode, the width of the non-unique region (the region between *SCL* and *BF* points in the ε_0, δ -diagram) increases with the increase of the relativistic factor of the injected beam γ_0 .

Similar to the case of the non-relativistic Bursian diode with the transverse magnetic field, the $\varepsilon_0 - -\delta$ -diagram demonstrates a new oscillatory region as r approaches to 1. It arises due to the fact that in the presence of strong magnetic field, the longitudinal velocity of the injected electrons has a tendency to vanish for more than once within the inter-electrode space. When r is very close to 1, the period and the amplitude of the velocity oscillations tend to zero. However, for higher values of γ_0 , as the kinetic energy of the emitted energy increases, the

oscillatory region gets suppressed.

Chapter 6

Effect of transverse magnetic field on non-neutral plasma diodes

This chapter covers an analytical study of the non-neutral plasma diodes in the presence of an external transverse magnetic field for an arbitrary neutralization parameter γ . Investigations are restricted up to the regime where no electrons are turned around by the magnetic field. A new family of solutions appears along with the Bursian ones. Unlike the vacuum diode, there are steady state solutions for the negative values of the emitter field strength too. For $\gamma > 1$, the value of the emitter's electric field strength at the space charge limit ($E_{0,SC}$) turns out to be negative.

6.1 Introduction

The development of non-linear oscillations is typical for the Knudsen mode of a TIC [118, 133]. It was reported in Refs. [5, 118], that with the increase of the external transverse magnetic field, first, oscillation amplitude decreases, and finally these oscillations are suppressed. The presence of the magnetic field is found to be responsible for quenching instabilities and oscillations too. As shown in Refs. [171, 172], the physical processes of the Knudsen TIC can be successfully modeled by means of the Pierce-like diode [44] in which the electrons have the beam-like velocity distribution function. Therefore, it is necessary to perform an analytical treatment emphasizing the effect of the external magnetic field on the Pierce-like diode which is driven by a mono-energetic beam of charged particles.

In previous chapters, we have studied the steady state solutions of the vacuum diode driven by an electron beam (the Bursian diode) in the presence of an external transverse magnetic field. We have found that the external magnetic field can strongly influence the electron flow, when the Larmor radius becomes comparable with the inter-electrode distance.

In this present chapter, we study the time-independent solutions of a non-neutral diode where an electron beam is transported between the electrodes through the uniform background of immobile ions, in the presence of an external transverse magnetic field. Similar type of problem was studied in Ref. [173]. But, a set of specific features of the time-independent solutions were passed unnoticed. Particularly, the solutions with a potential maximum just near the emitter as well as the regime of solution corresponding to the electron turning by the magnetic field were missed. Note that the time-independent solutions of the generalized Pierce diode

in the absence of the magnetic field were studied in detail in Refs. [109, 150]. A full list of the solutions of different types was obtained, and new family of the solutions co-existing together with the Bursian ones was found. In the present paper, we show how the non-Bursian branches disappear gradually with increasing value of the applied magnetic field.

6.2 Basic equations

It is assumed that the diode region is occupied uniformly by the infinitely massive ions of constant density n_i . The emitter surface injects a non-relativistic and monoenergetic electron beam with density n_b and injection velocity v_b and the electrons travel through the uniform background of immobile ions. To measure the effect of the ion background, we have introduced the dimensionless neutralization parameter which is

$$\gamma = n_i/n_b. \quad (6.1)$$

Theoretically, γ can take any arbitrary value. This implies that the charge neutralization ($\gamma = 1$) is the only one state of many possible options. We name this kind of device as the Pierce diode [44]. For Bursian diodes $\gamma = 0$, i.e., the ions are totally absent [35]. The ions are treated as immobile. As our focus is on the fast electron processes, this type of dynamical situation can be safely assumed to be valid in lowest approximation. A practical example, where the ions do not participate in the dynamics, is mentioned in Ref. [150].

With the help of the above description, we now study the time-independent states that a plasma diode can adopt. In the presence of a transverse magnetic field, electrons move on $\{z, x\}$ plane, perpendicular to the magnetic field and have

two components of velocity: v_z and v_x . In the 1D time-independent case, we start with the basic governing equations which are continuity, momentum and the Poisson's equations:

$$\begin{aligned} \frac{d}{dz}(nv_z) &= 0, \\ v_z \frac{dv_z}{dz} &= -\frac{e}{m}E - \omega v_x, & v_z \frac{dv_x}{dz} &= \omega v_z, \\ E &= -\frac{d\varphi}{dz}, & \frac{dE}{dz} &= -\frac{e}{\epsilon_0}(n - \gamma). \end{aligned} \quad (6.2)$$

The beam accelerating voltage $V_b = W_b/e = mv_b^2/(2e)$ is in Volts, the beam current density $j_b = en_bv_b$ in Amperes per square cm and B is in Teslas; e and m are the electron charge and mass; the free-space permittivity $\epsilon_0 = 8.854 \cdot 10^{-12} C^2/Nm^2$; Larmor frequency $\omega = eB/m$ and Larmor radius $\lambda_L = mv_b/(eB)$.

To rewrite the Eqs. (6.2) in terms of dimensionless quantities, we use the energy and length units which are the kinetic energy of electrons at the emitter [$W_b = mv_b^2/2$] and the beam Debye length [$\lambda_D = \{(2\epsilon_0 W_b)/(e^2 n_b)\}^{1/2}$], respectively [58, 66]. The dimensionless coordinate, time, velocity, potential and electric field strength are defined as, $(\zeta, \chi) = (z, x)/\lambda_D$, $\tau = t\omega_b$, $(u_\zeta, u_\chi) = (v_z, v_x)/\sqrt{2W_b/m}$, $\eta = e\varphi/(2W_b)$, $\varepsilon = eE\lambda_D/(2W_b)$; here $\omega_b = [e^2 n_b/(m\epsilon_0)]^{1/2}$ is the characteristic frequency. Dimensionless inter-electrode gap and voltage between collector and emitter are denoted via δ and V respectively. Notice that in the presence of the ion background the solutions also depend on the additional parameter γ .

Now Eqs. (6.2) are written in a dimensionless form as:

$$\begin{aligned} \frac{d}{d\zeta}(nu_\zeta) &= 0, \\ u_\zeta \frac{du_\zeta}{d\zeta} &= -\varepsilon - \Omega u_\chi, & u_\zeta \frac{du_\chi}{d\zeta} &= \Omega u_\zeta, \\ \varepsilon &= -\frac{d\eta}{d\zeta}, & \frac{d\varepsilon}{d\zeta} &= -n + \gamma. \end{aligned} \quad (6.3)$$

Here Ω is the dimensionless Larmor frequency ($\Omega = \omega/\omega_b$). The boundary conditions to be used are, density $n(\zeta = 0) = 1$, components of velocity $u_\zeta(\zeta = 0) = 1$, $u_\chi(\zeta = 0) = 0$, electric potential $\eta(\zeta = 0) = 0$, and electric field $\varepsilon(\zeta = 0) = \varepsilon_0$. The emitter electric field ε_0 will be used as a variable parameter for our following analysis. The third equation of Eqs. (7.3) and the boundary condition for the χ -component of the electron velocity give $u_{chi} = \Omega\zeta$. After substituting u_χ into the second equation of (7.3) and integrating we obtain the energy conservation law:

$$\frac{1}{2}u_\zeta^2 - \eta + \frac{1}{2}\Omega^2\zeta^2 = \frac{1}{2}. \quad (6.4)$$

It is obvious that the potential distribution (PD) should be consistent with the distributions of the electrons within the diode region. Therefore, when there is a magnetic field in the transverse direction, from the above equation it follows that the PD $\eta(\zeta)$ should be restricted within a region limited by a square parabola $p(\zeta; \Omega)$

$$\eta(\zeta) \geq p(\zeta; \Omega) \equiv \frac{1}{2}(\Omega^2\zeta^2 - 1). \quad (6.5)$$

And interestingly, this condition does not depend on the ion background.

6.3 The steady state solutions

To solve the non-linear equations (6.3), we introduce the Lagrangian coordinate τ and the Lagrange transformation,

$$\zeta = \int_0^\tau u_\zeta(\tau') d\tau'.$$

Thus, $u_\zeta d/d\zeta = d/d\tau$. Then the equations (6.3) take the form

$$\begin{aligned} \frac{d}{d\tau}(nu_\zeta) &= 0, \\ \frac{du_\zeta}{d\tau} &= -\varepsilon - \Omega u_\chi, \quad \frac{du_\chi}{d\tau} = \Omega u_\zeta, \\ \frac{d\eta}{d\tau} &= -u_\zeta \varepsilon, \quad \frac{d\varepsilon}{d\tau} = -1 + \gamma u_\zeta. \end{aligned} \quad (6.6)$$

Combining Eq. (6.6) we can have

$$\frac{d^2}{d\tau^2} u_\zeta + \alpha^2 u_\zeta = 1. \quad (6.7)$$

with the initial conditions

$$u_\zeta(0) = 1, \quad \frac{d}{d\tau} u_\zeta(0) = -\varepsilon_0. \quad (6.8)$$

Here we have introduced an effective ‘‘frequency’’ $\alpha = \sqrt{\gamma + \Omega^2}$. Using these initial conditions, the solution of Eq. (6.7) in terms of the Lagrangian coordinate can be obtained as

$$u_\zeta(\tau) = \frac{1}{\alpha^2} + \left(1 - \frac{1}{\alpha^2}\right) \cos(\alpha \tau) - \frac{\varepsilon_0}{\alpha} \sin(\alpha \tau). \quad (6.9)$$

Integrating Eq. (6.9) we obtain

$$\zeta(\tau) = \frac{1}{\alpha^2} \tau + \frac{1}{\alpha} \left(1 - \frac{1}{\alpha^2}\right) \sin(\alpha \tau) + \frac{\varepsilon_0}{\alpha^2} [\cos(\alpha \tau) - 1]. \quad (6.10)$$

Now the 3rd equation of (6.6) gives

$$u_\chi(\tau) = \Omega \zeta(\tau) = \frac{\Omega}{\alpha^2} \tau + \frac{\Omega}{\alpha} \left(1 - \frac{1}{\alpha^2}\right) \sin(\alpha \tau) + \frac{\varepsilon_0 \Omega}{\alpha^2} [\cos(\alpha \tau) - 1]. \quad (6.11)$$

The 5th equation of (6.6) gives

$$\varepsilon(\tau) = \varepsilon_0 - \tau + \gamma \zeta(\tau) = \frac{\Omega^2}{\alpha^2} (\varepsilon_0 - \tau) + \frac{\gamma}{\alpha} \left(1 - \frac{1}{\alpha^2}\right) \sin(\alpha \tau) + \frac{\gamma \varepsilon_0}{\alpha^2} \cos(\alpha \tau). \quad (6.12)$$

And at last, from the energy conservation law we obtain for the potential

$$\eta(\tau) = \frac{1}{2} [u_{\zeta}^2(\tau) + \Omega^2 \zeta^2(\tau) - 1]. \quad (6.13)$$

Note that at $\gamma = 0$, we can get back the corresponding formulas for the vacuum diodes (check chapter two).

At the collector position [$\tau = T$, $\zeta = \delta$, $\eta(\delta) = V$], we have

$$\begin{aligned} \delta &= \frac{1}{\alpha^2} T + \frac{1}{\alpha} \left(1 - \frac{1}{\alpha^2}\right) \sin(\alpha T) + \frac{\varepsilon_0}{\alpha^2} [\cos(\alpha T) - 1], \\ V &= \frac{1}{2} [u_{\zeta}^2(T) + \Omega^2 \delta^2 - 1], \\ u_{\zeta}(T) &= \frac{1}{\alpha^2} + \left(1 - \frac{1}{\alpha^2}\right) \cos(\alpha T) - \frac{\varepsilon_0}{\alpha} \sin(\alpha T). \end{aligned} \quad (6.14)$$

Here, T is the time-of-flight of an electron between electrodes. For particular values of γ , Ω and ε_0 , we can determine the profiles of relevant quantities (like electron velocity, density, electric field and potential) from Eqs. (6.9)–(6.13), by gradually increasing τ up to the moment ($\tau = T$) when the potential η takes the value equal to the collector potential V . As a result, we find the value of the inter-electrode gap δ , as well as the time T when an electron arrives at the collector surface.

Fig. 6.1 demonstrates the profiles of the potential $\eta(\zeta)$ [6.1(a) and 6.1(b)] and of the longitudinal velocity of the electrons $u_{\zeta}(\zeta)$ [6.1(c) and 6.1(d)] within the inter-electrode region for $\gamma = 1.1$ and a set of Ω -values. In these figures, the maximum value of Ω corresponds to the case when $u_{\zeta}(\zeta)$ vanishes for the first time. We can see that in the absence of the magnetic field ($\Omega = 0$), the PD is a wavy-type function, and for a fixed external voltage V , several solutions can exist. With increasing values of Ω , the shape of the potential changes gradually and when

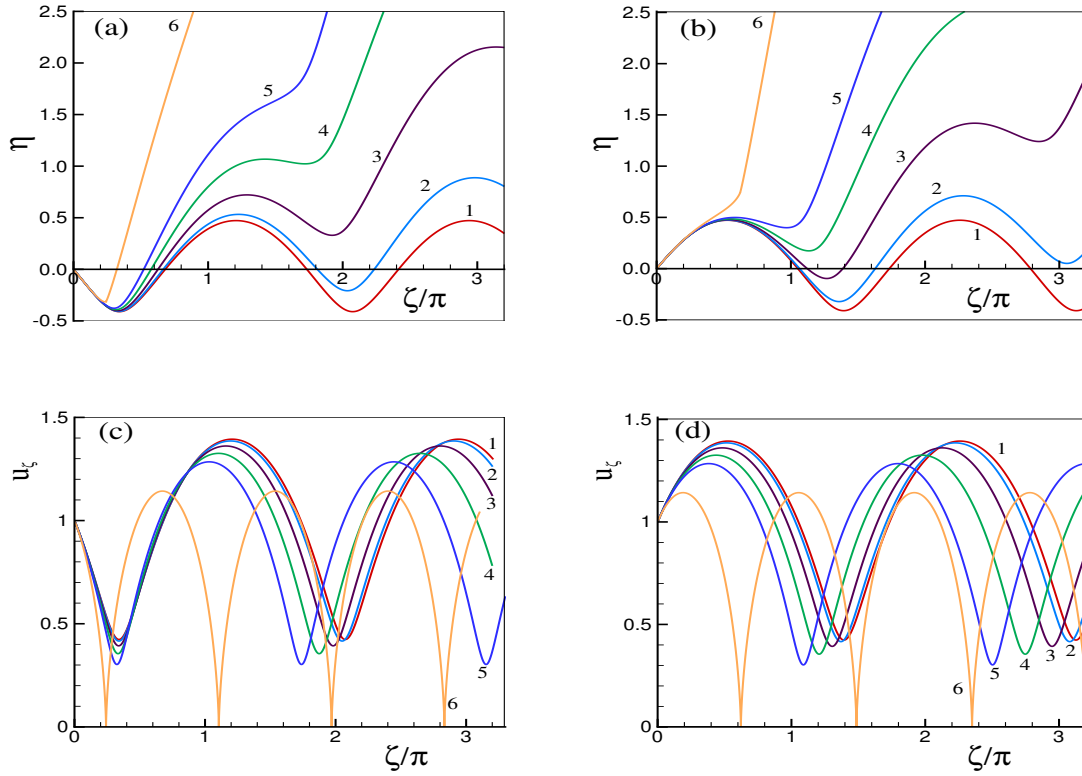


Figure 6.1: (a), (b) Potential distribution and (c), (d) electron longitudinal velocity one within the inter-electrode space drawn for various values of Ω : (1) $\Omega = 0$, (2) 0.1, (3) 0.2, (4) 0.3, (5) 0.4 and (6) 0.806225; (a), (c) $\varepsilon_0 = 0.5$; (b), (d) $\varepsilon_0 = -0.5$; $\gamma = 1.1$.

Ω exceeds a certain magnitude ($\Omega_{lim} \approx 0.3$ for the cases under consideration), the PD loses its wavy-type nature. Unlike the PD, $u_\zeta(\zeta)$ conserves wavy form with a period of about $2\pi(\gamma + \Omega^2)^{-3/2}$ for any Ω [see, e.g., Figs.6.1(c) and 6.1(d)]. Formula (6.9) also demonstrates this periodicity.

For fixed γ and V , the steady states lie on a continuous curve which represents a branch of solutions in $\varepsilon_0 - \delta$ -plane. In Fig.6.2, these branches are shown for three values of γ and a number of Ω values. Here each curve ends at such a value of ε_0 for which the longitudinal velocity turns out to be tangent to the line $u_\zeta = 0$ for the first time. The Bursian branches are located at the left part of Fig.6.2 (for $\delta \lesssim \pi$) [136, 66]. This family demonstrates also a region of non-unique solutions.

On the right boundary of this region, there is a bifurcation point – the *SCL* point. The end point, at the left part, refers to the solution containing a point within the gap in which the velocity u_ζ vanishes for the first time (“zero-point”). We mark it by an index “0”. With increasing magnetic field, the width of the region of ambiguous solutions (the region between δ_0 and δ_{SCL}) narrows and it shrinks at $\Omega = \sqrt{2 - \gamma}$ [the curve $\varepsilon_0(\delta)$ degenerates into the point $\varepsilon_0^0 = 0, \delta = 0$]. The formulas for the parameters of *SCL* and “0” points are also derived [Eqs. (6.18)–(6.24) and Eqs. (6.30)–(6.32)]. Note that for $\gamma > 1$, the *SCL* points appear only for larger values of Ω . [for example, Fig. 6.2(c) is drawn for $\gamma = 1.1$ and *SCL* point appears only at $\Omega \geq 0.3$].

The parameters related to the SCL points can be derived from the condition $d\delta/d\varepsilon_0 = 0$ [see Fig. 6.2]. We can calculate this derivative as a complex function utilizing Eq. (6.14):

$$\begin{aligned} \frac{d\delta}{d\varepsilon_0} &= \frac{\partial\delta}{\partial\varepsilon_0} + \frac{\partial\delta}{\partial T} \frac{dT}{d\varepsilon_0} = \frac{\partial\delta}{\partial\varepsilon_0} - \frac{\partial\delta}{\partial T} \frac{(\partial V/\partial\varepsilon_0)}{(\partial V/\partial T)} \\ &= \left(\frac{\partial\delta}{\partial\varepsilon_0} \frac{\partial u_\zeta}{\partial T} - u_\zeta \frac{\partial u_\zeta}{\partial\varepsilon_0} \right) / \left(\frac{\partial u_\zeta}{\partial T} + \Omega^2 \delta \right). \end{aligned} \quad (6.15)$$

Calculating the partial derivatives in (6.15) and reducing the similar terms in numerator we obtain

$$\frac{1}{\alpha} \sin(\alpha T) - \frac{\varepsilon_0}{\alpha^2} [1 - \cos(\alpha T)] = 0. \quad (6.16)$$

Transferring to half-index argument in trigonometric functions, Eq (6.16) is reduced to an equation as below

$$\frac{2}{\alpha} \sin\left(\frac{\alpha}{2} T\right) \left[\cos\left(\frac{\alpha}{2} T\right) - \frac{\varepsilon_0}{\alpha} \sin\left(\frac{\alpha}{2} T\right) \right] = 0. \quad (6.17)$$

This equation gives a relationship of T with ε_0 . Let us consider the cases $\varepsilon_0 > 0$

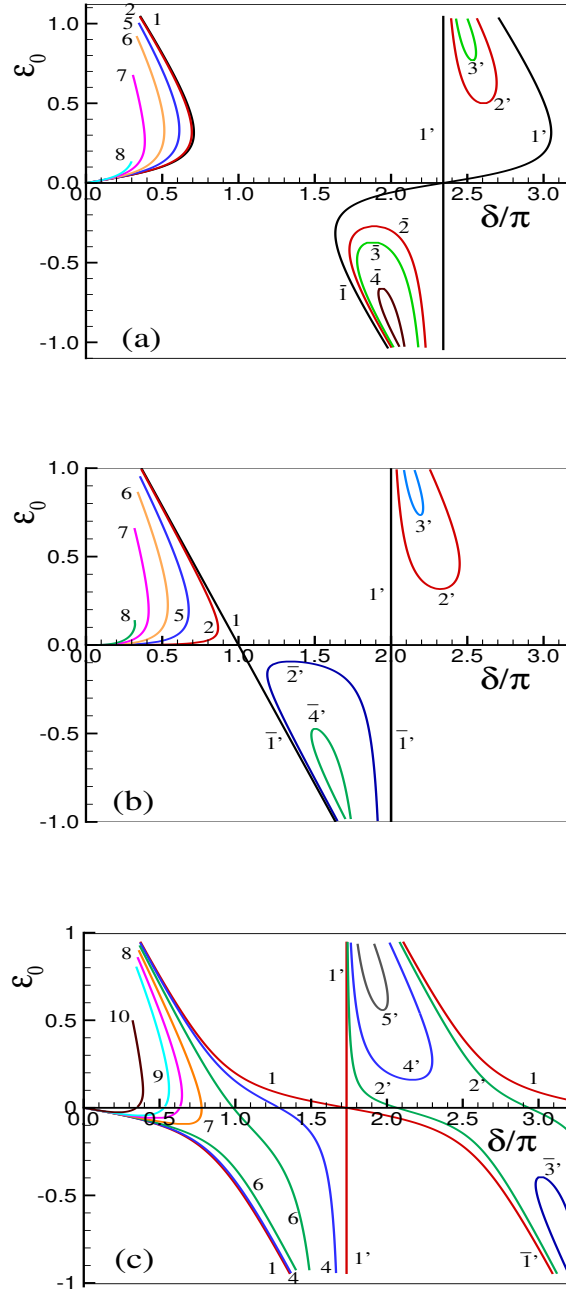


Figure 6.2: Curves $\varepsilon_0(\delta)$ drawn for three values of γ and various values of Ω : (a) $\gamma = 0.9$; $\Omega = 0$ (curve 1), 0.1 (2), 0.12 (3), 0.15 (4), 0.3 (5), 0.5 (6), 0.8 (7) and 1.04 (8); (b) $\gamma = 1.0$; $\Omega = 0$ (curve 1), 0.1 (2), 0.14 (3), 0.18 (4), 0.3 (5), 0.5 (6), 0.75 (7) and 0.99 (8); (c) $\gamma = 1.1$; $\Omega = 0$ (curve 1), 0.05 (2), 0.09 (3), 0.1 (4), 0.15 (5), 0.2 (6), 0.3 (7), 0.4 (8), 0.5 (9) and 0.806225 (10). $V = 0$. In the curves, $u_\zeta(\zeta) > 0$ everywhere.

and $\varepsilon_0 < 0$ separately. At $\varepsilon_0 > 0$ we have

$$T_{SCL} = \frac{2}{\alpha} \arctan \frac{\alpha}{\varepsilon_{0,SCL}}. \quad (6.18)$$

Substituting T_{SCL} into the first equation of (6.14), we obtain δ_{SCL} :

$$\delta_{SCL} = \frac{2}{\alpha^2} \left[\frac{1}{\alpha} \arctan \frac{\alpha}{\varepsilon_{0,SCL}} - \frac{\varepsilon_{0,SCL}}{\varepsilon_{0,SCL}^2 + \alpha^2} \right]. \quad (6.19)$$

Now we have to calculate the value ε_0 for the SCL point. First, $u_\zeta(\delta)$ is calculated, then, the law of energy conservation, [i. e. the second equation in (6.14)] is utilized.

Substituting T_{SCL} into the 3rd equation of (6.14), we obtain

$$u_\zeta = \frac{2}{\varepsilon_0^2 + \alpha^2} - 1. \quad (6.20)$$

By substituting u_ζ into the 2nd equation of (6.14), we obtain the transcendental equation to calculate the required value of $\varepsilon_{0,SCL}$:

$$\frac{4\Omega^2}{\alpha^4} \left(\frac{1}{\alpha} \arctan \frac{\alpha}{\varepsilon_{0,SCL}} - \frac{\varepsilon_{0,SCL}}{\varepsilon_{0,SCL}^2 + \alpha^2} \right)^2 + \left(\frac{2}{\varepsilon_{0,SCL}^2 + \alpha^2} - 1 \right)^2 = 1 + 2V. \quad (6.21)$$

Relationships (6.19) and (6.21) represent the maximum current in a diode for the Bursian family in presence of a transverse magnetic field [because $J_{max} \sim \delta_{SCL}^2$].

At $\varepsilon_0 < 0$ we have

$$T_{SCL} = \frac{2}{\alpha} \left(\pi - \arctan \frac{\alpha}{|\varepsilon_{0,SCL}|} \right), \quad (6.22)$$

$$\delta_{SCL} = \frac{2}{\alpha^2} \left[\frac{1}{\alpha} \left(\pi - \arctan \frac{\alpha}{|\varepsilon_{0,SCL}|} \right) + \frac{|\varepsilon_{0,SCL}|}{\varepsilon_{0,SCL}^2 + \alpha^2} \right], \quad (6.23)$$

and the relevant $\varepsilon_{0,SCL}$ is calculated from the following equation:

$$\begin{aligned} \frac{4\Omega^2}{\alpha^4} \left[\frac{1}{\alpha} \left(\pi - \arctan \frac{\alpha}{|\varepsilon_{0,SCL}|} \right) + \frac{|\varepsilon_{0,SCL}|}{\varepsilon_{0,SCL}^2 + \alpha^2} \right]^2 \\ + \left(\frac{2}{\varepsilon_{0,SCL}^2 + \alpha^2} - 1 \right)^2 = 1 + 2V. \end{aligned} \quad (6.24)$$

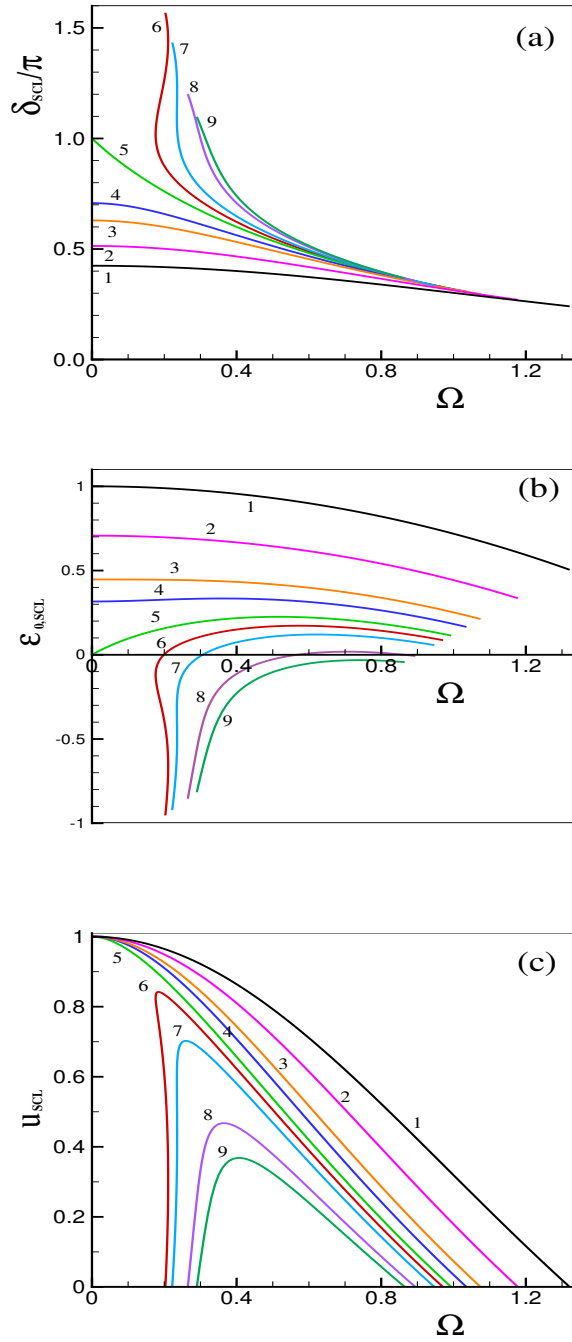


Figure 6.3: Dependencies of (a) $\delta_{SCL}(\Omega)$, (b) $\varepsilon_{0,SCL}(\Omega)$ and (c) u_{SCL} for various values of γ : (1) $\gamma = 0$, (2) 0.5, (3) 0.8, (4) 0.9, (5) 1.0, (6) 1.05, (7) 1.1, (8) 1.2 and (9) 1.25. $V = 0$.

In Fig. 6.3, the dependencies of δ_{SCL} and $\varepsilon_{0,SCL}$ on Ω are presented for a set of γ values. We can see that the value of ε_0 for the *SCL* point gets shifted to the area of negative values with the growth of γ . When γ exceeds ≈ 1.21 , $\varepsilon_{0,SCL} - \Omega$ curve stays below the line $\varepsilon_0(\Omega) = 0$. This feature was not observed in both the Pierce diode (in the absence of a magnetic field) and the Bursian diode (with and without magnetic field). These curves can be ambiguous at $\gamma > 1$. Fig. 6.3(c) shows the dependence of $u_{\zeta,SCL}$ on Ω for several γ values which are relevant to the curves shown in Figs. 6.3(a) and 6.3(b). One can see that the curves are nonmonotonic and they start and terminate at the points of zero longitudinal velocity.

We can easily find the relation between Ω and γ corresponding to $\varepsilon_{0,SCL} = 0$. The relevant value of T_{SCL} is determined from Eq. (6.16):

$$T_{SCL}^0(\Omega, \gamma) = \frac{\pi}{\alpha}, \quad (6.25)$$

then δ_{SCL} and $u_{\zeta}(T_{SCL})$ can be obtained from Eqs. (6.19) and (6.20):

$$\delta_{SCL}^0(\Omega, \gamma) = \frac{\pi}{\alpha^3}, \quad u_{\zeta} = \frac{2}{\alpha^2} - 1, \quad (6.26)$$

and after substituting them into the 2nd equation of (6.14) we obtain the relation between Ω and γ :

$$\left(\frac{2}{\gamma + \Omega^2} - 1 \right)^2 + \frac{\pi^2 \Omega^2}{(\gamma + \Omega^2)^3} - (1 + 2V) = 0. \quad (6.27)$$

For example, for $V = 0$, one can obtain an explicit dependence Ω on γ

$$\Omega = \left[\frac{\pi^2 + 4 - 8\gamma \pm \sqrt{(\pi^2 + 4)^2 - 16\pi^2\gamma}}{8} \right]^{1/2}. \quad (6.28)$$

This dependency is shown in Fig. 6.4. It is seen that the curve $\varepsilon_{0,SCL}(\Omega)$ can cross the zero line if $\gamma < \gamma_r \equiv [(\pi^2 + 4)/(4\pi)]^2 \approx 1.2114$, and the relevant Ω_r is

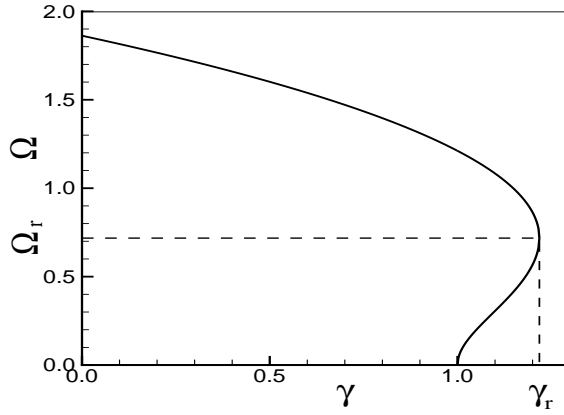


Figure 6.4: Dependence $\Omega(\gamma)$ corresponding to $\varepsilon_{0,SC L} = 0$; $V = 0$.

equal to $[(\pi^2 + 4 - 8\gamma_r)/8]^{1/2} \approx 0.7180$. It is also seen that two solutions can occur within the interval $1 < \gamma < \gamma_r$. These features are evident from Fig. 6.3(b).

To find the coordinates of the zero-point, we have to use two conditions: $u_\zeta(\tau) = 0$ and $du_\zeta(\tau)/d\tau = 0$. Based on these conditions, we obtain two equations from Eq. (6.9) to determine ε_0^0 and τ_0 (the value of the electric field strength at the emitter and time when velocity vanishes)

$$\begin{aligned} (1 - \alpha^2) \cos(\alpha \tau_0) + \varepsilon_0 \alpha \sin(\alpha \tau_0) &= 1, \\ - (1 - \alpha^2) \sin(\alpha \tau_0) + \varepsilon_0 \alpha \cos(\alpha \tau_0) &= 0. \end{aligned} \quad (6.29)$$

Solving this system of equations, we find

$$\begin{aligned} \varepsilon_0^0 &= \pm \sqrt{2 - (\gamma + \Omega^2)}, \\ \sin(\alpha \tau_0) &= \pm \alpha \sqrt{2 - \alpha^2}, \quad \cos(\alpha \tau_0) = 1 - \alpha^2. \end{aligned} \quad (6.30)$$

We can see from the 1st equation of Eqs. (6.30) that such solutions can only exist at $\Omega \leq \sqrt{2 - \gamma}$. This condition predicates that the solutions corresponding to the situation when no electron is reflected by the magnetic field cannot exist at $\gamma > 2$.

Substituting the terms from Eq. (6.30) into Eq. (6.9), we find the coordinate of the point ζ_0 where the electron velocity vanishes. Depending on the values of γ and Ω , the function $\zeta_0(\gamma, \Omega)$ reads for $\varepsilon_0^0 \geq 0$

$$\begin{aligned} & \alpha^{-3} \left[\arcsin(\alpha\sqrt{2-\alpha^2}) - \alpha\sqrt{2-\alpha^2} \right], \text{ if } \Omega^2 \leq 1-\gamma, \\ & \alpha^{-3} \left[\pi - \arcsin(\alpha\sqrt{2-\alpha^2}) - \alpha\sqrt{2-\alpha^2} \right], \text{ if } \Omega^2 > 1-\gamma. \end{aligned} \quad (6.31)$$

We should note that with no magnetic field, $\varepsilon_0^0 = \sqrt{2-\gamma}$, and the relevant $\zeta_0 = \gamma^{-3/2} [\arcsin \sqrt{2\gamma-\gamma^2} - \sqrt{2\gamma-\gamma^2}]$. This coincides with formulae (9) of Ref. [136].

On the other hand, for $\varepsilon_0^0 < 0$ the function $\zeta_0(\gamma, \Omega)$ reads

$$\begin{aligned} & \alpha^{-3} \left[2\pi - \arcsin(\alpha\sqrt{2-\alpha^2}) + \alpha\sqrt{2-\alpha^2} \right], \text{ if } \Omega^2 \leq 1-\gamma, \\ & \alpha^{-3} \left[\pi + \arcsin(\alpha\sqrt{2-\alpha^2}) + \alpha\sqrt{2-\alpha^2} \right], \text{ if } \Omega^2 > 1-\gamma. \end{aligned} \quad (6.32)$$

In order to calculate the relevant inter-electrode distance δ_0 , we have to continue our calculation of the PD using Eqs. (6.9), (6.10) and (6.13), starting from $\tau = \tau_0$ until the moment T when $\eta(T) = V$. We need to keep in our mind that at some value of ε_0 , the condition $\eta = V$ is not fulfilled anymore. It is seen from Figs. 6.1(a) and 6.1(b) that the point of minimum of each curve $\eta(\zeta)$ goes up as Ω increases, i.e. height of the potential minimum reduces and ultimately it exceeds the applied value of the potential, V . For this reason, there is a limit for ε_0^0 .

Fig. 6.5 shows the variation of the position ζ_0 (at which the longitudinal velocity of the electrons vanishes for the first time within a gap), the relevant inter-electrode distance δ_0 as well the electric field at the emitter ε_0^0 with Ω for various values of γ . We see that two values of ζ_0 can exist for some fixed value of Ω (excluding $\Omega = 0$) corresponding to positive or negative ε_0^0 value. We can also see that a portion of the curves in these figures are cut off. It is due to the fact that the PD does not

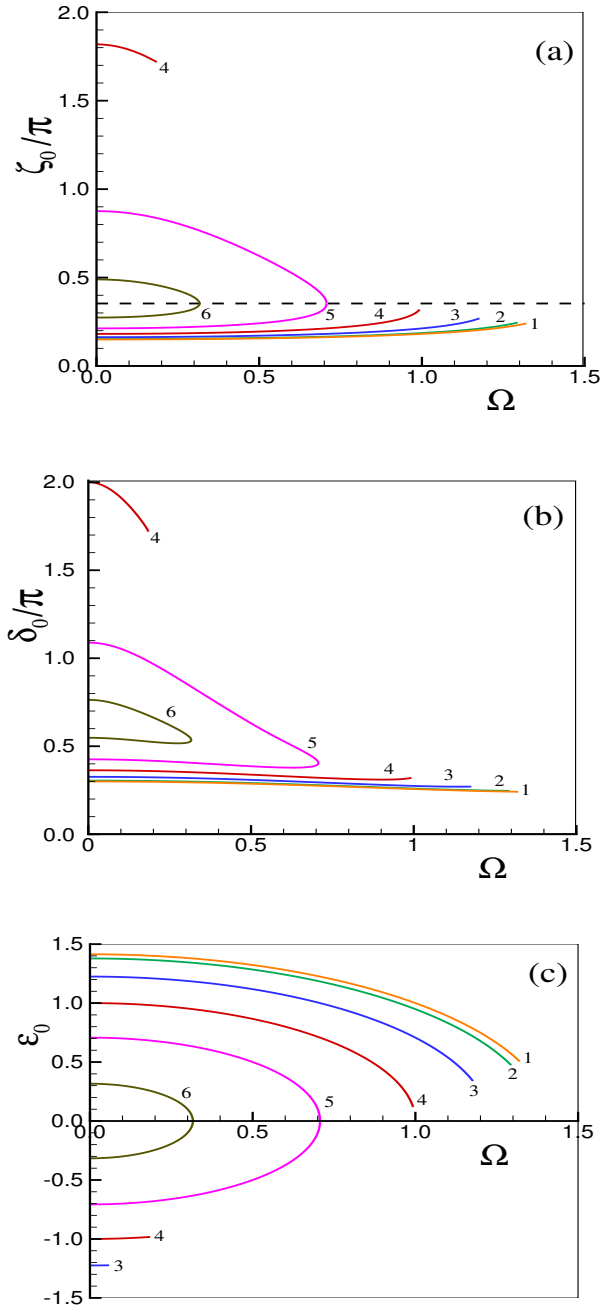


Figure 6.5: Dependencies of (a) ζ_0 , (b) δ_0 , and (c) ε_0^0 for various values of γ : (1) $\gamma = 0$, (2) 0.1, (3) 0.5, (4) 1.0, (5) 1.5, (6) 1.9. The dashed line in Fig. (a) corresponds to $\varepsilon_0^0 = 0$. $V = 0$.

intersect the line $\eta(\tau) = V$ for $\tau > \tau_0$.

For some particular values of Ω and ε_0 , the *SCL* and zero points coincide (both lie on the collector) with each other and their positions are determined from the 2nd equation of (6.14) with $u_\zeta(T) = 0$:

$$\delta_{SCL}^0(\Omega, \gamma; V) = \frac{\sqrt{1+2V}}{\Omega}. \quad (6.33)$$

It seems at first sight that $\delta_{SCL}^0(\Omega)$ does not depend on γ . However, it is not true. When the relevant $\varepsilon_{0,SCL}^0$ is calculated from the 1st formula of (6.30), we can check that it depends on γ too. We can calculate the corresponding value of Ω_0 from the equation which can be obtained after substituting the expression of $\varepsilon_{0,SCL}^0$ into Eq. (6.21) or Eq. (6.24):

$$\frac{2\Omega}{\alpha^2} \left(\frac{1}{\alpha} \arctan \frac{\alpha}{\sqrt{2-\alpha^2}} - \frac{\sqrt{2-\alpha^2}}{2} \right) = \sqrt{1+2V}, \quad \text{if } \varepsilon_{0,SCL}^0 \geq 0, \quad (6.34)$$

$$\frac{2\Omega}{\alpha^2} \left[\frac{1}{\alpha} \left(\pi - \arctan \frac{\alpha}{\sqrt{2-\alpha^2}} \right) + \frac{\sqrt{2-\alpha^2}}{2} \right] = \sqrt{1+2V}, \quad \text{if } \varepsilon_{0,SCL}^0 < 0. \quad (6.35)$$

The value of Ω_0 depends on γ , and thus δ_{SCL}^0 depends on γ too. Figs. 4(b) shows the variation of $\varepsilon_{0,SCL}$ with Ω . The curves representing $\varepsilon_{0,SCL}(\Omega)$ finish at $\Omega = \Omega_0(\gamma)$.

In the presence of ion background, new families of the branches appear. They are located at the right part of Figs. 6.2(a)–6.2(c) (e. g., for $\gamma = 0.9$ it occurs at $\delta > 1.5\pi$). Existence of such a family is typical for the diode with an ion background [136]. This occurs due to the fact that the corresponding PDs are wavy-type curves [see, Figs. 6.1(a) and 6.1(b)]. With the increase of the magnetic field, these families die away gradually (e. g., for $\gamma = 0.9$ this happens at $\Omega \approx 0.15$).

6.4 Summary

In this chapter we have studied a generalized Pierce diode in the presence of a transverse magnetic field by using the Lagrange technique. Analytical formulas for the electron trajectories as well as for the potential and the electric field were obtained. It is found that the potential profile is a wavy-type function for either weak magnetic field or when it is absent. The spatial period of the wavy PD is about $2\pi(\gamma + \Omega^2)^{-3/2}$. The wavy potential profile brings a new family of solutions which exists along with the Bursian one. As the magnitude of the applied magnetic field is increased, the PDs gradually lose the wavy nature, and non-Bursian branches disappear slowly. When the strength of the external magnetic field crosses a critical value only Bursian branches remain. Unlike the Bursian diode, the emitter field strength ε_0 can take both positive and negative values. When neutralization parameter is greater than unity ($\gamma > 1$), the ε_0 value of the *SCL* point may turn out to be negative.

Relatively strong magnetic field causes severe velocity spreading in the electron distribution function and the beam features are lost. This, in its turn, can weaken the “Bursian-Pierce instability” and the aperiodic oscillations in the diode.

Chapter 7

The regime of electron-reflection of a non-neutral plasma diode in the presence of a transverse magnetic field

In this chapter we investigate a non-neutral plasma diode when electrons are reflected back to the emitter by the transverse magnetic field for arbitrary values of the neutralization parameter. Both the Bursian and non-Bursian families of solutions are explored for the regime of electron-reflection with the help of Lagrangian formalism.

7.1 Introduction

In last chapter, assuming the monoenergetic emission of electron beam, we studied the influence of the transverse magnetic field on the steady-state solutions for the generalized Pierce diode [150] (non-neutral diode). All steady state solutions are visualized by the “emitter field strength vs diode gap” diagram. This diagram shows that, for relatively weak magnetic field, a new family of solutions arises along with the Bursian one. This new non-Bursian solutions appear because of the wavy potential distributions (PD) within the inter-electrode gap [136, 150]. The investigation was restricted up to the limit, when the longitudinal component of the electron velocity vanishes within the inter-electrode region for the first time (“zero-point”). At this condition potential barrier height acquires a threshold value and all electrons are turned back to the emitter by the potential barrier (as the emitted beam is monoenergetic). But the situation of partial electron reflection comes when there is a small velocity spread in the emitted electron beam. In this case, a small portion of the emitted electrons may overcome the barrier with a velocity little higher than the zero.

In this chapter, we intend to look beyond the “zero-point”. We study the time-independent solutions of a generalized Pierce diode when a fraction of the emitted electrons experiences reflection at a point within the diode gap in the presence of an external transverse magnetic field. Our primary motive is to explore both the Bursian and non-Bursian solutions in this regime.

7.2 Model and the dimensionless variables

We assume the same planar model for the Pierce diode as it was taken in previous chapter. A non-relativistic electron beam is supplied by the emitter surface with density n_b and velocity v_b . The emitted electrons are transported through the inter-electrode gap which is uniformly occupied by the infinitely massive immobile ions of constant density n_i . Ion background is taken into account through the dimensionless neutralization parameter $\gamma = n_i/n_b$.

Let us consider that the longitudinal velocity of an electron, emitted with a velocity v_b , vanishes at a point z_r . Now to incorporate the “electron beam splitting” at the point z_r , a reflection coefficient r is introduced [67]. In this case, there are two types of flow in the region between the emitter and the point z_r : the direct and the reverse flow. Therefore, for $z < z_r$, the electron flux carries a weight $1 + r$. To the right of the point z_r , there is the direct electron flow with a weight $1 - r$.

In this situation, the product of the density and the electron velocity longitudinal component (coming from the continuity equation at steady state) at a point z should be modified as

$$\begin{aligned} n(z)u_z(z) &= j_b H(z; z_r, r) \\ &\equiv j_b [(1 + r)\Theta(z_r - z) + (1 - r)\Theta(z - z_r)]. \end{aligned} \quad (7.1)$$

Here $j_b = en_b v_b$ is the beam current density, and the Heavyside function $\Theta(x) = 1$ for $x > 0$ and $\Theta(x) = 0$ for $x < 0$.

In the 1D time-independent case, we start with the basic governing equations

which are the equation of continuity and the momentum equations and the Poisson's equation:

$$\begin{aligned} \frac{d}{dz}(nv_z) &= 0, \\ v_z \frac{dv_z}{dz} &= -\frac{e}{m}E - \omega v_x, & v_z \frac{dv_x}{dz} &= \omega v_z, \\ E &= -\frac{d\varphi}{dz}, & \frac{dE}{dz} &= -\frac{e}{\epsilon_0}(n - \gamma). \end{aligned} \quad (7.2)$$

To describe the above equations in terms of the dimensionless variables, we use the same unit system as introduced in chapter six. In terms of the dimensionless variables, Eqs. (7.2) can be written as

$$\begin{aligned} nu_\zeta &= H(\zeta; \zeta_r, r), \\ u_\zeta \frac{du_\zeta}{d\zeta} &= -\varepsilon - \Omega u_\chi, & u_\zeta \frac{du_\chi}{d\zeta} &= \Omega u_\zeta, \\ \varepsilon &= -\frac{d\eta}{d\zeta}, & \frac{d\varepsilon}{d\zeta} &= -n + \gamma. \end{aligned} \quad (7.3)$$

The dimensionless Larmor frequency, Ω is defined in unit of ω_b [$\Omega = (eB/m)/\omega_b$]. The boundary conditions for the relevant variables at the position of the emitter surface can be taken in following forms, the density $n(\zeta = 0) = 1$, components of velocity $u_\zeta(\zeta = 0) = 1$, $u_\chi(\zeta = 0) = 0$, the electric potential, $\eta(\zeta = 0) = 0$, and the electric field $\varepsilon(\zeta = 0) = \varepsilon_0$. We shall use the emitter electric field ε_0 as a parameter to characterize the steady states.

In previous chapter, it was explained from the energy conservation principle that, in the presence of transverse magnetic field, the PD $\eta(\zeta)$ should be restricted within a region limited by a square parabola $p(\zeta; \Omega)$

$$\eta(\zeta) \geq p(\zeta; \Omega) \equiv \frac{1}{2} (\Omega^2 \zeta^2 - 1). \quad (7.4)$$

7.3 Steady state solutions

To solve Eqs. (7.3), we introduce the Lagrangian coordinate τ and the Lagrange transformation,

$$\zeta = \int_0^\tau u_\zeta(\tau') d\tau'.$$

Thus, $u_\zeta d/d\zeta = d/d\tau$ and Eqs. (7.3) become

$$\begin{aligned} nu_\zeta &= H(\zeta; \zeta_r, r), \\ \frac{du_\zeta}{d\tau} &= -\varepsilon - \Omega^2 \zeta, \\ \frac{d\eta}{d\tau} &= -u_\zeta \varepsilon, \quad \frac{d\varepsilon}{d\tau} = -1 + \gamma u_\zeta. \end{aligned} \quad (7.5)$$

In the first equation of Eqs. (7.5), we have taken into account the electron beam splitting at the point ζ_r through the Heavyside function $H(\zeta; \zeta_r, r)$. Combining Eqs. (7.5) we have

$$\frac{d^2}{d\tau^2} u_\zeta + \alpha^2 u_\zeta = H(\zeta; \zeta_r, r). \quad (7.6)$$

and the initial conditions related to the above equation are

$$u_\zeta(0) = 1, \quad \frac{d}{d\tau} u_\zeta(0) = -\varepsilon_0. \quad (7.7)$$

In Eq. (7.6), we have introduced an effective “frequency” $\alpha = \sqrt{\gamma + \Omega^2}$. Using these initial conditions, the solution of Eq. (7.6) in terms of the Lagrangian coordinate to the left of the point ζ_r can be obtained as

$$u_\zeta(\tau) = \frac{1+r}{\alpha^2} + \left(1 - \frac{1+r}{\alpha^2}\right) \cos(\alpha \tau) - \frac{\varepsilon_0}{\alpha} \sin(\alpha \tau). \quad (7.8)$$

Integrating Eq. (7.8) we obtain

$$\zeta(\tau) = \frac{1+r}{\alpha^2} \tau + \frac{1}{\alpha} \left(1 - \frac{1+r}{\alpha^2}\right) \sin(\alpha \tau) + \frac{\varepsilon_0}{\alpha^2} [\cos(\alpha \tau) - 1]. \quad (7.9)$$

If electrons are not turned back at all, then $r = 0$ and the formulas (7.8) and (7.9) coincide with the relevant formulas given in chapter six.

To calculate the time τ_r when the electron is turned around at the point ζ_r , as well as to get a relation between r and ε_0 , we have two conditions

$$u_\zeta(\tau = \tau_r) = 0, \quad \frac{d}{d\tau}u_\zeta(\tau = \tau_r) = 0. \quad (7.10)$$

With the help of Eqs. (7.8) and (7.10), these two conditions lead us to

$$\begin{aligned} (1 + r - \alpha^2) \cos \alpha \tau_r + \varepsilon_0 \alpha \sin \alpha \tau_r &= 1 + r, \\ (1 + r - \alpha^2) \sin \alpha \tau_r - \varepsilon_0 \alpha \cos \alpha \tau_r &= 0. \end{aligned} \quad (7.11)$$

From Eq. (7.11), we find

$$\begin{aligned} r &= \frac{\varepsilon_0^2 + \alpha^2}{2} - 1, \quad \varepsilon_0 = \pm \sqrt{2(1+r) - \alpha^2}, \\ \sin \alpha \tau_r &= \frac{\alpha}{1+r} \varepsilon_0, \quad \cos \alpha \tau_r = 1 - \frac{\alpha^2}{1+r}. \end{aligned} \quad (7.12)$$

First two equations of (7.12) are the relations between the emitter field strength ε_0 and the coefficient r . They also allow us to calculate the maximum value of ε_0 for which r takes the value one

$$|\varepsilon_{0,max}(\gamma, \Omega)| = \sqrt{4 - \gamma - \Omega^2}. \quad (7.13)$$

From the 3rd and 4th equations of (7.12), we can calculate the time τ_r when the electron velocity u_ζ vanishes. Depending on the values of γ and Ω , the function $\tau_r(\gamma, \Omega)$ reads for $\varepsilon_0 \geq 0$ as

$$\begin{aligned} &\frac{1}{\alpha} \sin^{-1} \frac{\alpha \sqrt{2(1+r) - \alpha^2}}{1+r}, \quad \text{if } \Omega^2 \leq 1+r-\gamma, \\ &\frac{1}{\alpha} \left(\pi - \sin^{-1} \frac{\alpha \sqrt{2(1+r) - \alpha^2}}{1+r} \right), \quad \text{if } \Omega^2 \geq 1+r-\gamma. \end{aligned} \quad (7.14)$$

and for $\varepsilon_0 < 0$ τ_r is equal to

$$\begin{aligned} & \frac{1}{\alpha} \left(2\pi - \sin^{-1} \frac{\alpha \sqrt{2(1+r) - \alpha^2}}{1+r} \right), \text{ if } \Omega^2 \leq 1+r-\gamma, \\ & \frac{1}{\alpha} \left(\pi + \sin^{-1} \frac{\alpha \sqrt{2(1+r) - \alpha^2}}{1+r} \right), \text{ if } \Omega^2 \geq 1+r-\gamma. \end{aligned} \quad (7.15)$$

Depending on the sign of ε_0 , when we substitute Eq. (7.14) or (7.15) into Eq. (7.9), we can get the coordinate of the point where the electron velocity u_ζ vanishes

$$\zeta_r = \frac{1}{\alpha^2} [(1+r)\tau_r - \varepsilon_0]. \quad (7.16)$$

To deduce the parameters of the electron trajectory for the region locating to the right of ζ_r , we need to solve Eq. (7.5) with the initial conditions (7.10). Thus, for $\zeta > \zeta_r$, we have

$$\begin{aligned} u_\zeta(\tau) &= \frac{1-r}{\alpha^2} [1 - \cos \alpha(\tau - \tau_r)], \\ \zeta(\tau) &= \zeta_r + \frac{1-r}{\alpha^2} (\tau - \tau_r) - \frac{1-r}{\alpha^3} \sin \alpha(\tau - \tau_r). \end{aligned} \quad (7.17)$$

From the energy conservation law we obtain for the potential

$$\eta(\tau) = \frac{1}{2} [u_\zeta^2(\tau) + \Omega^2 \zeta^2(\tau) - 1]. \quad (7.18)$$

At the collector [$\tau = T$, $\zeta = \delta$, $\eta(\delta) = V$], we have

$$\begin{aligned} \delta &= \zeta_r + \frac{1-r}{\alpha^2} (T - \tau_r) - \frac{1-r}{\alpha^3} \sin \alpha(T - \tau_r), \\ V &= \frac{1}{2} [u_\zeta^2(T) + \Omega^2 \delta^2 - 1], \\ u_\zeta(T) &= \frac{1-r}{\alpha^2} [1 - \cos \alpha(T - \tau_r)]. \end{aligned} \quad (7.19)$$

Here, T is the time required for the electron to cross the inter-electrode gap.

Figs. 7.1(a) and 6.1(b) show the PDs for two cases: for the regime when all electrons can arrive at the collector and for the regime when a portion of the

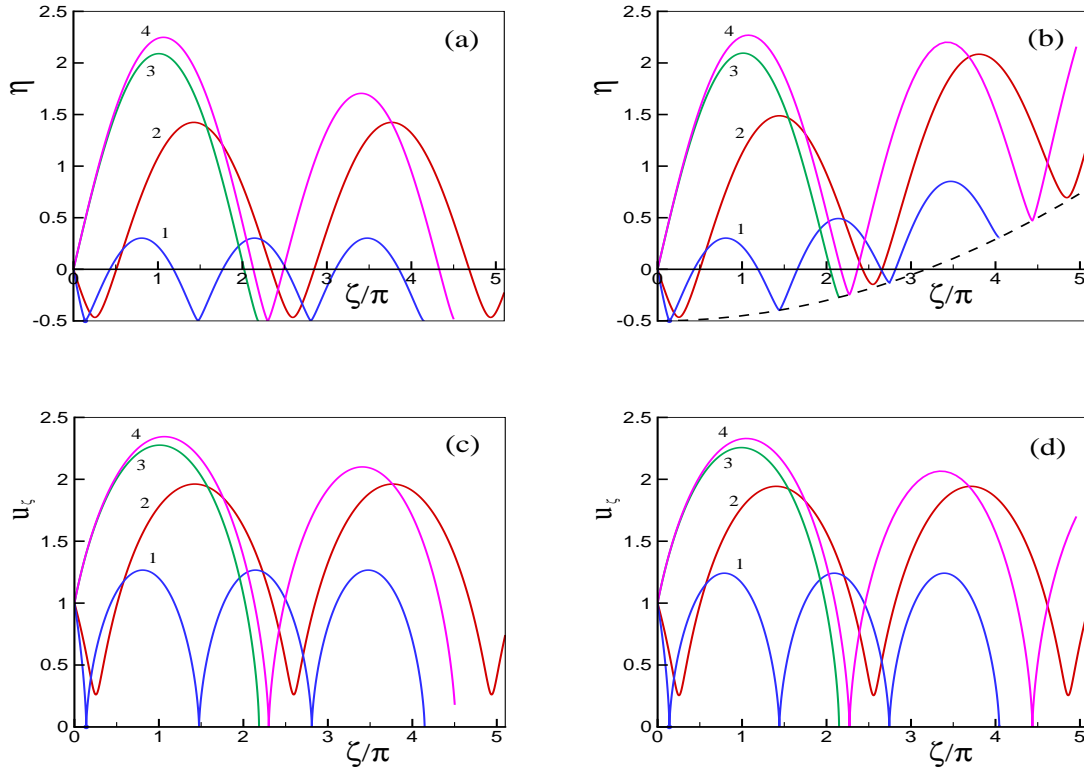


Figure 7.1: (a), (b) Potential distribution and (c), (d) electron longitudinal velocity profile within the inter-electrode space drawn for various values of ε_0 : (1) $\varepsilon_0 = 1.4$, (2) 0.8, (3) -1.1, (4) -1.1. Fig. (a), (c) correspond to $\Omega = 0$ with $r = 0.43$ on curve (1), 0 (2), 0 (3), 0.055 (4); Fig. (b), (d) – $\Omega = 0.1$ with $r = 0.435$ on curve (1), 0 (2), 0 (3), 0.06 (4). $\gamma = 0.9$. The real PDs terminate at points with $V = 0$. The dashed line corresponds to Eq. 10.

emitted electrons are turned back to the emitter by the magnetic field. PDs are shown for $\gamma = 0.9$ and two values of Ω ($\Omega = 0$ and 0.1) in those figures. One can see that the potential distribution $\eta(\zeta)$ has wavy profile. Because of this wavy potential profile, a number of steady state solutions is possible. Let us determine the steady states when the collector potential is fixed at V . For a certain value of ε_0 , the number of possible values of δ can be more than one. For some definite values of Ω and ε_0 , the corresponding values of δ can be obtained from the positions where the relevant PD $[\eta(\zeta)]$ intersects with the line $\eta = V$. In the absence of the magnetic field the PDs are periodic functions and each of the potential minima

have equal magnitude. This is also true for the potential maxima. On the other hand, when the magnetic field is applied, the magnitudes of the minima start to differ with each other in such a way that, below the line $\eta = V$, the minimum at larger ζ takes smaller magnitude than the minimum at lower ζ . When Ω crosses a certain critical value (say, Ω_{cr}), only one solution remains. This happens because of the fact that, for $\Omega > \Omega_{cr}$ (e. g., $\Omega_{cr} \approx 0.12$ for $\gamma = 0.9$), the second and all following potential minima stay above the straight line $\eta(\zeta) = V$. Therefore, if the collector is placed at the point where η is equal to V then for $\Omega > \Omega_{cr}$ there is only one solution in the region between the electrodes.

For a fixed value of V , the steady states lie on a continuity curve representing a branch of solutions in $\varepsilon_0 - \delta$ -plane. At first, we build $\varepsilon_0 - \delta$ -curves for the solutions without electron reflection ($r = 0$). In this case, $|\varepsilon_0| \leq |\varepsilon_0^0| = \sqrt{2 - \alpha^2}$, where ε_0^0 corresponds to the emitter field strength for which the turning point arises for the first time. Then we calculate the solutions related to the regime with electron reflection. We begin to increase the parameter r , starting from $r = 0$. For each value of r , we calculate ε_0 and δ . The ε_0 vs δ parametric plots are shown in Fig. 7.2 for three γ values. We can see two types of solutions which can be categorized in Bursian and non-Bursian families. The Bursian branches occur for small δ -values and the non-Bursian branches appear for relatively large δ -values. With the increase of Ω the Bursian branches shift to the left. For $\Omega < \Omega_{cr}(\gamma)$, we can see that the Bursian branches meet with the non-Bursian ones (see curves 1 and 2 in Fig. 7.2) and in these branches the coefficient r is limited within a value which is smaller than unity ($r < r_{lim} < 1$). However, for $\Omega > \Omega_{cr}$ the non-Bursian branches disappear. In the remaining Bursian branches r can take values from 0

to 1. As the value of r becomes close to 1, a zigzag segment appears in the $\varepsilon_0(\delta)$ curves. This segment corresponds to the ambiguous solutions. With the increase of Ω the width of this region gets narrowed.

For negative values of ε_0 , a potential maximum is formed near the emitter [see, curve 4 in Fig. 7.1(a) and 3 in Fig. 7.1(b)]. The non-Bursian branches are shown both for the cases when the electrons do not suffer reflection and when they are turned back to the emitter by the magnetic field. For $\Omega > \Omega_{cr}$ these branches disappear.

The Bursian branches in the Pierce diode contains two bifurcation points which are the *SCL* point and the *BF* point. Formulas for the *SCL* point were calculated in previous chapter and for this purpose the condition $d\delta/d\varepsilon_0 = 0$ was used. For $\varepsilon_0 > 0$,

$$T_{SCL} = \frac{2}{\alpha} \arctan \frac{\alpha}{\varepsilon_{0,SCL}}, \quad (7.20)$$

$$\delta_{SCL} = \frac{2}{\alpha^2} \left[\frac{1}{\alpha} \arctan \frac{\alpha}{\varepsilon_{0,SCL}} - \frac{\varepsilon_{0,SCL}}{\varepsilon_{0,SCL}^2 + \alpha^2} \right]. \quad (7.21)$$

A transcendental equation can be derived to calculate $\varepsilon_{0,SCL}$ also:

$$\frac{4\Omega^2}{\alpha^4} \left(\frac{1}{\alpha} \arctan \frac{\alpha}{\varepsilon_{0,SCL}} - \frac{\varepsilon_{0,SCL}}{\varepsilon_{0,SCL}^2 + \alpha^2} \right)^2 + \left(\frac{2}{\varepsilon_{0,SCL}^2 + \alpha^2} - 1 \right)^2 = 1 + 2V. \quad (7.22)$$

For $\varepsilon_0 < 0$, the relevant formulas take the form

$$T_{SCL} = \frac{2}{\alpha} \left(\pi - \arctan \frac{\alpha}{|\varepsilon_{0,SCL}|} \right), \quad (7.23)$$

$$\delta_{SCL} = \frac{2}{\alpha^2} \left[\frac{1}{\alpha} \left(\pi - \arctan \frac{\alpha}{|\varepsilon_{0,SCL}|} \right) + \frac{|\varepsilon_{0,SCL}|}{\varepsilon_{0,SCL}^2 + \alpha^2} \right], \quad (7.24)$$

$$\frac{4\Omega^2}{\alpha^4} \left[\frac{1}{\alpha} \left(\pi - \arctan \frac{\alpha}{|\varepsilon_{0,SCL}|} \right) + \frac{|\varepsilon_{0,SCL}|}{\varepsilon_{0,SCL}^2 + \alpha^2} \right]^2 + \left(\frac{2}{\varepsilon_{0,SCL}^2 + \alpha^2} - 1 \right)^2 = 1 + 2V. \quad (7.25)$$

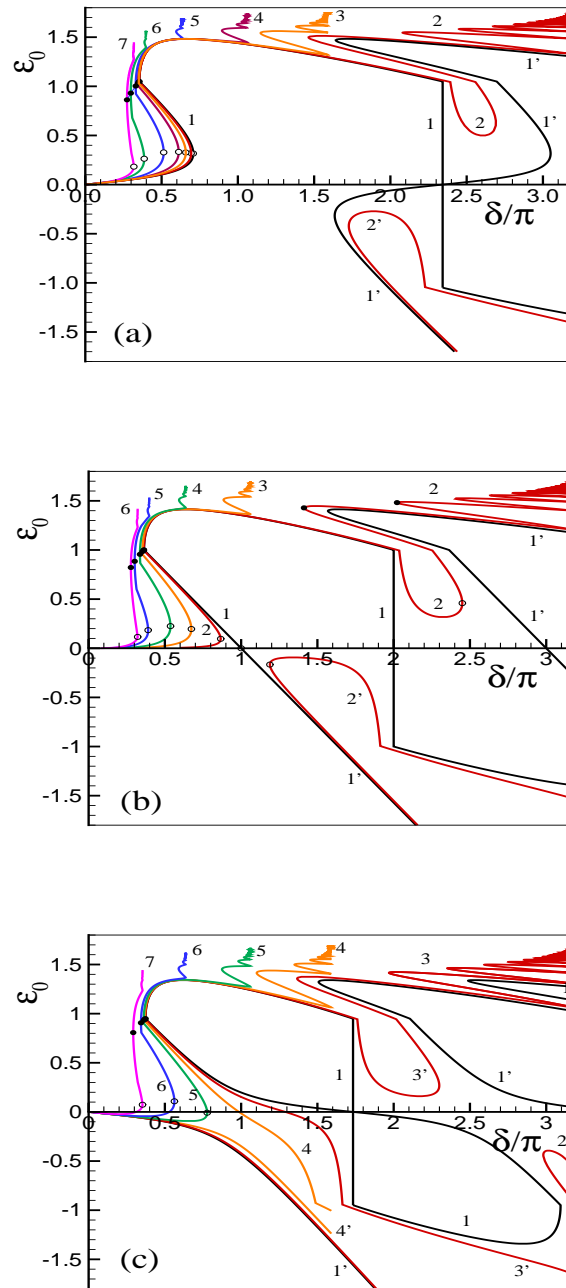


Figure 7.2: Curves $\varepsilon_0(\delta)$ drawn for three values of γ and various values of Ω : (a) $\gamma = 0.9$; $\Omega = 0$ (curve 1), 0.1 (2), 0.2 (3), 0.3 (4), 0.5 (5), 0.8 (6) and 1.0 (7); (b) $\gamma = 1.0$; $\Omega = 0$ (curve 1), 0.1 (2), 0.3 (3), 0.5 (4), 0.8 (5) and 0.99 (6); (c) $\gamma = 1.1$; $\Omega = 0$ (curve 1), 0.09 (2) 0.1 (3), 0.2 (4), 0.3 (5), 0.5 (6) and 0.9 (7). Open circles correspond to the *SCL* points, closed circles – to the *BF* points.

It can be seen from Fig. 7.2 that the bifurcation points of the *SCL* type can also arise for non-Bursian branches. They are marked by the open circles in Fig. 2(b).

Now we calculate the parameters of the BF point. A condition $d\delta/dr = 0$ has to hold at this point. We can calculate this derivative as a complex function using Eqs. (7.19)

$$\frac{d\delta}{dr} = \left[\frac{\partial u_\zeta}{\partial(T - \tau_r)} \frac{\partial \delta}{\partial r} - u_\zeta \frac{\partial u_\zeta}{\partial r} \right] / \left[\frac{\partial u_\zeta}{\partial(T - \tau_r)} + \Omega^2 \delta \right]. \quad (7.26)$$

For particular terms, we obtain

$$\begin{aligned} \frac{\partial u_\zeta}{\partial(T - \tau_r)} &= \frac{1-r}{\alpha} \sin \alpha(T - \tau_r), \\ \frac{\partial u_\zeta}{\partial r} &= -\frac{1}{\alpha^2} [1 - \cos \alpha(T - \tau_r)], \\ \frac{\partial \delta}{\partial r} &= \frac{\partial \zeta_r}{\partial r} - \frac{1}{\alpha^2} (T - \tau_r) + \frac{1}{\alpha^3} \sin \alpha(T - \tau_r), \\ \frac{\partial \zeta_r}{\partial r} &= \frac{1}{\alpha^2} \left[\tau_r - \frac{2}{\varepsilon_0} \right]. \end{aligned} \quad (7.27)$$

Substituting the related terms from Eqs. (7.27) into Eq. (7.26) and multiplying the result by α^4 , we obtain

$$\begin{aligned} &[\alpha\tau_r - 2\alpha/\varepsilon_0 - \alpha(T - \tau_r) + \sin \alpha(T - \tau_r)] \sin \alpha(T - \tau_r) \\ &+ [1 - \cos \alpha(T - \tau_r)]^2 = 0. \end{aligned} \quad (7.28)$$

Here, τ_r is determined by Eq. (7.15) and Eq. (7.16). After transforming the trigonometrical functions to half arguments, Eq. (7.28) breaks into two equations

$$\begin{aligned} &[\alpha\tau_r - 2\alpha/\varepsilon_0 - \alpha(T - \tau_r) + \sin \alpha(T - \tau_r)] \cos \frac{\alpha(T - \tau_r)}{2} \\ &+ 2 \left[\sin \frac{\alpha(T - \tau_r)}{2} \right]^3 = 0. \end{aligned} \quad (7.29)$$

and

$$\sin \frac{\alpha(T - \tau_r)}{2} = 0. \quad (7.30)$$

In order to calculate the parameters corresponding to the BF point, we have to use Eq. (7.29). This gives the first equation relating $(T - \tau_r)$ and r . The second equation which relates these parameters can be obtained as

$$u_\zeta^2(T - \tau_r, r; \alpha) + \Omega^2 \delta^2(T - \tau_r, r; \alpha) - (1 + 2V) = 0. \quad (7.31)$$

From the system of equations (7.29) and (7.31), we can calculate $(T - \tau_r)_{BF}$ and r_{BF} . Substituting them into Eqs. (7.9) and (7.12), we can have $\varepsilon_{0,BF}$ and δ_{BF} for the BF point.

Fig. 7.3 shows the dependencies of the bifurcation point on Ω . Here the variations of the δ_0 and ε_0^0 with respect to Ω are also shown. They correspond to the zero-point solutions where the longitudinal electron velocity vanishes for the first time. One can see that δ_{BF} is very closed to δ_0 for $\Omega < 0.6$. At a certain value of Ω the SCL and 0 points merge with each other (both lie at the collector). In this case the related parameters can be determined from the 2nd equation of (7.19) with $u_\zeta(T) = 0$.

We can see from Fig. 2 that each $\varepsilon_0 - \delta$ -curve contains a oscillating segment as $r \rightarrow 1$, i. e. it is many-valued over a certain range of the δ 's and it has many bifurcation points. This situation arises due to the fact that, for a particular value of $r(\varepsilon_0)$, the electron velocity u_ζ can vanish for several times in the region where $\zeta > \zeta_r$. It is quite evident from the third equation of (7.19) [see, also curves 1 and 4 in Fig. 1]. Figure 2 shows that the amplitude of the oscillations diminishes with r for each corkscrew line. It is also found that the maximum width of the oscillating segment shrinks with the increase of Ω .

The values of the coefficient r and T for the left bifurcation points can be calculated from the system of equations (7.29) and (7.31). Then, they are used to

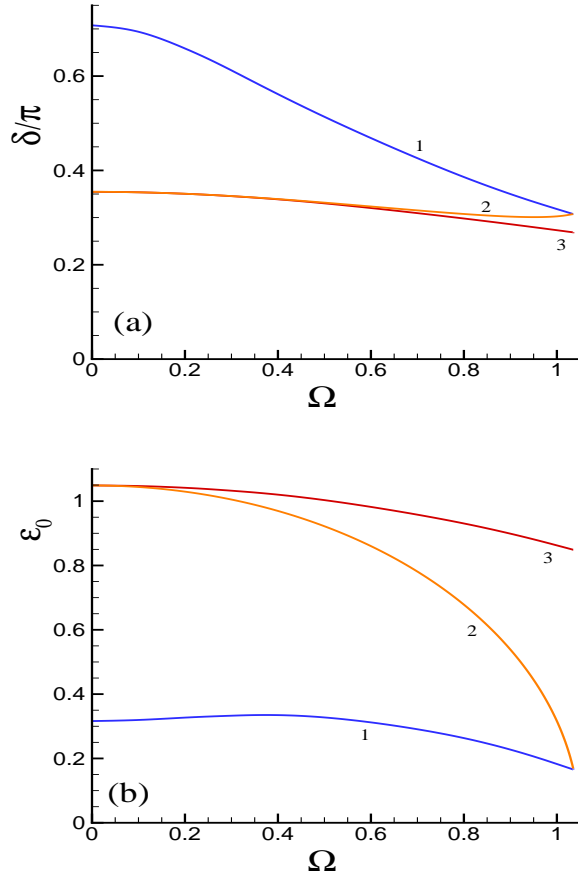


Figure 7.3: Dependencies of characteristic points (*SCL*, *BF* and 0-points) on the Bursian family $\varepsilon_0(\delta)$ for $\gamma = 0.9$ and $V = 0$; (a) $\delta(\Omega)$, (b) $\varepsilon_0(\Omega)$. Curve 1 corresponds to *SCL* point, 2 – 0-point, 3 – *BF* point.

find relevant parameters like ε_0 and δ from Eqs. (7.12) and (7.19). It turns out that each right bifurcation point on the zigzag segments corresponds to the condition $u_\zeta(\delta) = 0$. The second equation of (7.19) also reveals that, at these points, all relevant δ have the same value δ_{max} :

$$\delta_{max}(V; \Omega) = \sqrt{1 + 2V}/\Omega, \quad (7.32)$$

and it does not depend on γ . This particular value of the inter-electrode gap is maximum for the regime where only a portion of the injected electrons is turned around

by the magnetic field. Corresponding time can be calculated from Eq. (7.30):

$$T_i = \tau_r(r; \gamma, \Omega) + \frac{2\pi}{\alpha}i. \quad (7.33)$$

Here, $\tau_r(r; \gamma, \Omega)$ is determined by Eqs. (7.14)–(7.15) and the index i takes the positive integer values (i.e., $i = 1, 2, \dots$). The coefficient r corresponding to δ_{max} can be obtained when we substitute T_i from Eq. (7.33) into Eqs. (7.19) and (7.31) :

$$\zeta_r(r; \gamma, \Omega) + \frac{2\pi}{\alpha^3}(1-r)i = \frac{\sqrt{1+2V}}{\Omega}. \quad (7.34)$$

Here ζ_r is determined by Eq. (7.16). Relevant values of ε_0 are calculated from Eq. (7.12). In Fig. 2, several bifurcation points are marked with the closed circles.

Thus, our study shows that, similar to the case of the Bursian diode, there is also an ambiguity of the solutions for non-netral diodes in the vicinity of δ_{max} . The related parameters for the new bifurcation points are also calculated. In our next paper, we'll show that each bifurcation point on the curve $\varepsilon_0(\delta)$ separates the regions containing aperiodic stable and unstable steady state solutions.

7.4 Summary

In this chapter we have presented a comprehensive analysis on the steady states of a generalized Pierce diode which includes both the regime where all electrons arrive at the collector and the regime where a part of them is reflected back to the emitter by the magnetic field. It was found that the potential profile is a wavy-type function for zero and relatively weak magnetic field. This wavy PD brings a new family of solutions which exists along with the Bursian one. With the increase of the magnetic field, the wavy nature of the potential profile is lost. As a result,

the non-Bursian branches disappear gradually and only Bursian branches remain. Unlike the Bursian diode, the emitter field strength ε_0 can take both positive and negative values.

The (ε_0, δ) -diagram carries a region where the solutions are non-unique. Hence, the magnetic field can be used to design a fast electronic switch on the basis of the generalized Pierce diode too. It was also observed that non-Bursian solutions are very sensitive to the external magnetic field and they appear only when the strength of the magnetic field is either zero or weak enough. The transition of the states between the non-Bursian and Bursian branches makes it possible to control and regulate very high current density in diodic systems. We should also note that there is always an inherent magnetic field in real devices which is produced by the electron beam current. For this reason, it is very difficult to detect the non-Bursian solutions in an experiment.

Chapter 8

Conclusion

In this chapter, a quick recapitulation has been made on the works discussed in this thesis and the general conclusions are summarized. Some future prospects of our study have also been discussed in addition.

8.1 A quick recapitulation

With its nonlinear nature and a number of interesting features, a plasma diode has drawn the attention of many researchers since the beginning of the twentieth century. The derivation of the famous current-voltage relationship for planar diode by Child and Langmuir is the inception and till now it is a central topic of research. Many physical systems, such as, Q-machines, thermionic energy converters, microwave generators, low-pressure discharges and processing device etc. follow diodic character in their basic structure. The operational conditions in these systems are severely affected by the space-charge-limited flow which is a common feature of all types of plasma diodes. The space charge limit indicates a transition point between a state with high current density and a state with negligible current. When diode current exceeds a critical value, an aperiodic instability is developed in the system and as a result of it the transition of states occurs. The state with very low current density arises due to the formation of the virtual cathode within the inter-electrode region. The virtual cathode is a potential barrier which is sufficiently strong to block the passage of the charge particles. Let us consider that a monochromatic beam of charge particle is injected into the diode with a finite velocity. When the kinetic energy of the charge particle at emitter becomes equal to the potential barrier height, the charge particle loses all its longitudinal kinetic energy at some point and gets reflected by the virtual cathode. In practical situations, emitter does not emit charge particles in monoenergetic way. Therefore, there is always a very small fraction of emitted charges which can overcome the barrier.

The presence of inherent magnetic field is inevitable for the the systems like

thermionic energy converters, microwave generators etc, which operate with high current density. This magnetic field is generally transversal to the motion of the charge particle and it influences the space charge limit by reorienting their trajectories. In this thesis, we have assumed a planar model for a plasma diode, where a constant magnetic field is applied externally in transverse direction and studied the effect of the magnetic field on the space charge limit and on other characteristic parameters. The analysis is performed with the aid of the Eulerian and Lagrangian descriptions. A numerical scheme is developed to inspect the stationary state properties of a plasma diode in terms of the Eulerian variables. Whereas, the Lagrangian formalism provides us the exact analytical formulas for the potential and velocity profiles as well as the expressions for the parameters which define characteristic bifurcation points like space charge limit, zero-point etc. A brief summary of our obtained results is given below:

- Chapter II covers the analysis when there is no electron reflection, i.e., potential distribution within diode region does not correspond to the virtual cathode (VC). The results show that when there is a transverse magnetic field, the potential distributions remain the single minimum functions, but the height of the minimum turns out to be lower than the initial kinetic energy of the electrons. The magnetic field converts a portion of the longitudinal kinetic energy into the transverse one. The steady state solutions are represented through the (ε_0, δ) -curves. The (ε_0, δ) -diagram contains two distinct regions one of which is shown to be non-unique (C-overlap branch). The boundaries of the non-unique regions are defined by two characteristic-points. The right boundary point is “space charge limit” or *SCL*-point and

it corresponds to the state with maximum diode current. The left boundary point is “zero-point” which defines the situation when longitudinal component of electron velocity vanishes for the first time within inter-electrode gap. The effect of the magnetic field becomes dominant when the Larmor radius becomes comparable with the Bursian threshold. The distribution function of the emitted electrons start to lose its beam nature. As a consequence, the width of the non-unique region reduces until it vanishes at a particular strength of the magnetic field. At this condition, the *SCL* and “zero-point” of the (ε_0, δ) -curve merge with each other. The (ε_0, δ) -curves get displaced as the strength of the magnetic field increases. The value of the parameters at *SCL* point and zero-point also changes with this displacement. The critical value of the diode current also decreases with the increasing magnetic field.

- In chapter III, we have performed a stability analysis of the steady states of a vacuum diode which is kept under the uniform transverse magnetic field. The analysis does not include the steady states with virtual cathode. With the help of Lagrangian description and by employing a perturbative technique, a dispersion relation is derived. It is shown that the solutions corresponding to branch I ($\varepsilon \leq \varepsilon_{0,SCL}$) are always stable, and those of branch II ($\varepsilon_{0,SCL} < \varepsilon_0 \leq \varepsilon_0^0$) are unstable with respect to the small aperiodic perturbation. When the strength of the magnetic field is increased, the width of the unstable region (branch II) gradually decreases and vanishes at some particular value.
- In Chapter IV, we have studied the steady states of a Bursian diode with a constant magnetic field in the transverse direction when the electrons of the

emitted beam are reflected back to the emitter. The emitted electrons can be turned around partially or totally, depending on the values of the applied magnetic field and the electric field strength at emitter. The steady states with electron reflection are represented with an extra branch in the $\varepsilon_0 - \delta$ -curves (virtual cathode branch or B-branch). In this case, the left boundary of the non-unique region (C-overlap branch) is defined by *BF*-point.

However, unlike the classical Bursian diode, a new oscillatory region is observed in the (ε_0, δ) -diagram. This region arises because of the fact that the longitudinal velocity of the injected electrons can vanish for several times within the inter-electrode space. In this region, the reflection coefficient r is close to the value 1. When $r \rightarrow 1$, the period and the amplitude of the velocity oscillations gradually become zero.

Based on the transition of states between normal C branch and B branch, a basic model to design a fast electronic switches is suggested.

- Chapter V contains the basic properties of a relativistic Bursian diode in the presence of a transverse magnetic field. All steady state solutions including the solutions with electron reflection is inspected in generalized way. The width of the C-overlap branch increases with the increasing value of the relativistic factor (γ_0) of the emitted electron beam. The variations of the characteristic bifurcation points (zero-point, BF point and SCL point) with respect to γ_0 are shown. The magnitude of the diode current at space charge limit increases with γ_0 . It is found that the magnetic field and γ_0 has opposite effects on the steady state properties. Like the non-relativistic Bursian diode with the transverse magnetic field, the (ε_0, δ) -diagram displays a oscillatory

or zig-zag region when the reflection coefficient r is close to unity. The reason lies in the fact that the presence of strong magnetic field can cause multiple turning points, i.e., longitudinal velocity of the electrons can vanish for more than once. However, for higher values of γ_0 , as the kinetic energy of the emitted energy increases, the oscillatory region gets suppressed.

- In chapter VI, an effort has been made to study the steady state properties of a generalized Pierce diode when an external magnetic field is applied along the transverse direction. The study only includes the regime of no electron reflection. In absence of magnetic field as well as when the strength of the magnetic field is weak, a new family of solutions arises along with the Bursian families. The wavy potential profile has been identified to be responsible for the existence of the non-Bursian brunches.
- Chapter VII presents the analysis on the steady states of a generalized Pierce diode when a portion of the emitted electrons are turned around by the the magnetic field. The Bursian and non-Bursian branches are developed for the solutions representing electron-reflection. When the strength of the magnetic field is increased beyond a critical value, the non-Bursian branches disappear and only the Bursian branches survive.

8.2 Future prospects and conclusive remarks

The motivation behind the works contained in this thesis is to provide a clear understanding on the basic features of a plasma diode. The thesis provides an extensive discussion on the steady state properties of a plasma diode in presence of an external magnetic field which is applied along transverse direction. However,

few unanswered questions still remain to address in future.

- In our study, we have considered a delta-function for the velocity distribution of the injected electrons. The beam was assumed cold too. The appearance of electron reflection has been incorporated by assuming a small velocity spread in the injected electron beam profile. But in the devices like TIC where charge carriers are produced by the surface ionization process, it would be more practical, to assume a half-Maxwellian velocity distribution for the injected electrons. Therefore, assuming a thermal spreading of the longitudinal velocity (v_z) around v_0 , the velocity distribution function of the emitted electrons can be taken as

$$f_0(v_z) = \frac{n_0}{v_0} A(\alpha) \exp \left\{ -\alpha \left(\frac{v_z^2}{v_0^2} - 1 \right) \right\} \Theta(v_z - v_0),$$

$$A(\alpha) = \frac{2\sqrt{\alpha}}{\sqrt{\pi} \operatorname{exers}(\alpha)}.$$

where, $\alpha = v_0^2/(2kT/m)$ with T being the effective “temperature” of the beam and $\operatorname{exers}(\alpha) = \exp(\alpha)(1 - \operatorname{erf}\sqrt{\alpha})$ [$\operatorname{erf}(\alpha)$ being the error integral]. It will be interesting to check how the properties of the solutions and space charge limit change for this type of velocity distribution function.

- The stability properties of the Normal C branch and C overlap branch is studied with the help of $\eta - \varepsilon_0$ -diagram and a dispersion relation derived by the Lagrangian technique. The $\eta - \varepsilon_0$ -diagram technique allows us to study the solutions with respect to aperiodic perturbations. However, it does not say anything about oscillatory perturbations. It will be interesting to derive a dispersion relation for the states with electron reflection and check its stability criteria with respect to aperiodic perturbation.

- An attempt could be made to study the stability properties of the different branches of steady state solutions (Normal C branch, C-overlap branch and virtual cathode branch) of a relativistic Bursian diode in the presence of a transverse magnetic field.
- For generalized Pierce diodes, ions are assumed to form uniform background and their motion is ignored. But inclusion of finite ion velocity may bring some new features in the diode characteristics. In addition, an analysis on the plasma diodes with a nonuniform density distribution of ions is also necessary. Steady-state properties and the transition processes should be examined by varying spatial distributions of the ions.
- In our works, we have considered a planar model for the plasma diodes. It should be examined how the space charge limited flow and other properties of a plasma diode depends on the geometries (for example cylindrical or spherical geometry).
- In this thesis work, electrons are assumed to travel the diode region without collisions. We can check further the role of particle collisions on the Bursian-Pierce instability and space charge limit. Note that such a problem for the Bursian diode was partially attempted in Ref. [174].
- As an important application of our works on the plasma diodes in the presence of the transverse magnetic field, we have suggested to build an electron switch which works on the basis of the transition of states. It is discussed in detail in the summary sections of chapter two and three. In order to

understand the working mechanism of the switches, we need to study time-dependent processes of transition between the states with different currents. It also provides an opportunity to study the whole mechanics experimentally.

The investigation presented in this dissertation on the beam plasma diodes with an external magnetic field in perpendicular direction opens up new prospects to study the thermionic energy converters, microwave generators, high effective switches and other devices of the plasma electronics. To deal with the main challenges for the future investigations, we need to use an accurate numerical methods. Because when the picture becomes more complex, it is very difficult to find an exact analytical solutions. We sincerely hope that the works elaborated in this thesis can help us to understand the complex and nonlinear aspects of the plasma diodes and enlighten our way to proceed furthermore in this direction.

Appendix

(Related to Chapter-5)

Using approximation (5.29), each integral (5.28) becomes as follows:

$$\begin{aligned}
 G(\zeta_{k-1}, \eta_{k-1}, \varepsilon_{k-1}, \eta_k, \varepsilon_k) &= \int_{\eta_{k-1}}^{\eta_k} \frac{[2(\gamma_0 - 1)w + \gamma_0]dw}{[2(\gamma_0 - 1)w^2 + 2\gamma_0w + (\gamma_0 + 1)/2 - \Omega^2(\zeta')^2]^{1/2}} \\
 &= \int_0^{\eta_k - \eta_{k-1}} \frac{(D + Et)dt}{\sqrt{A + Bt + Ct^2}} \\
 &= \left(D - \frac{BE}{2C} \right) \int_0^{\eta_k - \eta_{k-1}} \frac{dt}{\sqrt{A + Bt + Ct^2}} + \frac{E}{C} \sqrt{A + Bt + Ct^2} \Big|_0^{\eta_k - \eta_{k-1}} \quad (\text{A.1})
 \end{aligned}$$

Here

$$\begin{aligned}
 A &= (\gamma_0 + 1)/2 + 2\gamma_0\eta_{k-1} + 2(\gamma_0 - 1)\eta_{k-1}^2 - \zeta_{k-1}^2\Omega^2 > 0, \\
 B &= 2 \left[\gamma_0 + 2(\gamma_0 - 1)\eta_{k-1} + (\zeta_{k-1}/\varepsilon_k)\Omega^2 \right], \\
 C &= 2(\gamma_0 - 1) - (1/\varepsilon_k^2)\Omega^2, \\
 D &= \gamma_0 + 2(\gamma_0 - 1)\eta_{k-1}, \quad E = 2(\gamma_0 - 1). \quad (\text{A.2})
 \end{aligned}$$

and

$$\Delta = 4AC - B^2 < 0. \quad (\text{A.3})$$

At $\Omega > 0$, the integral in (A.1) reads as (formulae (2.261) in [175])

$$-\frac{1}{|C|} \left\{ \arcsin \left[\frac{B + 2C(\eta_k - \eta_{k-1})}{\sqrt{-\Delta}} \right] - \arcsin \left(\frac{B}{\sqrt{-\Delta}} \right) \right\} \quad (\text{A.4})$$

at $C < 0$ and

$$\frac{1}{\sqrt{C}} \ln \frac{2\sqrt{C}\sqrt{A + B(\eta_k - \eta_{k-1}) + C(\eta_k - \eta_{k-1})^2} + B + 2C(\eta_k - \eta_{k-1})}{2\sqrt{AC} + B} \quad (\text{A.5})$$

at $C > 0$, while at $\Omega = 0$ $E/C = 1$, $D - BE/2C = 0$ and the function G reads as

$$\sqrt{(\gamma_0 + 1)/2 + 2\gamma_0\eta_k + 2(\gamma_0 - 1)\eta_k^2} - \sqrt{(\gamma_0 + 1)/2 + 2\gamma_0\eta_{k-1} + 2(\gamma_0 - 1)\eta_{k-1}^2} \quad (\text{A.6})$$

Bibliography

- [1] R.G. McIntyre, J. Appl. Phys. **33**, 2485 (1962).
- [2] R. W. Motley, *Q-Machines*, Academic Press, New York, (1975).
- [3] F.G. Baksht et al., in: Moizhes, Pikus (Eds.), *Thermionic Converters and Low-Temperature Plasma*, Washington, DC, (1976).
- [4] V.I. Kuznetsov and A.Ya. Ender, Sov. Phys. Tech. Phys. **17**, 1859 (1973).
- [5] V.I. Babanin, I.N. Kolyshkin, V.I. Kuznetsov, A.S. Mustafaev, V.I. Sitnov, A.Ya. Ender, Sov. Phys. Tech. Phys. **27**, 793 (1982).
- [6] E.A. Coutsiias and D.J. Sullivan, Phys. Rev. A **27**, 1535 (1983).
- [7] V.L. Granatstein and I. Alexeff (Eds.), *High-Power Microwave Sources*, Artech House, Norwood (1987).
- [8] W. Hertz, Phys. Technol. **10**, 195 (1979).
- [9] R.T. Farouki, M. Dalvie and L.F. Pavarino, J. Appl. Phys. **68**, 6106 (1990).
- [10] M. A. Lieberman and A. J. Lichtenbarg, *Principles of Plasma Discharges and Material processing*, Wiley, New York (1994).
- [11] N. Rostoker and M. Reiser, *Collective Methods of Acceleration*, Harwood Academic, London (1979).

- [12] R.B. Miller, *Introduction to the Physics of Intense Charged Particle Beams*, Plenum Press, New York, (1982).
- [13] J.W. Poukey, J.P. Quintenz and C.L. Olson, *Appl. Phys. Lett.* **38**, 20 (1981).
- [14] J.W. Poukey, J.P. Quintenz and C.L. Olson, *J. Appl. Phys.* **52**, 3016 (1981).
- [15] D. S. Lemons and J. R. Cary, *J. Appl. Phys.* **53**, 4093 (1982).
- [16] M. Carr and J. Khachan, *Phys. Plasmas* **17**, 052510 (2010).
- [17] D. Hinshelwood, P. Ottinger, J. Schumer, R. Allen, J. Apruzese, R. Comisso, G. Cooperstein, S. Jackson, D. Murphy, D. Phipps *et al.*, *Phys. Plasmas* **18**, 053106 (2011).
- [18] Yu. N. Gartstein and P.S. Ramesch, *J. Appl. Phys.* **83**, 2037 (1998).
- [19] M. A. Lampert and P. Mark, *Current Injection in Solids*, Academic, New York (1970).
- [20] E. Hernandez, *Cryst. Res. Technol.* **33**, 285 (1998).
- [21] P.D. Mumford and M. Cahay, *J. Appl. Phys.* **84**, 2754 (1998).
- [22] S. A. Sultz and M. P. Desjarlais, *J. Appl. Phys.* **67**, 6705 (1990).
- [23] S. A. Sultz, J. W. Poukey and T. D. Pointon, *Phys. Plasmas* **1**, 2072 (1994).
- [24] P. F. Ottinger, P. J. Goodrich, D. D. Hinshelwood, D. Mosher, J. M. Neri, D. V. Rose, S. J. Stephanakis and F. C. Young, *Proc. Ieee* **80**, 1010 (1992).
- [25] K. L. Jensen, M. A. Kodis, R. A. Murphy and E. Zeidman, *J. Appl. Phys.* **82**, 845 (1997).

- [26] V. T. Binh and Ch. Adessi, *Phys. Rev. Lett.* **65**, 864 (2000).
- [27] K. Jensen *Phys. World* **13**, 25 (2000).
- [28] C. K. Birdsall and W. B. Bridges, *Electron dynamics of Diode Regions*, Academic Press, New York (1966).
- [29] P. T. Kirstein, G. S. Kino and W. E. Waters, *Space Charge Flow*, McGraw-Hill, New York (1967).
- [30] L. S. Bogdankevich and A. A. Rukhadze, *Sov. Phys. Usp.* **14**, 163 (1971).
- [31] R. C. Davidson, *Physics of Nonneutral Plasmas*, Addison-Wesley, Redwood City, CA, (1990).
- [32] C. D. Child, *Phys. Rev.*, Ser. 1, **32** 492 (1911).
- [33] I. Langmuir, *Phys. Rev.* **2**, 450 (1913).
- [34] W. Schottky, *Z. Phys.* **14**, 63 (1923) (in German).
- [35] V. R. Bursian and V. I. Pavlov, *Zh. Rus. Fiz.-Khim. Obshch* **55**, 71 (1923) (in Russian).
- [36] G. Plato, W. Kleen and H. Rothe, *Z. Phys.* **101**, 509 (1936).
- [37] W. Kleen and H. Rothe, *Z. Phys.* **104**, 711 (1937) (in German).
- [38] B. Salzberg and A. V. Haeff, *RCA Rev.* **2**, (336) (1938).
- [39] M. J. O. Strutt and van der Ziel, *Physics* **5**, 705 (1938).
- [40] G. Jaffe, *Phys. Rev.* **65**, 91 (1944).

- [41] P. F. Ottinger, P. J. Goodrich, D. D. Hinshelwood et al., Proc. IEEE **80**, 1100 (1992).
- [42] A. A. G. Driskill-Smith, D. G. Hasko and H. Ahmed, Appl. Phys. Lett. **75**, 2845 (1999).
- [43] W. A. de Heer and R. Martel, Phys. World **13**, 49 (2000).
- [44] J.R. Pierce, Appl. Phys. **15**, 721 (1944).
- [45] O. M. Bulashenko, J. M. Rubi, and V. A. Kochelap, Phys. Rev. B **61**, 5511 (2000).
- [46] M. C. Lin, J. Vac. Sci. Technol. B **23**, 636 (2005).
- [47] P. Yi and Z. Geng-Min, Chin. Phys. Lett. **22**, 648 (2005).
- [48] Y. Feng and J. P. Verboncoeur, Phys. Plasmas **13**, 073105 (2006).
- [49] E. W. B. Gill, Philos. Mag. **49**, 993 (1925).
- [50] J. H. O. Harries, *Wireless Engineer* **13**, 190 (1936).
- [51] E. W. Mueller, Z. Phys. **108**, (668) (1938).
- [52] J. P. Barbour, W. W. Dolan, J. K. Trolan, E. E. Martin, and W. P. Dyke, Phys. Rev. **92**, 45 (1953).
- [53] W. A. Anderson, J. Vac. Sci. Technol. B **11**, 383 (1993).
- [54] J. H. O. Harries, *Television Soc.* **2**, 106 (1936).
- [55] C. E. Fay, A. L. Samuel and W. Shockly, Bell Syst. Tech. J. **17**, 49 (1938).

- [56] F.B. Llewellyn, *Electron Inertia Effect*, Cambridge Univ. Press, London, 1941.
- [57] R.J. Lomax, Proc. IEE Pt C **108**, 119 (1961).
- [58] M.V. Nezlin, *Dynamics of Beams in Plasma*, Moscow, Energoizdat, 1982 (in Russian); *Physics of Intense Beams in Plasmas*, IOP publ., Bristol, 1993 (in English).
- [59] E.A. Coutsias, J. Plasma Phys. **31**, 313 (1984).
- [60] E.A. Coutsias, J. Plasma Phys. **40**, 369 (1987).
- [61] I.M. Alyeshin and L.S. Kuz'menkov, Vestnik Mosk. Univ. Ser. 3, Fizika Astronomiya **35**, 46 (1994) (in Russian).
- [62] C. K. Birdsall and W. Bridges, J. Appl. Phys. **34**, 2946 (1963).
- [63] V. I. Kuznetsov and A. Ya. Ender, Sov. Phys. Tech. Phys. **22**, 1295 (1977).
- [64] V. I. Kuznetsov, A. V. Solov'yev and A. Ya. Ender, Sov. Phys. Tech. Phys. **39**, 1207 (1994).
- [65] V. I. Kuznetsov, A. Ya. Ender, H Schamel and P. V. Akimov, Phys. Plasmas **11**, 3224 (2004).
- [66] V. I. Kuznetsov and A. Ya. Ender, Plasma Phys. Rep. **36**, 226 (2010).
- [67] V. I. Kuznetsov and A. Ya. Ender, Tech. Phys. **58**, 1705 (2013).
- [68] P. V. Akimov, H. Schamel, A. Ya. Ender, and V. I. Kuznetsov, J. Appl. Phys. **93**, 1246 (2003).

- [69] A. Y. Ender, V. I. Kuznetsov and H. Schamel, *Phys. Plasmas* **18**, 033502 (2011).
- [70] H. Matsumoto, H. Yokoyama and D. Summers, *Phys. Plasmas* **3**, 177 (1996).
- [71] P. V. Akimov, A. Ya. Ender and H. Kolinsky, *et. al.*, *Vopr. At. Nauki Tekh.* **1**, 155 (2000).
- [72] H. Kolinsky, H. Schamel, *J. Plasma Phys.* **57**, 403 (1997).
- [73] S. Kuhn, *Phys. Rev. Lett.* **50**, 217, (1983).
- [74] S. Kuhn, *Phys. Fluids* **27**, 1834 (1984).
- [75] T. L. Crystal and S. Kuhn, *Phys. Fluids* **28**, 2116 (1985).
- [76] J. Frey and C. K. Birdsall, *J. Appl. Phys.* **36**, 2962 (1965).
- [77] M.V. Nezlin and A.M. Solntzev, *Sov. Phys. JETP* **26**, 290 (1968).
- [78] V.I. Kuznetsov and A.Ya. Ender, *Sov. Phys. Tech. Phys.* **25**, 37 (1980).
- [79] J.R. Cary and D.S. Lemons, *J. Appl. Phys.* **53**, 3303 (1981).
- [80] T.M. Burinskaya and A.S. Volokitin, *Sov. J. Plasma Phys.* **9**, 261 (1983).
- [81] A.N. Mosiyuk, *Sov. Phys. Tech. Phys.* **29**, 1388 (1984).
- [82] S. Kuhn and M. Horhager, *J. Appl. Phys.* **60**, 1952 (1986).
- [83] B.B. Godfrey, *Phys. Fluids* **30**, 1553 (1987).
- [84] M. Hörhager and S. Kuhn, *Phys. Fluids* **B2**, 2741 (1990).

- [85] A.Ya. Ender, S. Kuhn and V.I. Kuznetsov, Czech. J. Phys. **48** (Suppl. S2), 251 (1998).
- [86] V.M. Smirnov, Sov. Phys. JETP **23**, 668 (1966).
- [87] V.P. Shumilin, Sov. Phys. Tech. Phys. **26**, 1484 (1981).
- [88] S.I. Vybornov, Sov. J. Plasma Phys. **12**, 537 (1986).
- [89] X. Chen and P.A. Lindsay, *H.E. Brandt (Ed.), Intense Microwave Pulses III, SPIE Proc.*, Vol. 2557, San Diego, USA, (1995).
- [90] K. Yuan, J. Appl. Phys. **48**, 133 (1977).
- [91] I.N. Kolyshkin, V.I. Kuznetsov and A.Ya. Ender, Sov. Phys. Tech. Phys. **29**, 882 (1984).
- [92] H. Schamel and S. Bujarbarua, Phys. Fluids B **5**, 2278 (1993).
- [93] H. Schamel and V. Maslov, Phys. Rev. Lett. **70**, 1105 (1993).
- [94] H. Kolinsky and H. Schamel, Phys. Plasmas **1**, 2359 (1994).
- [95] H. Kolinsky and H. Schamel, Phys. Rev. E **52**, 4267 (1995).
- [96] H. Kolinsky, F. Greiner and T. Klinger, J. Phys. D: Appl. Phys. **30**, 2979 (1997).
- [97] Y.Y. Lau, D. Chernin and D.G. Colombant, P. T. Ho, Phys. Rev. Lett. **66**, 1446 (1991).
- [98] Y.Y. Lau, P.J. Christensen and D. Chernin, Phys. Fluids B **5**, 4486 (1993).

- [99] A.W. Hull, Phys. Rev. **18**, 31 (1921).
- [100] Y.Y. Lau, Y. Liu and R.K. Parker, Phys. Plasmas **1**, 2082 (1994).
- [101] Y. Y. Lau, Phys. Rev. Lett. **87**, 278301 (2001).
- [102] A. Valfells, D. W. Feldman, M. Virgo, P. G. OShea, and Y. Y. Lau, Phys. Plasmas **9**, 2378 (2002).
- [103] J. W. Luginsland, Y. Y. Lau, R. J. Ulmstattd and J. J. Watrous, Phys. Plasmas **9**, 2371 (2002).
- [104] D. A. Dunn and I. T. Ho, AIAA J. **1**, 2770 (1963).
- [105] V. D. Selemir, B. V. Alekhin, V. E. Vatrugin, A. E. Dubinov *et. al.*, Plasma Phys. Rep. **20**, 621 (1994).
- [106] P. V. Akimov, H. Kolinsky V. I. Kuznetsov, H. Schamel and A. Ya. Ender, *Proceedings of the All-Russia Conference on Low Temperature Plasmas, Petrozavodsk.* **1**, 513 (1998).
- [107] V. I. Kuznetsov and A. Ya. Ender, *Proceedings of the All-Russia Conference on Low Temperature Plasmas, Petrozavodsk.* **2**, 148 (1995).
- [108] V. I. Kuznetsov, A. Ya. Ender, H. Schamel and P. V. Akimov, Phys. Plasmas **11**, 3224 (2004).
- [109] V. F. Tarasenko, Plasma Phys. Rep. **37**, 409 (2011).
- [110] A. Roy, A. Patel, R. Menon, A. Sharma, D. P. Chakravarthy, and D. S. Patil, Phys. Plasmas **18**, 103108 (2011).

- [111] A. Pedersen, A. Manolescu, and A. Valfells, *Phys. Rev. Lett.* **104**, 175002 (2010).
- [112] R. E. Caffisch and M. S. Rosin, *Phys. Rev. E* **85**, 056408 (2012).
- [113] M. S. Rosin and H. Sun, *Phys. Rev. E* **87**, 043114 (2013).
- [114] V. I. Kuznetsov and A. Ya. Ender, *Plasma Phys. Rep.* **41**, 905 (2015).
- [115] V. I. Babanin, I. N. Kolyshkin, V. I. Kuznetsov, V. I. Sitnov, and A. Ya. Ender, *Physics of thermionic energy converters, in 2nd Intersociety Conference on Nuclear Power Engineering in Space*, Sukhumi, Georgia (Vekua Institute of Physics and Technology, Sukhumi, 1991), p. 9.
- [116] A.Ya. Ender et al., in H.S. El-Genk (Ed.), *Proceedings of the 11th Symposium on Space Nuclear Power and Propulsion*, CONF-940101, AIP Conf. Proc., no. 301, **2**, p. 861; Amer. Inst. Phys., NY, (1994).
- [117] A.Ya. Ender, I.N. Kolyshkin, V.I. Kuznetsov, V.I. Sitnov and D.V. Paramonov, *Next generation solar bimodal systems*, Proc. 32-IECEC, AIChE, p. 427 (1997).
- [118] G. Gverdtziteli, V.Ya. Karakhanov, E.A. Kashirskii, R.Ya. Kucherov and Z.A. Oganezov, *Sov. Phys. Tech. Phys.* **17**, 78 (1972).
- [119] V.I. Babanin, I.N. Kolyshkin, V.I. Kuznetsov, V.I. Sitnov and A.Ya. Ender, *Proceedings of the second Intersociety Conference on Nuclear Power Engineering in Space*, Physics of Thermionic Energy Converters, Sukhumi, USSR, Ministry of Atomic Energy, p. 95 (1991).

- [120] S. Iizuka, P. Michelsen, J.J. Rasmussen, R. Schrittwieser, R. Hatakeyama, K. Saeki and N. Sato, *J. Phys. Soc. Japan* **54**, 2516 (1985).
- [121] A. M. Ignatov and A. A. Rukhadze, *Kratk. Soobsh. Fiz.* **1**, 13 (1977).
- [122] D. Sullivan, *Proceedings Vth International Top. Conference on High Power Electron and Ion Beam Research and Technology*, San Francisco, p. 557 (1983).
- [123] Y. Modukuru, M. Cahay, H. Kolinsky, and P. Mumford, *J. Appl. Phys.* **87**, 3386 (2000).
- [124] P. V. Akimov, V. I. Kuznetsov, H. Schamel and A. Ya. Ender, *Proceedings of the All-Russia Conference on Low Temperature Plasmas, Petrozavodsk.* **1**, 25 (2001).
- [125] G. N. Hatsopoulos and E. P. Gyftopoulos, *Thermionic Energy Conversion, Vol. I, Processes and Devices*, MIT Press, Cambridge, M. A. (1973).
- [126] G. N. Hatsopoulos and E. P. Gyftopoulos, *Thermionic Energy Conversion, Vol. II, Theory, Technology and Application*, MIT Press, Cambridge, M. A. (1979).
- [127] N. S. Rasor, *IEEE Trans. Plasma Sci.* **19**, 1191 (1991).
- [128] A. Kadish, R. J. Faehl and C. M. Snell, *Phys. Fluids* **29**, 4192 (1986).
- [129] L. E. Thode, *High Power Microwave Sources*, Artech House, Norwood, M. A. (1987).

- [130] R. J. Barker and E. Schamiloglu, *High-Power Microwave Sources and Technologies*, IEEE, New York, (2002).
- [131] J. D. Ivers, L. Schachter, J. A. Nation, G. S. Kerslick and R. Advani, *J. Appl. Phys.* **73**, 2667 (1993).
- [132] L. Schachter, J. D. Ivers, J. A. Nation and G. S. Kerslick, *J. Appl. Phys.* **73**, 8097 (1993).
- [133] V. I. Kuznetsov and A. Ya. Ender, *Sov. Phys. Tech. Phys.* **28**, 1431 (1983).
- [134] W. Jiang and M. Kristiansen, *Phys. Plasmas* **8**, 3781 (2001).
- [135] P. V. Akimov, H. Schamel, H. Kolinsky, A. Ya. Ender and V. I. Kuznetsov, *Phys. Plasmas* **8**, 3788 (2001).
- [136] A. Ya. Ender, V. I. Kuznetsov, H. Schamel, and P. V. Akimov, *Phys. Plasmas* **11**, 3212 (2004).
- [137] V. I. Kuznetsov, A. Ya. Ender, H. Schamel and P. V. Akimov, *Phys. Plasmas* **11**, 3224 (2004).
- [138] A. E. Dubinov and D. I. Selemir, *J. Comm. Technol. Electron.* **47**, 575 (2002).
- [139] A. Shock, *J. Appl. Phys.* **31**, 1978 (1960).
- [140] F. G. Block, F. H. Corregan, G. J. Eastman, J. R. Fendley, K. G. Hernqvist and E. J. Hills, *Proc. IRE*, 1846 (1960).
- [141] J. Kramář, *Czech. J. Phys.* **15**, 190 (1965).

- [142] A. Ya. Ender, Sov. Phys. Tech. Phys. **13**, 1546 (1969).
- [143] A. Ya. Ender, Sov. Phys. Tech. Phys. **14**, 762 (1969).
- [144] A. Ya. Ender, Sov. Phys. Tech. Phys. **15**, 426 (1970).
- [145] Yu. G. Morosov and A. Ya. Ender, Sov. Phys. Tech. Phys. **16**, 1914 (1972).
- [146] D. Li, J. Zhang, and X. Chen. Phys. Plasmas **15**, 023110 (2008).
- [147] A. V. Paschenko and B. N. Rutkevich, Sov. J. Plasma Phys. **3**, 437 (1977).
- [148] V. I. Kuznetsov, A. V. Solov'ev, and A. Ya. Ender, Tech. Phys. **39**, 1207 (1994).
- [149] I. N. Bronstein, K. A. Semendjajew, G. Musiol, and H. Muhlig, *Taschenbuch der Mathematik, 3rd ed. Verlag Harri Deutsch, Frankfurt am Main*, (1997).
- [150] A. Ya. Ender, H. Kolinsky, V. I. Kuznetsov, and H. Schamel, Phys. Rep. **328**, 1, (2000).
- [151] S. Pramanik, A. Ya. Ender, V. I. Kuznetsov, and N. Chakrabarti, Phys. Plasmas **22**, 042110 (2015).
- [152] V. I. Kuznetsov and A. Ya. Ender, Plasma Phys. Rep. **36**, 236 (2010).
- [153] H. Sze, J. Benford and B. Harteneck, Phys. Fluids **29** 5875 (1986).
- [154] D. J. Sullivan, J. E. Walsh, and E. A. Coutsiias, *Virtual Cathode Oscillator (Vircator) Theory*, High Power Microwave Sources Vol.13, Artech House Microwave Library, NY, (1987).

- [155] J. Benford, J. A. Swegle, and E. Schamiloglu. *High Power Microwaves*, CRC Press, Taylor and Francis, (2007).
- [156] R. A. Mahaffey, P. A. Sprangle, J. Golden, and C. A. Kapetanacos, *Phys. Rev. Lett* **39**, 843 (1977).
- [157] W. Jiang, K. Masugata, and K. Yatsui, *Phys. Plasmas* **2**, 982 (1995).
- [158] R. A. Filatov, A. E. Hramov, Y. P. Bliokh, A. A. Koronovskii, and J. Felsteiner, *Phys. Plasmas* **16**, 033106 (2009).
- [159] Y. A. Kalinin, A. A. Koronovskii, A. E. Khramov, E. N. Egorov, and R. A. Filatov, *Plasma Phys. Rep.* **31**, 938 (2005).
- [160] E. W. V. Action, *J. Electron. Control* **3**, 203 (1957).
- [161] J. E. Boers and D. Kelleher, *J. Appl. Phys.* **40**, 2409 (1969).
- [162] H. R. Jory and A. W. Trivelpiece, *J. Appl. Phys.* **40**, 3924 (1969).
- [163] V. S. Voronin, Y. T. Zozulya and A. N. Lebedev, *Sov. Phys. Tech. Phys.* **17**, 432 (1972).
- [164] Y. Feng and J. P. Verboncoeur, *Phys. Plasmas* **15**, 112101 (2008).
- [165] P. A. Lindsay, D. Li, and X. Chen, *Phys. Plasmas* **16**, 073303 (2009).
- [166] M. C. Lin and D. S. Chuu, *Appl. Phys. Lett.* **80**, 4262 (2002).
- [167] M. Lopez, Y. Y. Lau, J. W. Luginsland, D. W. Jordan, and R. M. Gilgenbach, *Phys. Plasmas* **10**, 4489 (2003).
- [168] F. G. Smith. *Pulsars*, Cambridge University Press, (1977).

- [169] Alexander Hramov, Alexey Koronovskii, Mikhail Morozov and Alexander Mushtakov, *Phys. Lett. A* **372**, 876 (2008).
- [170] S.A. Kurkin, A.E. Hramov, and A.A. Koronovskii, *App. Phys. Lett.* **103**, 043507 (2013).
- [171] A.Ya. Ender, S. Kuhn and V.I. Kuznetsov, *Phys. Plasmas* **13**, 113506 (2006).
- [172] A. Ya. Ender, V. I. Kuznetsov, *Journal of Physics: Conference Series* **510** 012046 (2014).
- [173] D. Li, J. Zhang, and X. Chen, *Phys. Plasmas* **15**, 023110 (2008).
- [174] P. V. Akimov and H. Schamel, *J. Appl. Phys.* **92**, 1690 (2002).
- [175] I.S. Gradshteyn and I.M. Ryzhik, *Table of Integrals, Series and Products*, Academic, New York, (1980).